

UNIVERSIDADE FEDERAL DE SANTA MARIA CENTRO DE TECNOLOGIA
PROGRAMA DE PÓS-GRADUAÇÃO EM ENGENHARIA QUÍMICA

Victoria Ximenes Nascimento

**PREPARAÇÃO E CARACTERIZAÇÃO DE CARVÃO ATIVADO MAGNÉTICO
OBTIDO A PARTIR DA SERRAGEM DE MADEIRA SAPELLI (*Entandrophragma
cylindricum*) PARA ADSORÇÃO DO CORANTE AZUL BRILHANTE**

Santa Maria, RS
2023

Victoria Ximenes Nascimento

**PREPARAÇÃO E CARACTERIZAÇÃO DE CARVÃO ATIVADO MAGNÉTICO
OBTIDO A PARTIR DA SERRAGEM DE MADEIRA SAPELLI (*Entandrophragma
cylindricum*) PARA ADSORÇÃO DO CORANTE AZUL BRILHANTE**

Dissertação apresentada ao Curso de mestrado do Programa de Pós-Graduação em Engenharia Química, da Universidade Federal de Santa Maria (UFSM, RS), como requisito parcial para obtenção do título de Mestre em Engenharia Química.

Orientador: Prof. Dr. Guilherme Luiz Dotto

Coorientador: Prof. Dr. Éder Cláudio Lima

This study was financed in part by the Coordenação de Aperfeiçoamento de Pessoal de Nível Superior - Brasil (CAPES) - Finance Code 001

Nascimento, Victoria Ximenes
PREPARAÇÃO E CARACTERIZAÇÃO DE CARVÃO ATIVADO
MAGNÉTICO OBTIDO A PARTIR DA SERRAGEM DE MADEIRA SAPELLI
(*Entandrophragma cylindricum*) PARA ADSORÇÃO DO CORANTE
AZUL BRILHANTE / Victoria Ximenes Nascimento.- 2023.
139 p.; 30 cm

Orientador: Guilherme Luiz Dotto
Coorientador: Éder Cláudio Lima
Dissertação (mestrado) - Universidade Federal de Santa
Maria, Centro de Tecnologia, Programa de Pós-Graduação em
Engenharia Química, RS, 2023

1. Adsorção 2. Carvão ativado magnético 3. Corante 4.
Pirólise de etapa única I. Dotto, Guilherme Luiz II.
Lima, Éder Cláudio III. Título.

Sistema de geração automática de ficha catalográfica da UFSM. Dados fornecidos pelo autor(a). Sob supervisão da Direção da Divisão de Processos Técnicos da Biblioteca Central. Bibliotecária responsável Paula Schoenfeldt Patta CRB 10/1728.

Declaro, VICTORIA XIMENES NASCIMENTO, para os devidos fins e sob as penas da lei, que a pesquisa constante neste trabalho de conclusão de curso (Dissertação) foi por mim elaborada e que as informações necessárias objeto de consulta em literatura e outras fontes estão devidamente referenciadas. Declaro, ainda, que este trabalho ou parte dele não foi apresentado anteriormente para obtenção de qualquer outro grau acadêmico, estando ciente de que a inveracidade da presente declaração poderá resultar na anulação da titulação pela Universidade, entre outras consequências legais.

Victoria Ximenes Nascimento

**PREPARAÇÃO E CARACTERIZAÇÃO DE CARVÃO ATIVADO MAGNÉTICO
OBTIDO A PARTIR DA SERRAGEM DE MADEIRA SAPELLI (*Entandrophragma cylindricum*) PARA ADSORÇÃO DO CORANTE AZUL BRILHANTE.**

Dissertação apresentada ao Curso de mestrado do Programa de Pós-Graduação em Engenharia Química, da Universidade Federal de Santa Maria (UFSM, RS), como requisito parcial para obtenção do título de **Mestre em Engenharia Química**.

Aprovada em 10 de Março de 2023:

Guilherme Luiz Dotto, Dr (UFSM)
(videoconferencia)

Éder Cláudio Lima, Dr (UFRGS)
(videoconferencia)

Maria Amélia Zazycki, Dra (UFN)
(videoconferencia)

Jivago Schumacher de Oliveira, Dr (UFN)
(videoconferencia)

Santa Maria, RS
2023

AGRADECIMENTOS

A Deus agradeço pela vida, por me abençoar, iluminar e guiar meu caminho.

Aos meus pais, Maria Nilda Ximenes e Antônio Carlos Nascimento, pelo amor e carinho, e pelo incentivo a educação. Obrigada por estarem ao meu lado sem vocês nada seria possível.

Ao meu marido Leonardo Teixeira, por todo amor e compreensão, por estar ao meu lado nos dias bons e ruins, por ser meu porto seguro, por me incentivar e cuidar de mim.

Aos meus sogros, por todo amor, afeto, cuidado e suporte.

À Sabrina Lutke, por todas as horas compartilhadas no laboratório e na pesquisa, por sua dedicação, paciência e ensinamentos, você foi essencial nessa trajetória. Obrigada por tanto! Te admiro e torço pelo seu sucesso.

À Maria Caroline Ferreira por ser minha parceira nessa jornada, nos momentos de angustia e nos momentos de vitória, obrigada por toda ajuda e carinho amiga. Agradeço a sua família por ter me acolhido e me dado suporte. Obrigada Leiza e Zoilo.

Ao meu orientador, professor Dr. Guilherme Dotto, pela confiança e orientação. Sou grata pela oportunidade de fazer parte do grupo ENGEPAC.

Ao meu coorientador, professor Dr. Éder Lima, por todo auxílio e dedicação.

A todos os meus amigos e familiares, que de alguma forma torceram para que este momento chegasse. Agradeço a amizade e o carinho e por vibrarem comigo a cada conquista, pelo apoio e pelas palavras de incentivo.

À Universidade Federal de Santa Maria e ao Programa de Pós-Graduação em Engenharia Química muito obrigada pela oportunidade e por terem me recebido de braços abertos.

Ao Secretário Marcos, obrigada por toda atenção e dedicação ao seu trabalho, por sempre solucionar minhas dúvidas e estar disposto ajudar.

Agradeço aos demais professores, funcionários e colegas do PPGEQ.

À CAPES pelo apoio financeiro.

RESUMO

PREPARAÇÃO E CARACTERIZAÇÃO DE CARVÃO ATIVADO MAGNÉTICO OBTIDO A PARTIR DA SERRAGEM DE MADEIRA SAPELLI (*Entandrophragma cylindricum*) PARA ADSORÇÃO DO CORANTE AZUL BRILHANTE

AUTORA: Victoria Ximenes Nascimento

ORIENTADOR: Guilherme Luiz Dotto

COORIENTADOR: Éder Lima

A contaminação dos corpos d'água por corantes tem sido um problema a ser combatido devido às grandes quantidades de efluentes lançados nos corpos hídricos serem prejudiciais ao meio ambiente e aos seres vivos. Desse modo é preciso desenvolver e aprimorar tecnologias que promovam o tratamento eficiente de efluentes. Neste contexto, no presente estudo, dois carvões ativados magnéticos foram preparados a partir da serragem da madeira Sapelli, usando pirólise de etapa única com KOH e NiCl₂ como agentes de ativação e magnetização. Na preparação a proporção de biomassa, KOH e NiCl₂ foi de 1:1:0,5 e 1:1:1 sendo assim os carvões foram denominados CAM1105 e CAM111, respectivamente, de acordo com a porporção utilizada. Os carvões foram caracterizados e aplicados como adsorventes para remoção do corante azul brilhante. A caracterização foi realizada usando diferentes técnicas como MEV/EDS, FTIR, BET, TGA, DRX, VSM e pH_{PCZ}. De acordo com a caracterização obteve-se materiais mesoporosos com propriedades ferromagnéticas e a presença de partículas nanoestruturadas de Ni. Os CAMs, apresentaram potencial para serem reutilizados em 4 ciclos de adsorçãoe apresentaram alta eficácia (até 90% de remoção) no tratamento de um efluente simulado. O CAM111 apresentou, maior área superficial (331,543 m² g⁻¹), cinética mais rápida (em torno de 10 min) e maior capacidade de adsorção. A capacidade de adsorção foi em torno de 40 mg g⁻¹ para CAM1105 e 96 mg g⁻¹ para CAM111. Dessa forma, o CAM111 foi selecionado, e experimentos de adsorção foram realizados do ponto de vista cinético, de equilíbrio e termodinâmico. Nos experimentos de adsorção, a dosagem de adsorvente foi 0,75 g L⁻¹ e o pH da solução foi 4,0. Além disso, os dados cinéticos e de equilíbrio foram adequadamente representados pelos modelos de pseudo-segunda ordem (PSO) e Sips, respectivamente. A capacidade máxima de adsorção foi de 111,50 mg g⁻¹ a 55 °C. O estudo termodinâmico revelou que a adsorção foi um processo espontâneo, favorável e endotérmico. Além disso, a elucidação mecanística sugeriu que interações eletrostáticas, pontes de hidrogênio, interações π–π e n–π estavam envolvidas na adsorção do corante azul brilhante no CAM 111.

Palavras-chaves: Adsorção; Adsorvente magnético; Corante aniônico; Pirólise de etapa única.

ABSTRACT

PREPARATION AND CHARACTERIZATION OF MAGNETIC ACTIVATED CARBON OBTAINED FROM SAPELLI WOOD SAWDUST (*Entandrophragma cylindricum*) FOR ADSORPTION OF BRILLIANT BLUE DYE

AUTHOR: Victoria Ximenes Nascimento

ADVISOR: Guilherme Luiz Dotto

CO-ADVISOR: Éder Lima

The contamination of water bodies by dyes has been a problem to be fought because the large amounts of effluents released into water bodies are harmful to the environment and living beings. Thus, it is necessary to develop and improve technologies that promote the efficient treatment of effluents. In this context, in the present study, two magnetic activated carbons were prepared from Sapelli wood sawdust, using single-step pyrolysis with KOH and NiCl₂ as activation and magnetization agents. In the preparation, the proportion of biomass, KOH and NiCl₂ was 1:1:0.5 and 1:1:1, therefore, the carbons were named MAC1105 and MAC111, respectively, according to the proportion used. The coals were characterized and applied as adsorbents to remove the brilliant blue dye. The characterization was performed using different techniques such as MEV/EDS, FTIR, BET, TGA, XRD, VSM and pHPCZ. According to the characterization, mesoporous materials with ferromagnetic properties and the presence of nanostructured Ni particles were obtained. The MACs showed the potential to be reused in 4 cycles of adsorption and showed high efficiency (up to 90% removal) in the treatment of a simulated effluent. CAM111 showed a higher surface area (331.543 m² g⁻¹), faster kinetics (around 10 min) and a higher adsorption capacity. The adsorption capacity was around 40 mg g⁻¹ for MAC1105 and 96 mg g⁻¹ for MAC111. Thus, MAC111 was selected, and adsorption experiments were carried out from the kinetic, equilibrium and thermodynamic points of view. In the adsorption experiments, the adsorbent dosage was 0.75 g L⁻¹ and the pH of the solution was 4.0. Furthermore, kinetic and equilibrium data were adequately represented by pseudo-second order (PSO) and Sips models, respectively. The maximum adsorption capacity was 111.50 mg g⁻¹ at 55 °C. The thermodynamic study revealed that the adsorption was a spontaneous, favorable and endothermic process. Furthermore, mechanistic elucidation suggested that electrostatic interactions, hydrogen bonding, π–π and n–π interactions were involved in the adsorption of brilliant blue dye on MAC 111.

Keywords: Adsorption; Anionic dye; Magnetic adsorbent; Single-step pyrolysis.

LISTA DE FIGURAS

REFERENCIAL BIBLIOGRÁFICO

- Figura 1- Tipos de classificações dos corantes
Figura 2 - Estrutura molecular do corante azul brilhante
Figura 3 – Técnicas de tratamento de águas residuais com corantes
Figura 4 - Processo de adsorção
Figura 5 – Comportamento típico das isotermas de adsorção
Figura 6- Classificação das isotermas de adsorção
Figura 7- Tipos de adsorventes usados para remoção de corantes

ARTIGO 1

- Fig. 1.** SEM images of (a) MAC1105 and (b) MAC111 and EDS spectra of (c) MAC1105 and (d) MAC111.
Fig. 2. FTIR vibrational spectra of (a) MAC1105 and (b) MAC111.
Fig. 3. Nitrogen adsorption/desorption isotherms and the BJH pore size distribution of (a) MAC1105 and (b) MAC111.
Fig. 4. TGA curves of (a) MAC1105 and (b) MAC111.
Fig. 5. XRD patterns of MAC1105 and MAC111.
Fig. 6. M-H hysteresis loops of MAC1105 and MAC111 at room temperature. The inset is a magnified view of the M-H curves.
Fig. 7. The kinetic curve of BB dye adsorption onto (a) MAC1105 and (b) MAC111.
Fig. 8. Equilibrium isotherms of BB blue dye adsorption onto (a) MAC1105 and (b) MAC111.
Fig. 9. Reuse cycles of (a) MAC1105 and (b) MAC111.
Fig. 10. Absorption spectra of simulated effluent before and after adsorption with 1 g L^{-1} : (a) MAC1105 and (b) MAC111; 5 g L^{-1} : (c) MAC1105 and (d) MAC111; 10 g L^{-1} : (e) MAC1105 and (d) MAC111.
Fig. 1S. Chemical structure of the brilliant blue dye.

ARTIGO 2

- Fig. 1** (a) SEM image and (b) EDS spectrum of SWSMAC.
Fig. 2 (a) Nitrogen adsorption/desorption isotherms and (b) BJH pore size distribution of SWSMAC.

Fig. 3 XRD pattern of SWSMAC.

Fig. 4 M-H hysteresis loop of SWSMAC at room temperature. The inset is a magnified view of the M-H curve.

Fig. 5 FTIR vibrational spectra of SWSMAC (a) before and (b) after the brilliant blue FCF dye adsorption.

Fig. 6 Determination of the pH_{PZC} of SWSMAC.

Fig. 7 Effect of SWSMAC dosage in the brilliant blue FCF dye adsorption.

Fig. 8 Effect of the pH of the solution in the brilliant blue FCF dye adsorption.

Fig. 9 Kinetic curve of the brilliant blue FCF dye adsorption onto SWSMAC.

Fig. 10 Equilibrium isotherms of the brilliant blue FCF dye adsorption onto SWSMAC.

Fig. 11 Proposed adsorption interactions of the brilliant blue FCF dye onto SWSMAC.

Fig. S1 Fitting of Van't Hoff equation for the calculation of the adsorption thermodynamic parameters.

LISTA DE TABELAS

REFERENCIAL BIBLIOGRÁFICO

Tabela 1- Principais diferenças entre adsorção física e química

Tabela 2- Adsorventes desenvolvidos a partir de resíduos agrícolas na remoção de corantes.

ARTIGO 1

Table 1. Textural characteristics of the magnetic activated carbons.

Table 2. Magnetic properties of the magnetic activated carbons.

Table 3. Kinetic parameters for the adsorption of BB dye.

Table 4. Equilibrium parameters for the adsorption of BB dyes.

Table 5. Adsorption capacities of different adsorbents for BB dye adsorption.

Table 6. Regeneration test using different regeneration agents in different concentrations.

ARTIGO 2

Table 1. Kinetic parameters of the brilliant blue FCF dye adsorption

Table 2. Equilibrium parameters of the brilliant blue FCF dye adsorption.

Table 3. Thermodynamic parameters of the brilliant blue FCF dye adsorption

SUMÁRIO

1.	INTRODUÇÃO	13
2.	OBJETIVOS	15
2.1.	OBJETIVO GERAL	15
2.2.	OBJETIVOS ESPECÍFICOS	15
3.	REFERENCIAL BIBLIOGRÁFICO.....	16
3.1	POLUIÇÃO DOS RECURSOS HÍDRICOS	16
3.2.	CORANTES	17
3.2.1.	Classificação e propriedades.....	18
3.2.2.	Corante Azul Brilhante	19
3.2.3.	Toxicidade dos corantes sintéticos.....	20
3.2.4.	Formas de Tratamento de águas residuais com corantes	21
3.3.	ADSORÇÃO	23
3.3.1.	Fatores que afetam a adsorção	24
3.3.1.1.	Área superficial	25
3.3.1.2.	Temperatura	25
3.3.1.3.	pH e Ponto de Carga Zero	26
3.3.1.4	Dosagem do Adsorvente.....	26
3.3.1.5.	Efeito da Concentração Inicial do Adsorbato	27
3.3.1.6.	Tempo de Contato	28
3.3.2.	Cinética de adsorção.....	28
3.3.2.1.	Modelo pseudo primeira ordem	28
3.3.2.2.	Modelo pseudo segunda ordem	29
3.3.3.	Equilíbrio de adsorção	30
3.3.3.1.	Isoterma de Langmuir.....	31
3.3.3.2.	Isoterma de Freundlich.....	32
3.3.3.3.	Isoterma de Sips	32

3.3.4. Termodinâmica de adsorção	33
3.4. ADSORVENTES	34
3.4.1. Carvão Ativado.....	35
3.4.1.1. Serragem como material precursor na preparação de carvões ativados.....	36
3.4.1.2. Carvões ativados magnéticos	37
3.4.1.3. Preparação carvão ativado.....	39
4. RESULTADOS E DISCUSSÕES	41
4.1. ARTIGO 1 - Adsorptive features of magnetic activated carbons prepared by a one-step process towards brilliant blue dye.....	42
4.2. ARTIGO 2 – Brilliant blue FCF dye adsorption using magnetic activated carbon from Sapelli wood sawdust	79
5. DISCUSSÕES.....	122
6. CONCLUSÃO GERAL.....	124
7. REFERENCIAS	126

1. INTRODUÇÃO

O acelerado avanço industrial e tecnológico desenfreado tem sido uma ameaça à saúde e ao meio ambiente principalmente em relação a poluição das águas. O descarte inadequado de efluentes é um dos principais fatores de contaminação da água doce. Segundo a Agência Nacional das Águas – ANA (2018), apenas 2,5% da água do mundo é água doce e a maior parte é de difícil acesso. Ou seja, a água doce disponível para o consumo humano representa uma parcela muito pequena, o que torna seu gerenciamento adequado indispensável para que essa parcela de água doce possa estar disponível em quantidade e qualidade adequada para atender as necessidades dos seres vivos.

Diversos estudos têm sido realizados no campo de tratamento de efluentes e remoção de poluentes das águas, como metais pesados, corantes, óleos, fármacos, entre outros. Os corantes por sua vez, quando lançados de forma inadequada no meio aquático podem ter efeitos nocivos tanto no ecossistema, quanto na saúde humana. Segundo Gupta et al (2012) mais de 700.000 toneladas de efluentes de corantes são gerados anualmente e cerca de 1.000 toneladas deles são descartados no sistema aquático. Além disso, os corantes possuem uma estrutura química complexa que dificulta sua degradação, assim as moléculas de corantes duram mais tempo no ambiente ampliando os riscos ambientais (HALEEM et al, 2023).

Implicações severas da presença de corantes na água foram relatadas, na vida aquática pode afetar a atividade fotossintética e a fonte de alimento dos organismos (CUSIOLI et al, 2019; PEREIRA et al, 2020). Na vida humana pode causar irritações da pele, doenças como o câncer, afetar o sistema nervoso e diversos órgãos como os rins e fígado, além de desenvolver hiperatividade em crianças (BHATTI et al, 2020; OMER et al, 2018; PATRA et al, 2021a; POTERA, 2010; WEKOYE et al, 2020).

Nos últimos anos, várias abordagens de tratamento foram amplamente desenvolvidas e testadas para minimizar esse cenário preocupante. Especificamente, a adsorção tem se mostrado uma técnica promissora para a remoção de contaminantes coloridos de águas residuais (TAHIR et al, 2016). A adsorção pode ser um processo vantajoso em relação a outras abordagens (coagulação, filtração, precipitação, troca iônica, osmose reversa, e processos oxidativos), principalmente por ser um método de projeto simples e de baixo custo, bem como eficaz para uma ampla gama de poluentes (CHIKRI et al, 2020; JAWAD et al, 2021). Atualmente, diversos estudos têm sido dedicados à preparação de materiais adsorventes para tratamento de águas residuais.

Materiais precursores naturais, resíduos agrícolas e industriais têm sido utilizados como adsorventes de baixo custo (GUPTA et al, 2022). A serragem por exemplo é um tipo de material precursor que está amplamente disponível de forma barata (MEEZ; RAHDAR; KYZAS, 2021). A estrutura da serragem juntamente com seus componentes a torna objeto de pesquisa quanto ao seu processo de adsorção (MEEZ; RAHDAR; KYZAS, 2021).

Ademais, pesquisas para melhorar as propriedades dos adsorventes têm sido investigada. Carvões ativados magnéticos tem se destacado, pois facilita a separação da fase sólida e da fase líquida sem a necessidade de centrifugação (VIEIRA et al, 2020). A magnetização de adsorventes permite a separação em soluções aquosas simplesmente usando um campo magnético externo (FEIQIANG et al, 2018; MOOSAVI et al, 2020), o que traz vantagens e resultados promissores no processo de tratamento de águas residuais.

Neste contexto, uma alternativa para o aproveitamento da serragem é a sua preparação e utilização como adsorvente, especialmente no tratamento de efluentes coloridos. Dessa forma, duas grandes questões ambientais podem ser solucionadas usando um carvão ativado proveniente de serragem na remoção de corantes em meio aquoso, são eles: a destinação correta de resíduos sólidos e o tratamento adequado de efluentes.

2. OBJETIVOS

2.1. OBJETIVO GERAL

O objetivo geral deste trabalho foi desenvolver carvões ativados magnéticos a partir de serragem de madeira sapelli (*Entandrophragma cylindricum*) e verificar seu potencial na remoção do corante azul brilhante em meio aquoso.

2.2. OBJETIVOS ESPECÍFICOS

- Desenvolver e caracterizar os carvões ativados magnéticos (CAMs) utilizando as técnicas:
 - Microscopia eletrônica de varredura (MEV);
 - Espectroscopia Dispersiva de Energia (EDS)
 - Análise da área superficial (BET/BJH)
 - Análise termogravimétrica (TGA)
 - Espectroscopia no infravermelho por transformada de Fourier (FTIR);
 - Difração de raio-X (DRX);
 - Magnetometria de Amostra Vibrante (VSM);
 - Ponto de carga zero (pHPCZ).
- Avaliar capacidade de regeneração;
- Analisar a capacidade de adsorção dos carvões em efluente simulado;
- Determinar o CAM com maior eficiência dentre os adsorventes testados;
- Determinar as condições ótimas na adsorção do CAM mais eficiente;
- Estudar a cinética de adsorção do corante azul brilhante no CAM;
- Estudar o equilíbrio de adsorção do corante azul brilhante no CAM;
- Avaliar a termodinâmica;
- Investigar o mecanismo de adsorção.

3. REFERENCIAL BIBLIOGRÁFICO

3.1. POLUIÇÃO DOS RECURSOS HÍDRICOS

Nas últimas décadas, a poluição dos recursos hídricos por contaminantes emergentes tem sido considerada uma preocupação global, devido aos diversos impactos negativos causados à saúde humana e ao meio ambiente (BELUCI et al, 2020; VIDOVIX et al, 2019). A classe de poluentes emergentes engloba um extenso grupo de substâncias sintéticas e naturais, incluindo fármacos, produtos de higiene pessoal, hormônios, esteroides, agroquímicos e corantes (QUESADA et al, 2019). O rápido progresso da industrialização nos últimos anos aumentou a descarga de poluentes no meio ambiente (DAS e DEY, 2020). Diversos contaminantes complexos de atividades domésticas e industriais são direta ou indiretamente lançados em corpos d'água (PATRA et al. 2021b).

No Brasil, apesar da abundância dos recursos hídricos (12% da água doce mundial), o acesso não chega na mesma qualidade e quantidade para todos. Segundo a Organização Mundial da Saúde - OMS (2008), 28 mil pessoas morrem por ano no Brasil de doenças provocadas por água contaminada ou de doenças relacionadas com a falta de higiene. Atividades humanas como, desmatamento, intensificação do uso de defensivos agrícolas e lançamento inadequado de efluentes, a falta de planejamento urbano, o desperdício e o constante desenvolvimento industrial, são alguns fatores que acabam por ocasionar mudanças e preocupações no que diz respeito à conservação da água potável. De acordo com alguns especialistas a crise da água no século XXI, é muito mais de gerenciamento do que uma crise real de escassez e estresse (ROGERS et al, 2005).

A disposição inadequada ou indireta de contaminantes, provenientes de diversas fontes pode ocasionar a incorporação em águas superficiais e subterrâneas. A OMS apresentou um relatório que diz que o tratamento de tingimento em várias indústrias desencadeou de 17% a 20% da poluição da água (KANT, 2011; ROY e SAHA, 2021). O procedimento de tingimento leva à liberação de 20% de corantes como descargas industriais, o que acaba contaminando as fontes de água potável (KANT, 2011). Os corantes são amplamente utilizados em diversos setores industriais, produzindo anualmente em todo o mundo um volume considerável de águas residuais coloridas, que podem causar diversos impactos nos corpos hídricos receptores (CUSIOLI et al, 2019). Quando estes efluentes são misturados com água limpa podem desequilibrar o nível recomendado de parâmetros orgânicos e inorgânicos em corpos d'água (JAVAID et al, 2019), impedindo os processos de autopurificação e degradação biológica devido à limitada transmitância da luz (COLLIVIGNARELLI et al,

2017). Dessa forma, no ecossistema aquático, a presença de uma quantidade mínima de corantes sintéticos na água pode afetar a transparência e a solubilidade gasosa dos corpos d'água, causando efeitos na atividade fotossintética e na fonte alimentar dos organismos (PEREIRA et al, 2020). Em humanos, pode causar disfunção renal e afetar o sistema reprodutivo, fígado, cérebro e sistema nervoso central (BHATTI et al, 2020; OMER et al, 2018; WEKOYE et al, 2020).

3.2. CORANTES

Os corantes são compostos aromáticos insaturados complexos que exibem boa cor, intensidade, solubilidade (NAVIA-MENDOZA et al, 2021) e absorvem radiação eletromagnética na faixa visível do espectro (~400 a 800 nm) (PEREIRA et al, 2020). Eles são compostos químicos orgânicos coloridos hidrossolúveis ou oleosos que geralmente são dissolvidos em água que podem se conectar a superfícies ou tecidos para dar cor. A maioria dos corantes são moléculas orgânicas complexas que são projetadas para se suportar uma ampla gama de efeitos externos (GUPTA et al, 2009; KANT, 2012; REHMAN et al, 2012). De modo geral, os corantes são geralmente grandes moléculas aromáticas, muitas vezes com uma estrutura de anel aromático ligada a uma cadeia lateral na estrutura da molécula do corante que é necessária para a ressonância e, portanto, para a transferência de cor (RÁPÓ e TONK, 2021).

Os corantes sintéticos são uma das classes mais importantes de compostos químicos utilizados em diversos campos de tecnologia avançada, por exemplo, eles são aplicados na produção de alimentos, têxteis, bioquímicos, fungicidas, ectoparasiticidas, farmacêuticos, indicadores colorimétricos e cosméticos, entre outros, ou seja, nota-se uma ampla gama de aplicação desses compostos em processos industriais (YAGUB et al, 2014; JANUÁRIO et al, 2021).

De acordo com o relatório da Allied Market Research (2019), o mercado global de corantes deverá atingir US\$ 15 bilhões até 2026. Atualmente, existem mais de 100.000 corantes comerciais disponíveis, estimando-se que sua produção mundial seja de 7×10^7 toneladas por ano (JUN et al, 2020). Consequentemente, cerca de 10-15% dos corantes geralmente chegam ao meio ambiente através de efluentes industriais sem tratamento prévio (ADEGOKE e BELLO, 2015), o que pode ameaçar o meio ambiente e a saúde humana (SHABBIR, 2017).

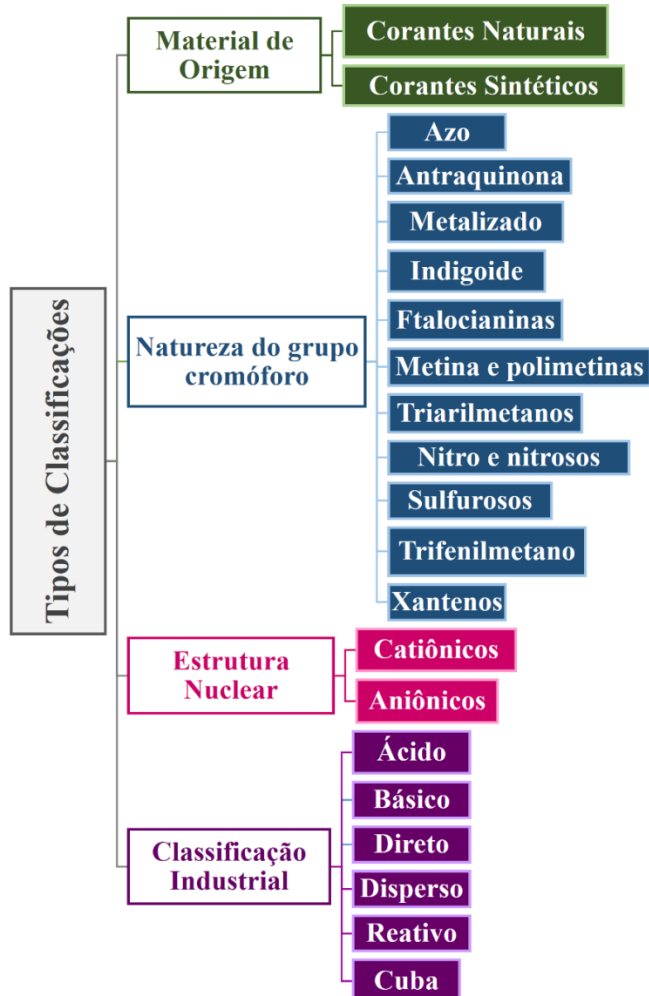
3.2.1. Classificação e propriedades

Existem várias maneiras de classificação de corantes comerciais, a literatura sobre a classificação dos corantes é complexa, devido ao fato que um mesmo corante poder possuir diferentes nomenclaturas (ZANONI e YAMANAKA, 2016). De modo geral, os corantes podem ser classificado em termos de estrutura, cor, método de aplicação (BENKHAYA et al, 2020; CLARKE e ANLIKER, 1980) ou com base em sua carga de partícula após a dissolução em meio de aplicação aquoso (PURKAIT et al, 2005; MISHRA e TRIPATHY, 1933), como catiônicos, aniônicos e não iônicos (YAGUB et al, 2014). No entanto, devido às complexidades da nomenclatura de cores do sistema de estrutura química, a classificação baseada na aplicação é muitas vezes favorável (GUPTA et al, 2009). Porém, segundo Hunger (2007) a maneira mais apropriada de classificar um corante é pela sua estrutura química, ou pelo seu grupo cromóforo, pois com essa classificação os corantes são rapidamente identificados por estarem agrupados em categorias que possuem características semelhantes e, desse modo, podem ser facilmente reconhecidos no setor têxtil (HUNGER, 2007).

Na literatura é comum encontrar os corantes têxteis sintéticos, classificado segundo sua estrutura química, sendo assim, as classes mais relevantes dos corantes têxteis são: Azo, antraquinona, metalizado, indigoide, ftalocianinas, metina e polimetinas (polienos e análogos), triarilmetanos, nitro e nitrosos e sulfurosos (ZANONI e YAMANAKA, 2016). Já os corantes alimentícios diferente das estruturas dos corantes alimentícios naturais e os corantes alimentícios sintéticos. Enquanto os naturais possuem estruturas muito diversificadas, os sintéticos possuem estrutura química semelhante aos usados na indústria têxtil, classificados quimicamente como, azo, indigoide, trifenilmetano e xantina (DAMODARAN; PARKIN, 2010; ZOLLINGER, 2003).

As principais classificações estão apresentadas na Figura 1, baseada no material de origem, estrutura química (natureza do cromóforo), estrutura nuclear e segundo a classificação industrial.

Figura 1- Tipos de classificações dos corantes.



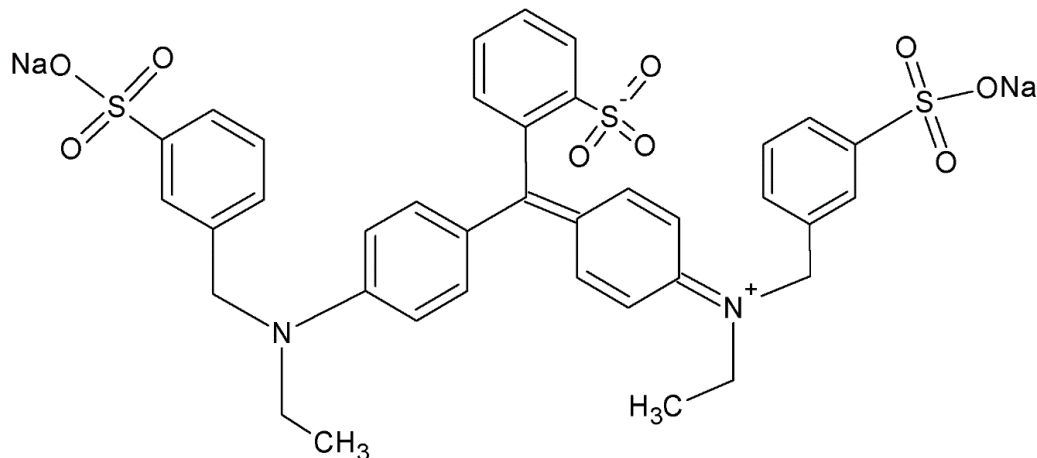
Fonte: (Autora, 2022).

3.2.2. Corante Azul Brilhante

O azul brilhante é um corante sintético amplamente encontrado na indústria alimentícia e têxtil sintetizado a partir de hidrocarbonetos aromáticos derivados do petróleo (MAIAN, 2022) e é descrito quimicamente pela fórmula $C_{27}H_{34}N_2Na_2O_9S_2$ representada na Figura 2. Sua absorção de luz máxima ocorre em 630 nm e sua molécula possui propriedades predominantemente aniônicas e grupos sulfonatos que o tornam altamente iônico e facilmente solúvel no meio aquoso (GERMAN-HEINS et al, 2000; WANG et al, 2019). O corante Azul brilhante encontra-se na classe dos corantes trifenilmetano (MAIAN, 2022; MISHRA e MAITI, 2018) e é encontrado em alimentos como, sucos, refrigerantes, balas, chicletes, xaropes, laticínios, entre outros. Além disso, é capaz de atribuir diversas tonalidades de azul

ao produto em produção, gerando um resultado atraente do ponto de vista visual, e pode ser combinado com diversos outros corantes, como o corante amarelo tartrazina, cuja combinação é capaz de gerar variados tons de verde (MAIAN, 2022).

Figura 2- Estrutura molecular do corante azul brilhante.



Fonte: (Dotto e Pinto, 2011, adaptado).

O corante Azul Brilhante foi banido na Alemanha, na Áustria, na França, na Bélgica, na Noruega, na Suécia e na Suíça por causar irritações cutâneas e constrição brônquica quando associado a outros corantes (ZANONI e YAMANAKA, 2016). O vermelho Bordeaux (composto por uma mistura de amaranto com azul brilhante) foi proibido nos Estados Unidos, na Áustria, na Noruega e na Rússia por causar crises asmáticas e eczemas. (ZANONI e YAMANAKA, 2016).

3.2.3. Toxicidade dos corantes sintéticos

A principal questão relacionada ao uso industrial de corantes é sua notável taxa de perda ao longo dos processos de fabricação. Por exemplo, a indústria têxtil perdeu cerca de 10 a 15% dos corantes sintéticos (PERIYASAMY e MILITKY, 2020). Ou seja, uma fração dos corantes utilizados na indústria passa a fazer parte dos efluentes industriais que, sem o tratamento adequado, quando lançados podem causar diversos impactos nos corpos hídricos receptores (CUSIOLI et al, 2019).

Considerando os corantes não biodegradáveis, os corantes quando não tratados podem conferir toxicidade à vida aquática e podem ser mutagênicos, carcinogênicos e teratogênico, podendo causar danos graves aos seres humanos (HOMEM et al, 2019; PAIXÃO et al, 2019;

PEREIRA, 2020). Devido ao seu alto potencial carcinogênico, mutagênico e teratogênico, a ingestão humana de água contaminada com corantes pode levar a disfunções do rim, sistema reprodutivo, fígado, cérebro e problemas no sistema nervoso central, (DINÇER et al, 2007; KADIRVELU et al, 2003; SHEN et al, 2009), principalmente pela presença de metais e substâncias aromáticas (PAIXÃO et al, 2019). Além disso, estudos indicam que o uso de corantes alimentícios sintéticos podem causar reações de hipersensibilidade e problemas comportamentais em crianças, como hiperatividade (POTERA, 2010).

No ecossistema aquático, a presença de uma quantidade mínima de corantes sintéticos na água (< 1 ppm) pode afetar a transparência e a solubilidade gasosa dos corpos d'água (PEREIRA et al, 2020) e o principal impacto está relacionado à redução da penetração solar, que afeta diretamente a atividade fotossintética e a fonte alimentar dos organismos. Dessa forma, proporciona redução na quantidade de oxigênio dissolvido, altera a cor e aumenta a demanda bioquímica de oxigênio da água, causando mortalidade de seres vivos (CUSIOLI et al, 2019; JANUÁRIO et al, 2020; PEREIRA et al, 2020). Segundo Gupta e Suhas (2009), os efluentes de corantes são considerados altamente tóxicos para a biota aquática e afetam o processo simbiótico ao perturbar o equilíbrio natural ao reduzir a atividade fotossintética e a produção primária devido à coloração da água. Além disso, diversos estudos confirmam que os corantes sintéticos podem exercer efeitos agudos e crônicos em organismos vivos, dependendo de sua concentração e extensão da exposição (PEREIRA et al, 2020).

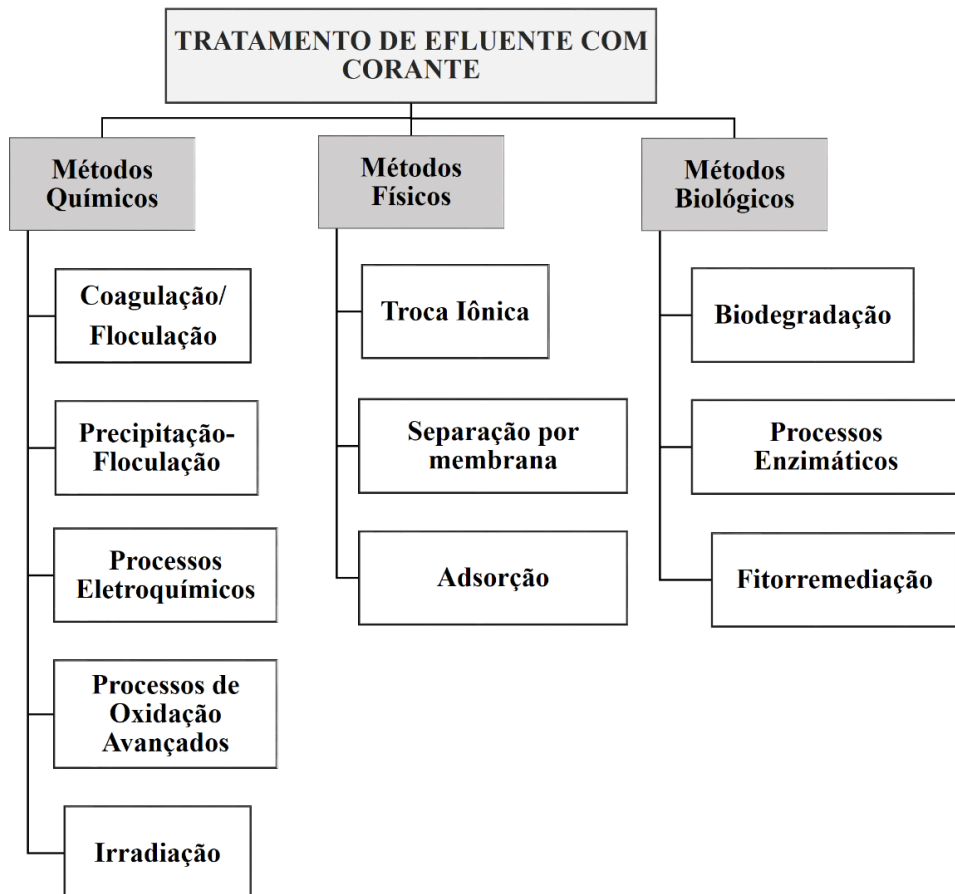
Sendo assim, nota-se a extrema relevância de garantir a remoção adequada desses contaminantes dos efluentes. O descarte de efluentes coloridos devem ser monitorados e devidamente removidos do meio ambiente (JANUÁRIO et al, 2020). A remoção de corantes de águas residuais é considerada um desafio ambiental e a legislação governamental exige que as águas residuais com corantes sejam tratadas, ou seja, há uma necessidade constante de ter processos de tratamento eficazes que possam remover esses corantes de forma eficiente no meio ambiente (LEE et al, 2006).

3.2.4. Formas de tratamento de águas residuais com corantes

Os poluentes industriais são um dos maiores problemas ambientais devido ao seu efeito nas águas subterrâneas e superficiais, juntamente com a saúde humana (SIVASUBRAMANIAM e FRANKS, 2016; ANAS et al, 2016; DE VIDALES et al, 2019). Diversas tecnologias, como processo de oxidação avançado, técnica de filtração por membrana, floculação/coagulação, tratamento biológico, degradação fotocatalítica, adsorção

entre outras técnicas são relatadas na literatura para o tratamento de águas residuais com corantes (ARUNPRASATH, et al, 2019; DOTTO et al, 2018; FOTEINIS et al, 2018; KHAKI et al, 2018; ORTIZ-MARTÍNEZ et al, 2021; YU et al, 2017). A Figura 3 apresenta algumas formas de tratamentos dos efluentes com corantes. De modo geral, todos os processos descritos na Figura 3 têm vantagens e desvantagens. As principais desvantagens são o altos custos operacionais, baixa eficiência, versatilidade limitada, manuseio complicado e poluição secundária (PEREIRA et al, 2020). Além disso, os corantes apresentam alta solubilidade em água e dificultam a remoção por procedimentos convencionais (HASSAN e CARR, 2018).

Figura 3 – Técnicas de tratamento de águas residuais com corantes.



Fonte: (Autora, 2022).

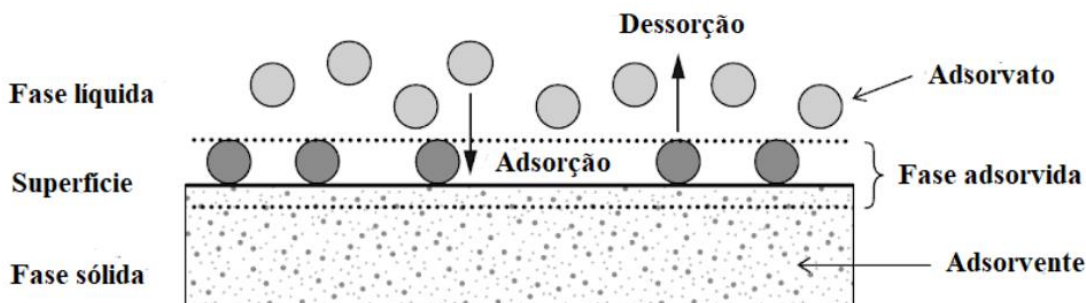
Atualmente na literatura, muitos pesquisadores consideram a adsorção como um método alternativo e econômico para remover corantes de águas e efluentes de maneira mais segura (ADEGOKE e BELLO, 2015; KATHERESAN et al, 2018). A adsorção é uma técnica que se destaca por apresentar diversos benefícios como baixo custo, operação simples, alta eficiência e possibilidade de regeneração dos adsorventes (SULTANA et al, 2022). As

características atrativas associadas à adsorção também motivaram (direta ou indiretamente) o desenvolvimento e aplicação de diferentes materiais adsorventes (PEREIRA et al, 2020).

3.3. ADSORÇÃO

A adsorção é um fenômeno físico-químico que se baseia na transferência de massa, em que certos sólidos têm a capacidade de concentrar em sua superfície determinadas espécies existentes em fluidos líquidos ou gasosos, possibilitando a separação dos componentes desses fluidos (SILVA, 2019; YAGUB et al, 2014). No processo de adsorção conforme ilustra a Figura 4, a substância que se acumula na interface é chamada de adsorbato e o sólido no qual ocorre a adsorção é adsorvente (RUTHVEN, 1984).

Figura 4 - Processo de adsorção.



Fonte: (RUTHVEN, 1984).

Considerando a natureza das ligações entre adsorvente e adsorbato, a adsorção pode ser classificada em dois tipos: adsorção química (quimiossorção) e adsorção física (fisiossorção) (NASCIMENTO et al, 2020). Na adsorção química a ligação envolve a troca ou partilha de elétrons entre as moléculas do adsorbato e a superfície do adsorvente, resultando em uma reação química (NASCIMENTO et al, 2020). Segundo Ruthven (1984), a quimiossorção normalmente apresenta características como, formação de uma única camada sobre a superfície sólida, irreversibilidade e liberação de uma quantidade considerável de energia. Por outro lado, na adsorção física, a ligação do adsorbato à superfície do adsorvente envolve uma interação relativamente fraca que pode ser atribuída às forças de Van der Waals, ligações de hidrogênio e dipolo-dipolo (NASCIMENTO et al, 2020; SILVA, 2019; ZAZYCKI, 2019). De acordo com Ruthven (1984) na fisiossorção, geralmente ocorre a deposição de mais de uma camada de adsorbato sobre a superfície do adsorvente. As

características gerais que diferenciam a adsorção física da química são apresentadas na Tabela 1.

Tabela 1– Principais diferenças entre adsorção física e química.

Adsorção Química	Adsorção Física
Possível em uma gama extensa de temperaturas.	Significante somente a temperaturas relativamente baixas.
Com transferência de elétrons	Sem transferência de elétrons
Especificidade alta	Especificidade baixa
Alto calor de adsorção	Baixo calor de adsorção
Pode ser lenta e irreversível	Rápida e reversível
Apenas em monocamada	Pode ocorrer em mono ou multicamadas
Difícil dessorção	Fácil dessorção

Fonte: (RUTHVEN, 1984, adaptado).

Diversos pesquisadores consideram a adsorção uma boa forma de tratamento de efluentes, dado que o processo possui vantagens significativas em comparação com os métodos convencionais, principalmente do ponto de vista econômico e ambiental (GUPTA e SUHAS, 2009; SALLEH et al, 2011). O processo de adsorção ganhou enorme atenção devido ao seu baixo custo, simplicidade de design, facilidade de operação e alta eficiência (JAWAD et al, 2020; KATHERESAN et al, 2018; SULTANA et al, 2022). Além disso, o potencial de reutilização do adsorvente e a recuperação do corante são aspectos adicionais relevantes associados ao processo de adsorção (PEREIRA et al, 2020).

3.3.1. Fatores que afetam a adsorção

A eficiência da adsorção da fase líquida e, portanto, a operação ideal do processo adsorção depende de vários parâmetros (RÁPÓ e TONK, 2021). Existem muitos fatores físico-químicos que afetam a adsorção, como a natureza do adsorvente (área superficial, tamanho do poro, densidade, grupos funcionais presentes na superfície e hidrofobidade do adsorvente), natureza do adsorbato (polaridade, tamanho da molécula, solubilidade) e condições operacionais (temperatura, pH e natureza do solvente) (COONEY, 1999; RAZI et al, 2017; SILVA, 2019). A otimização desses fatores é crucial para o desenvolvimento de um

bom processo de adsorção, dessa forma, os efeitos desses parâmetros devem ser levados em consideração (YAGUB et al, 2014).

3.3.1.1. Área superficial

A intensidade da adsorção é proporcional à área superficial específica, visto que a adsorção é um fenômeno de superfície. Para partículas maiores, a resistência à difusão é menor e grande parte da superfície interna da partícula não é disponibilizada para adsorção (SEKAR et al, 2004).

Os parâmetros texturais são relevantes para a adsorção de contaminantes de água com grandes tamanhos moleculares (por exemplo, corantes, produtos farmacêuticos, hidrocarbonetos com alto peso molecular). O tamanho molecular dos adsorbitos afeta a transferência de massa dentro dos mesoporos e microporos e, consequentemente, afeta a acessibilidade dos sítios de ligação disponíveis na estrutura interna do adsorvente. Ou seja, a quantidade adsorvida por unidade de massa de adsorvente é maior quanto mais finamente estiver dividido o adsorvente, e quanto mais poroso for o material (SILVA, 2005).

As propriedades adsortivas dependem na natureza sólida e do tamanho e distribuição do poro. Esses tamanhos podem ser classificados de acordo com a IUPAC em função do seu diâmetro (THOMMES et al, 2015):

- Macroporos: poros com diâmetros maiores que 50 nm;
- Mesoporos: poros com diâmetros entre 2 e 50 nm;
- Microporos: poros com diâmetros menores que 2 nm.

3.3.1.2. Temperatura

O efeito da temperatura é um fator físico-químico significativo, pois afeta o processo de tratamento, mudando a natureza da reação de endotérmica para exotérmica, ou vice-versa (YEOW et al, 2021). Podendo a temperatura alterar diretamente a capacidade de adsorção (ARGUN et al, 2008; BADAWY et al, 2020). Se a capacidade de adsorção aumenta com o aumento da temperatura, então a adsorção é um processo endotérmico (YAGUB et al, 2014). Na adsorção de corantes, isso pode ser devido ao aumento da mobilidade das moléculas do corante e ao aumento do número de sítios ativos para a adsorção com o aumento da temperatura. Já a diminuição da capacidade de adsorção com o aumento da temperatura indica

que a adsorção é um processo exotérmico (YAGUB et al, 2014). Isso pode ser devido ao aumento da temperatura diminuir as forças de adsorção entre as espécies de corantes e os sítios ativos na superfície adsorvente como resultado da diminuição da quantidade de adsorção (SALLEH et al, 2011).

Em processos de adsorção, o efeito da temperatura sobre o sistema afeta, principalmente, a constante de velocidade de adsorção. Um aumento na temperatura pode ocasionar aumento de energia cinética e na mobilidade das espécies do adsorbato, e ainda provocar um aumento na taxa de difusão intrapartícula do adsorbato (JIMENEZ et al, 2004). Além disso, um aumento na temperatura pode também danificar a estrutura física do adsorvente (RÁPÓ e TONK, 2021). De modo geral, a temperatura pode afetar a eficiência da adsorção de forma diferente dependendo do adsorvente e do poluente (RÁPÓ e TONK, 2021).

3.3.1.3. pH e ponto de carga zero

Um dos fatores mais importantes que afetam a capacidade do adsorvente e a eficiência do processo de adsorção é o pH da solução (YAGUB et al, 2014). O pH afeta a química da solução de contaminantes, alterando a atividade de grupos funcionais no adsorvente, o grau de ionização do íon adsorvido e a carga superficial do adsorvente (KHASRI et al, 2021). Ou seja, a eficiência da adsorção depende do pH da solução, uma vez que a variação do pH leva à variação do grau de ionização da molécula adsorvente e das propriedades de superfície do adsorvente (NANDI et al, 2009). Em relação a adsorção de corantes, não apenas o adsorvente, mas também a estrutura química do corante pode ser alterada pelo pH da solução (RÁPÓ e TONK, 2021). Um índice usado para quantificar ou definir a capacidade de uma superfície se tornar positiva ou negativamente carregada em função do pH é chamado ponto de carga zero (pH_{PZC}). A partir do pH da solução é possível determinar o ponto de carga zero e então, a carga superficial de um adsorvente. Para valores de pH inferiores ao ponto de carga zero ($pH < pH_{PZC}$) a carga superficial do adsorvente é positiva e a adsorção de ânions é favorecida; e para valores de pH superiores ao ponto de carga zero ($pH > pH_{PZC}$) a carga superficial é negativa e a adsorção de cátions é favorecida (THUE et al, 2020).

3.3.1.4. Dosagem do adsorvente

A quantidade de adsorvente utilizado em um processo de adsorção é um parâmetro importante, que influencia o processo através da relação quantitativa da dosagem do

adsorvente e a capacidade de remoção do adsorvente para uma dada concentração inicial do poluente (ŞENTÜRK e ALZEIN, 2020; RAPÓ e TONK, 2021). Em relação a adsorção de corantes, a porcentagem de remoção do corante aumenta com o aumento da dosagem do adsorvente, onde o número de sítios de sorção na superfície do adsorvente aumentará com o aumento da dosagem, e como resultado, aumentará a porcentagem de remoção do corante (OFOMAJA, 2008; SALLEH et al, 2011). Dessa forma, o aumento da dose de adsorvente está positivamente correlacionado com a eficiência e desempenho da remoção de corante em um processo de adsorção (RAPÓ e TONK, 2021). Entretanto, do ponto de vista econômico, é importante que a pesquisa do efeito da dosagem do adsorvente e da capacidade de remoção de um contaminante como o corante, seja realizado (SALLEH et al, 2011), visto que, uma boa remoção aliada a um mínimo de dosagem de adsorvente, representa custo, ou seja, quanto menor a dosagem necessária menor o custo do processo.

Sendo assim, um desafio na área de adsorção é o emprego de um material de baixo custo, com baixa dosagem e grande capacidade de adsorção, e, idealmente, que possa ser recuperado por processos simples e reutilizado (NASCIMENTO et al, 2020; WORCH, 2012).

3.3.1.5. Efeito da concentração inicial do adsorbato

A capacidade de adsorção para remoção de um poluente é altamente dependente da sua concentração inicial, uma vez que, afeta indiretamente a eficiência da remoção do poluente no processo adsorção (YAGUB et al, 2014). A respeito da concentração inicial do corante, o efeito do fator de concentração inicial depende da relação imediata entre a concentração do corante e os sítios de ligação disponíveis em uma superfície adsorvente, podendo reduzir ou aumentar a disponibilidade de sítios de ligação na superfície (SALLEH et al, 2011; RAPÓ e TONK, 2021).

De modo geral, a porcentagem de remoção do corante diminui com o aumento da concentração inicial do corante, o que pode ser devido à saturação dos sítios de adsorção na superfície adsorvente (EREN e ACAR, 2006; YAGUB et al, 2014). Em uma concentração baixa, haverá sítios ativos desocupados na superfície adsorvente, e quando a concentração inicial do corante aumenta, os sítios ativos necessários para a adsorção das moléculas do corante faltam (KANNAN e SUNDARAM, 2001). Além disso, o aumento na concentração inicial de corante pode causar um aumento na capacidade do adsorvente e isso pode ser devido à alta força motriz para a transferência de massa em uma alta concentração inicial de corante (BULUT e AYDIN, 2006).

3.3.1.6. Tempo de contato

O tempo de contato é um fator importante, visto que, indica o comportamento cinético da adsorção de um determinado adsorvente e adsorbato. O tempo de contato ou tempo de residência, é o tempo que envolve a transferência de massa de um ou mais componentes para o adsorvente, ou seja é o tempo necessário para atingir a concentração de remoção desejada de um poluente no processo de adsorção (NASCIMENTO et al, 2020). Um período rápido necessário para estabelecimento do equilíbrio no processo de adsorção de um poluente pode refletir a eficiência de um adsorvente. Estudos na literatura mostram que a adsorção é rápida nos estágios iniciais do período de contato e, posteriormente, mais lenta próxima ao equilíbrio. Este fato pode estar relacionado com a maior disponibilidade dos sítios de adsorção nos primeiros instantes e que nos momentos posteriores vão sendo ocupados pelas moléculas dos poluentes e com isso variando pouco a capacidade adsorção (KAVEESHWAR et al, 2018).

3.3.2. Cinética de adsorção

A cinética de adsorção descreve a taxa de remoção do adsorbato na fase fluida em relação ao tempo, sendo influenciada pelas características físicas e químicas do adsorvente e adsorbato, e das condições operacionais do processo em estudo. O estudo e os cálculos dos parâmetros cinéticos é fundamental em um processo de adsorção, visto que com isso, pode-se obter a velocidade de adsorção, o tempo necessário para remover os contaminantes, a quantidade adsorvida do adsorbato e o tempo de residência do adsorbato na interface sólido-líquido (HO e MCKAY, 1999).

Para análise e melhor compreensão sobre o comportamento cinético de um processo de adsorção, diversos modelos são relatados na literatura. As curvas experimentais são ajustadas de acordo com cada modelo, tais como, o modelo de pseudo primeira ordem (PPO), pseudo segunda ordem (PSO) e Elovich. Os modelos baseados em reações de adsorção, como as equações de PPO e PSO, são amplamente utilizados em estudos de adsorção relacionados ao tratamento de água (BONILLA-PETRICOLET et al, 2019).

3.3.2.1. Modelo pseudo primeira ordem

O modelo de PPO, foi proposto por Lagergren (1898). O modelo baseia-se na capacidade de adsorção, sendo amplamente utilizado em processos de adsorção em sistemas sólido/líquido e é representado pela Equação 1 (LAGERGREN, 1898). A equação do modelo, assume que a taxa de adsorção é diretamente proporcional ao número de sítios de adsorção livres, e ele baseando-se em interações reversíveis (SILVA, 2019).

$$q_t = q_i(1 - e^{-k_1 t}) \quad (1)$$

onde q_t é a quantidade adsorvida no tempo t (mg g^{-1}) e q_i é o valor teórico da capacidade de adsorção (mg g^{-1}); k_1 é a constante de velocidade de adsorção do modelo de PPO (min^{-1}) e t é o tempo (min).

3.3.2.2. Modelo pseudo segunda ordem

O modelo de PSO foi proposto por Ho e McKay (1999). O modelo considera que a taxa de adsorção é diretamente relacionada ao quadrado do número de sítios livres, dessa forma, a taxa de adsorção, segundo esse modelo é determinada de acordo com a Equação 2.

$$q_t = \frac{t}{(1/k_2 q_2^2) + (t/q_2)} \quad (2)$$

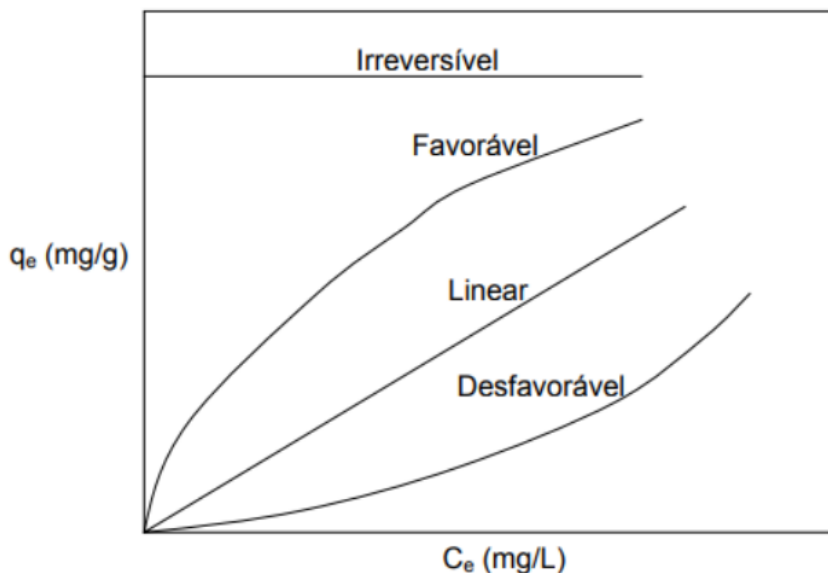
Onde q_2 é o valor teórico da capacidade de adsorção (mg g^{-1}), k_2 é a constante da taxa de adsorção do modelo PSO ($\text{g mg}^{-1} \text{ min}^{-1}$).

O modelo de PSO baseia-se na capacidade de adsorção do adsorvente e relata o comportamento do processo em toda a faixa de tempo de contato (ANDIA, 2009). Além disso, o modelo considera que a adsorção ocorre por natureza química e além de envolver apenas o processo de difusão como no modelo de PPO, também envolve o mecanismo de difusão interna (SKODRAS et al, 2008).

3.3.3. Equilíbrio de adsorção

O estudo das isotermas de equilíbrio é de fundamental importância para avaliar a eficiência de um adsorvente, como sua capacidade máxima de adsorção, por meio dos dados de equilíbrio, conhecidos como isotermas de adsorção. A partir das isotermas de adsorção é possível estabelecer uma relação de equilíbrio entre a concentração do adsorbato na fase fluida e a concentração do adsorbato na superfície do adsorvente em uma dada temperatura (PICCIN et al, 2017; SILVA, 2019). Elas fornecem informações sobre o mecanismo de adsorção e sua forma, e podem apresentar diferentes comportamentos típicos (NASCIMENTO et al, 2020), como mostrado na Figura 5.

Figura 5 – Comportamento típico das isotermas de adsorção

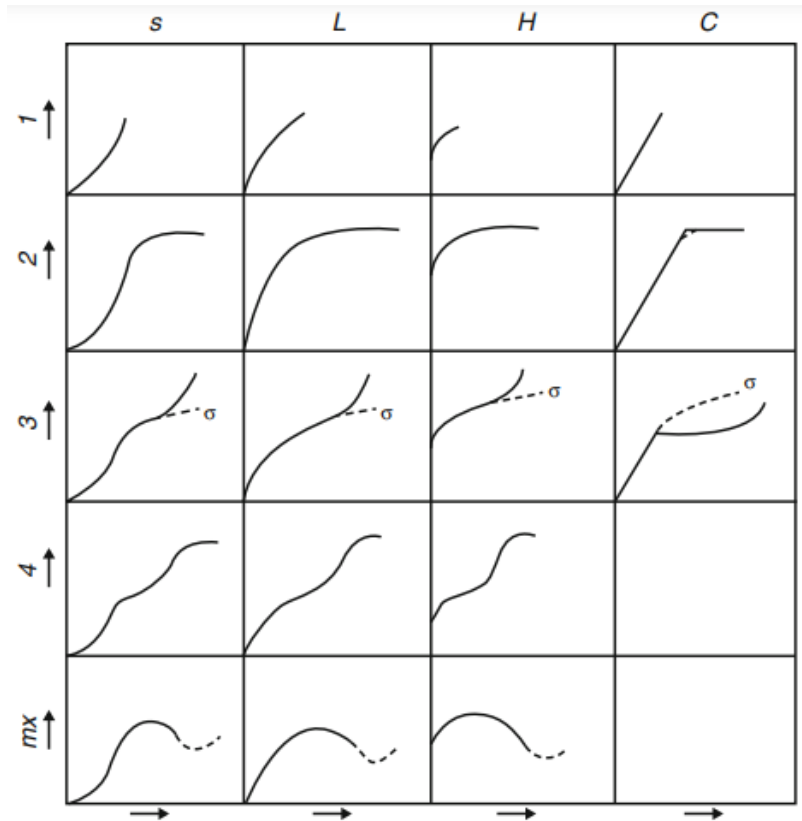


Fonte: (MCCABE et al, 2005).

As isotermas de adsorção são construídas a partir de dados experimentais e podem assumir variadas formas em um gráfico, onde relaciona a capacidade de adsorção (q_e) e a concentração final do adsorbato (C_e), medidas quando o sistema adsorvente atinge o equilíbrio. Dessa forma, a forma da curva de equilíbrio ajuda a explicar certos fenômenos associados à interação entre o adsorbato e o adsorvente (PICCIN et al, 2017).

Segundo Giles et al (1974) os tipos de isotermas podem ser divididas entre classes (S, L, H, C) e subclasses (1, 2, 3, 4), nesta classificação, as curvas de equilíbrio são identificadas de acordo com a inclinação inicial em quatro classes principais, e os subgrupos são descritos para cada classe, com base nas formas das partes superiores e mudanças de inclinação. A Figura 6 mostra a classificação proposta por Giles et al. (1974).

Figura 6- Classificação das isotermas de adsorção.



Fonte: (GILES et al. 1974).

Na literatura diversos modelos matemáticos de isotermas de adsorção foram propostos para ajustar e descrever os dados de equilíbrio de adsorção, como os modelos de Freundlich, Langmuir e Sips (NASCIMENTO et al, 2020).

3.3.3.1. Isoterma de Langmuir

O modelo de isoterma de Langmuir assume que a adsorção ocorre em uma monocamada, com superfície plana e com um número fixo de sítios ativos idênticos, e é representado pela Equação 3 (LANGMUIR, 1918).

$$q_e = \frac{q_m k_L C_e}{1 + k_L C_e} \quad (3)$$

Onde, q_e é a capacidade de adsorção no equilíbrio (mg g^{-1}), C_e é a concentração do adsorbato no equilíbrio (mg L^{-1}), q_m é a capacidade máxima de adsorção (mg g^{-1}) e k_L é a constante de Langmuir (L mg^{-1}) que expressa a afinidade entre o adsorvente e o adsorbato.

Dessa forma, o modelo de Langmuir assume que a distribuição dos grupos reativos sobre a superfície das partículas é homogênea e não há interação lateral entre as partículas, ou seja, cada sítio pode ser ocupado por apenas uma molécula e a energia de adsorção de cada sítio é igual, não havendo interações entre as moléculas adsorvidas em sítios vizinhos (RUTHVEN, 1984).

3.3.3.2. Isoterma de Freundlich

O modelo de Freundlich considera o sólido heterogêneo, ao passo que aplica uma distribuição exponencial para caracterizar os vários tipos de sítios de adsorção, os quais possuem diferentes energias adsorptivas, podendo ser representado pela Equação 4 (FREUNDLICH, 1906).

$$q_e = k_F C_e^{1/nF} \quad (4)$$

onde, k_F é a constante de Freundlich ($(\text{mg g}^{-1}) (\text{L mg}^{-1})^{1/n}$), $1/n$ é o fator de heterogeneidade.

Sendo assim, a isoterma de Freundlich assume que a adsorção ocorre em uma superfície, e a quantidade que é adsorvida aumenta infinitamente com o aumento da concentração (FREUNDLICH, 1906). Além disso, assume, que os sítios com ligação mais forte são ocupados primeiro e que a força de ligação diminui com o aumento do grau de ocupação do sítio, ou seja, prevendo a existência de multicamadas (COLPANI, 2012).

3.3.3.3. Isoterma de Sips

O modelo de isoterma de Sips é representado na Equação 5. O modelo representa uma combinação da isoterma de Langmuir e de Freundlich em que, em concentrações baixas, a adsorção reduz-se à isoterma de Freundlich e, em altas concentrações de adsorbato, prevê uma capacidade de adsorção em monocamada, característica da isoterma de Langmuir (SIPS, 1948).

$$q_e = \frac{q_s k_s C_e^{m_s}}{1 + k_s C_e^{m_s}} \quad (5)$$

onde, k_s é a constante de Sips (L mg^{-1}), q_s é a capacidade máxima de adsorção (mg g^{-1}) e m_s é a constante exponencial do modelo de Sips.

Desse modo, o modelo de isotermas de Sips foi desenvolvido para reconhecer e resolver o problema do aumento contínuo da quantidade adsorvida quando a concentração aumenta, o que geralmente é experimentado no modelo de isotermas de Freundlich (SIPS, 1948).

3.3.4. Termodinâmica de adsorção

Estimar os parâmetros termodinâmicos de adsorção é fundamental, visto que, fornece informações importantes sobre o processo de adsorção, como a influência da temperatura, características do processo e os mecanismos associados a adsorção (SCHIO, 2019; RÁPÓ e TONK, 2021).

Os parâmetros termodinâmicos de adsorção, são a variação da energia livre de Gibbs padrão (ΔG°), variação da entalpia padrão (ΔH°) e variação da entropia padrão (ΔS°). Os valores obtidos no cálculo desses parâmetros indicam a viabilidade do uso de qualquer material como adsorvente, pois revelam se o processo de adsorção é espontâneo, se seu caráter é endotérmico ou exotérmico e avalia o seu grau de desordem (SILVA, 2019; ZAZYCKI, 2019).

A energia livre de Gibbs padrão, pode ser calculada conforme a Equação 6, este parâmetro está relacionado com a espontaneidade do processo de adsorção. Se ΔG° for negativa, o processo é espontâneo e favorável, mas se ΔG° for positiva, o processo é desfavorável e não espontâneo (TRAN et al, 2021).

$$\Delta G^\circ = \Delta H^\circ - T\Delta S^\circ \quad (6)$$

A variação de entalpia indica se o processo de adsorção é exotérmico ou endotérmico. Valores negativos de ΔH° indica que o processo é exotérmico e valores positivos de ΔH° indica que o processo é endotérmico (TRAN et al, 2021). Além disso, a variação da entalpia está relacionada com a natureza do processo, indicando se a adsorção é física ou química

(TRAN et al, 2021). Já variação da entropia (ΔS°) mede o grau de desordem das partículas do sistema no processo (WANG et al, 2019). A variação da entalpia e entropia podem ser estimadas pela equação de Vant't Hoff (Equações 6, 7 e 8) (LIMA et al, 2019; TRAN et al, 2021; WANG et al, 2019).

$$\ln(K_D) = \frac{\Delta S^\circ}{R} - \frac{\Delta H^\circ}{RT} \quad (7)$$

$$K_D = \frac{(1000 \cdot K_s \cdot \text{molecular weight of adsorbato}) \cdot [\text{adsorbate}]^\circ}{\gamma} \quad (8)$$

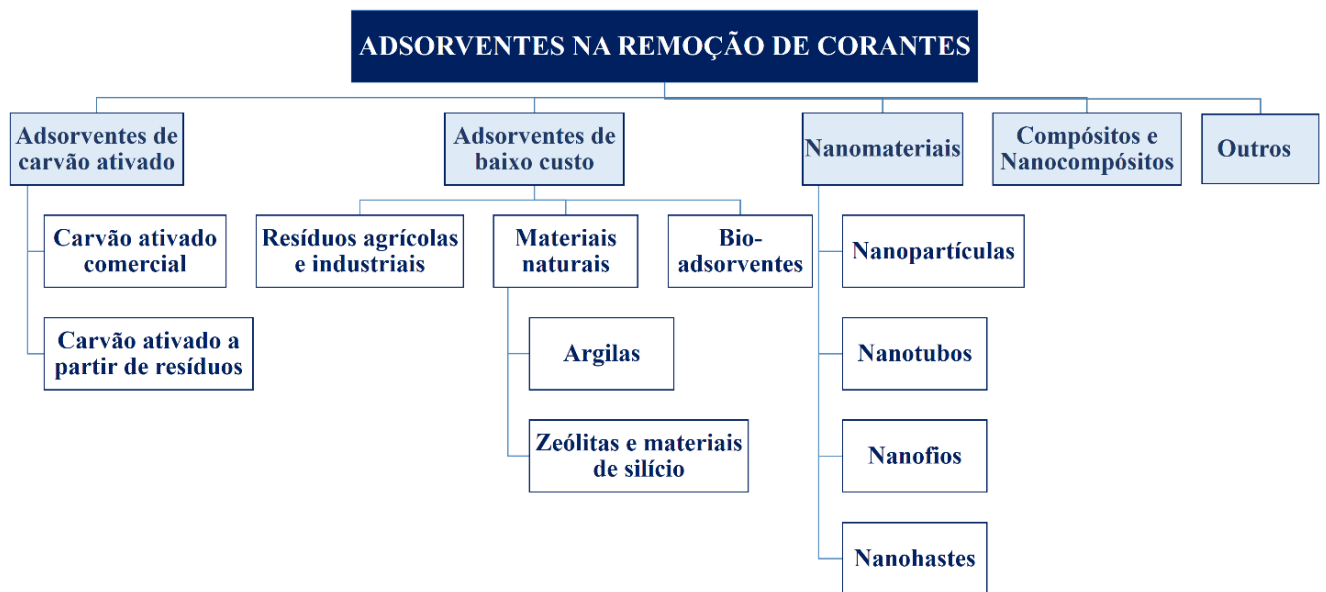
Onde, K_D é a constante de equilíbrio (adimensionalizada), R é a constante universal dos gases (8,314 kJ mol⁻¹ K⁻¹), T é a temperatura, K_s é constante do melhor modelo isotérmico ajustado e γ é o coeficiente de atividade.

A partir da Equação 7 é possível construir um gráfico $\ln K_D$ em função de $1/T$, com os dados experimentais da temperatura e da constante de equilíbrio (SILVA, 2019). Os valores de ΔH° e ΔS° são obtidos a partir da equação da reta do gráfico onde o coeficiente angular representa o valor de ΔH° e o coeficiente linear o valor de ΔS° (SILVA, 2005; SILVA, 2019).

3.4. ADSORVENTES

A eficiência de um processo de adsorção é diretamente dependente do adsorvente utilizado. Nos últimos anos, uma grande variedade de adsorventes com melhor custo-benefício e potencial foram desenvolvidos e estudados para remoção de uma gama de poluentes em meio aquoso, como os corantes. A Figura 7 ilustra os tipos de adsorventes estudados na remoção de corantes presentes na literatura (SINGH et al, 2018; ZHOU et al, 2019).

Figura 7- Tipos de adsorventes usados para remoção de corantes.



Fonte: (SINGH et al, 2018 adaptado).

3.4.1. Carvão ativado

O carvão ativado comercial é um dos adsorventes convencionais mais utilizado, visto que, apresenta alta eficiência no processo de adsorção (GUPTA e SUHAS, 2009). Entretanto, sua utilização acaba se tornando limitada por ser um material de alto custo, corrosivo e apresentar problemas na regeneração (YAGUB et al, 2014). Como ilustrado na Figura 7 diversas alternativas tem sido avaliadas além do carvão ativado comercial, a fim de combater as limitações de seu uso (SINGH et al, 2018).

Especificamente, a preparação de carvões ativados de baixo custo tem sido amplamente investigada para a remoção de corantes. De modo geral, o carvão ativado é um sólido carbonáceo que pode ser produzido a partir de qualquer material que contenha alto teor de carbono em sua composição (CHIKRI et al, 2020). Para desenvolver um adsorvente de baixo custo a partir de um determinado precursor, alguns fatores devem ser considerados, como por exemplo, o material precursor deve preferencialmente ser abundante, estar disponível gratuitamente ou de forma barata e não deve ser perigoso (CHIKRI et al, 2020; YAGUB et al, 2014). Potencialmente econômicos, os produtos residuais de operações industriais e agrícolas, materiais naturais e biossorventes tem sido alternativas promissoras (CHIKRI et al, 2020). Dentre os diversos materiais precursores possíveis para preparação de

um carvão ativado, destaca-se o uso de resíduos agrícolas como uma alternativa de baixo custo, tal como, casca de frutas, nozes, sementes, serragem, entre outros. A Tabela 2, apresenta estudos recentes de diferentes adsorventes desenvolvidos a partir de resíduos agrícolas para remoção de corantes.

Tabela 2- Adsorventes desenvolvidos a partir de resíduos agrícolas na remoção de corantes.

Material precursor	Corante	Referencia
Casca de coco	Azul de metileno	Yagmur e Kaya, 2021
Casca de romã	Azul de metileno	Jaward et al., 2021
Cascas de laranja e limão	Laranja de metila e azul de metileno Cristal violeta	Ramutshatsha-Makhwedzha et al., 2022 Homagai et Al., 2022
Casca de arroz	Violeta de Metila Verde de Malaquita	You et al., 2022
Casca de arroz e café	Índigo carmim	Paredes-Laverde et al., 2021
Casca da castanha de caju	Azul de Metileno Verde Brilhante Índigo Carmim	Thang et al., 2021 Samiyammal et al., 2022 Gupta et al., 2022
Serragem	Azul de metileno Azul Básico e Verde de Metileno	Yang e Cannon, 2022 Rahman et al., 2022

Fonte: Autora (2022).

3.4.1.1. Serragem como material precursor na preparação de carvões ativados

A serragem é subproduto abundante da indústria madeireira com preço baixo que pode ser utilizada como um material precursor sustentável para produção de carvão ativado (CHIKRI et al, 2020). A produção de carvão ativado a partir da serragem de madeira pode conferir vantagens no adsorvente, como alta porosidade, grande área superficial e baixo custo, além de ser favorável na adsorção de uma gama de poluentes, principalmente os corantes, visto que, contém numerosos grupos funcionais, como grupos carboxila, hidroxila, fenólica e amida em sua estrutura (ŠĆIBAN et al, 2007).

Nos últimos anos, os carvões ativados derivados da serragem têm sido investigados por muitos pesquisadores para a eliminação de vários tipos de corantes solúveis em água,

como azul de metileno, vermelho congo, violeta de metila, verde malaquita, azul brilhante, entre outros (CHIKRI et al, 2020). Yang e Cannon (2022) relaram uma alta capacidade de adsorção de 332 mg g^{-1} na remoção do corante azul de metileno. Garg et al (2003) usaram serragem tratada com formaldeído e ácido sulfúrico para adsorção do corante verde malaquita e mostraram que a serragem tratada com ácido foi mais eficiente atingindo cerca de 99% de remoção. Além disso, Benhabiles e Rida (2020) testaram a eficiência de carvões ativados preparados a partir de serragem e impregnados com NaOH e obtiveram eficiência superior a 94% na remoção dos corantes eritrosina e azul de metileno.

A madeira Sapelli (*Entandrophragma cylindricum*) usada como material percursor na preparação dos carvões ativados deste estudo, é comercialmente uma das mais importantes da África em termos de quantidades produzidas, bem como em termos de qualidade da madeira (KÉMEUZÉ, 2008). A madeira Sapelli é a segunda espécie mais explorada na África Central, principalmente em Congo e Camarões (BAYOL et al, 2012; RSR, 2018). A produção estimada da espécie é mais de 1 milhão de m^3 de toras por ano (RSR 2018). A madeira, geralmente comercializada como 'sapelli', 'sapele', 'abudikro' ou 'assié', é altamente valorizada para pisos, carpintaria de interiores, guarnição de interiores, painéis, escadas, móveis, marcenaria, instrumentos musicais, esculturas, construção naval, folheado e compensado (KÉMEUZÉ, 2008).

3.4.1.2. Carvões ativados magnéticos

Nos últimos anos a magnetização de carvões ativados tem sido proposta devido as suas excelentes propriedades físicas e químicas proporcionar uma forma de solução adequada para superar uma das principais desvantagens dos carvões ativados, sua difícil recuperação e separação no meio aquoso (MOOSAVI et al, 2020; ROCHA et al, 2020). Métodos tradicionais de separação como a filtração, podem causar o bloqueio dos filtros e perda do adsorvente (MOOSAVI et al, 2020). Além disso, a separação do adsorvente pode gerar uma poluição secundária (MOOSAVI et al, 2020). Neste contexto, a tecnologia de adsorção de partículas magnéticas mostra resultados promissores e eficazes para o tratamento de águas residuais devido à presença de um campo magnético externo facilitar a separação do adsorvente (FEIQIANG et al, 2018; MOOSAVI et al, 2020; ROCHA et al, 2020).

A separação dos adsorventes magnéticos obtida pela aplicação de um campo magnético externo (BADI et al, 2018) permite fácil isolamento, lavagem e redispersão, assim, evitando as etapas de filtração ou centrifugação (MOHAN et al, 2014; ROCHA et al, 2020).

Trabalhos investigando o uso de materiais precursores de baixo custo para a preparação de carvões ativados magnéticos na remoção de corantes são relatados na literatura (CHIKRI et al, 2020).

Diversos precursores metálicos podem ser utilizados na magnetização de carvões ativados, como compostos à base de ferro (Fe), níquel (Ni) e cobalto (Co) (ROCHA et al, 2020). Segundo Moosavi (2020) a introdução de carvão ativado magnético pode levar à remoção eficiente de corantes orgânicos. Entretanto, vale ressaltar que, o custo final de produção pode ser ligeiramente superior ao de carvões ativados não magnéticos (HAN et al, 2015).

Os carvões ativados magnéticos podem ser sintetizados utilizando diferentes processos que objetivam converter espécies de metais em partículas magnéticas, além de permitir que o material obtido exiba porosidade suficiente para ser utilizado em processos de adsorção (CAZETTA, 2014). Em geral, o adsorvente magnético é obtido pela impregnação de sais de metais de transição como $\text{FeSO}_4 \cdot \text{H}_2\text{O}$, $\text{FeCl}_3 \cdot \text{H}_2\text{O}$, $\text{Fe}(\text{NO}_3)_3 \cdot \text{H}_2\text{O}$ $\text{NiCl}_2 \cdot \text{H}_2\text{O}$, $\text{MnCl}_2 \cdot \text{H}_2\text{O}$, entre outros (DAMDIB et al, 2022). Dessa forma, tendo em vista a boa inoxidabilidade e ferromagnetismo (WANG et al, 2015) o cloreto de níquel (NiCl_2) foi utilizado neste trabalho para conferir características magnéticas aos materiais. O níquel metálico é um material ferromagnético, e tem chamado atenção ao fato das suas nanopartículas apresentarem propriedades magnéticas (CHEN e HSIEH, 2002).

A impregnação dos metais nos materiais porosos pode ser realizada com diferentes técnicas, diversos processos são descritos na literatura objetivando a obtenção de materiais carbonáceos magnéticos. Altintig et al (2017) avaliaram um carvão ativado magnético obtido da casca de bolota na remoção do corante azul de metileno em solução aquosa, a característica magnética foi adicionada ao carvão ativado pela ativação de ZnCl_2 , onde as cascas de bolota foram misturadas com ZnCl_2 com taxas de 1:3.

Feiqiang et al (2018) estudaram a adsorção de corante tóxico em carvões ativados magnéticos preparados por síntese modificada em uma etapa, a partir da casca de amendoim impregnando várias quantidades relativas de $\text{FeCl}_3 \cdot 6\text{H}_2\text{O}$.

Livani et al (2018) sintetizaram um carvão ativado a partir de cascas de avelã por ativação química com hidróxido de sódio a 600 °C em atmosfera de N_2 e depois combinado com nanopartículas magnéticas de NiFe_2O_4 por métodos hidrotérmicos e de coprecipitação.

Zhang et al (2020), preparam carvões ativados magnetizados ativando pó de palha de colza e pirolisando em diferentes temperaturas, e magnetizando pelo método hidrotérmico, para a aplicação na remoção de Pb(II) e Cd(II).

Jiang et al (2021) analisaram a adsorção do corante azul de metileno em meio aquoso usando um carvão ativado magnético preparado a partir do resíduo agrícola de bagaço de cana-de-açúcar e magnetizado com óxido de ferro, com uma proporção de massa de 1:1,5 por um método simples de micro-ondas.

Dentre os métodos citados, destaca-se o método de ativação e impregnação simultânea (em etapa única), pois é uma opção simples e rápida para o preparo de carvões ativados magnéticos quando comparadas a outras técnicas (DASTGHEIB et al., 2014).

3.4.1.3. Preparação carvão ativado

A produção de um carvão ativado é basicamente dividido em duas etapas principais: a carbonização/pirolise do material precursor e o processo de ativação (BORGES et al., 2003). A carbonização consiste de uma decomposição térmica do material carbonáceo, em atmosfera inerte a temperatura entre 400-800 °C, onde se removem componentes voláteis e gases leves como CO, H₂, CO₂, CH₄ (DI BERNARDO, 2005; SHARUDDIN, et al, 2016; YAHYA; AL-QODAH e NGAH, 2015), produzindo uma massa de carbono fixa com uma estrutura porosa rudimentar, com poros muito finos e fechados, assim, o produto carbonizado tem geralmente uma pequena capacidade de adsorção, ou seja, o carvão resultante tem uma área de superfície baixa e não é um produto ativo (YAHYA; AL-QODAH e NGAH, 2015). Segundo McDougall (1991), o objetivo da carbonização é reduzir o teor de voláteis do material precursor para converter o carvão resultante com maior teor de carbono fixo para fins de ativação.

O processo de ativação é uma etapa fundamental no preparo de carvões ativados, sua função principal é alterar as características do carvão para proporcionar melhores resultados através da formação de poros. O objetivo da ativação é basicamente desenvolver mais porosidade e criar algum ordenamento da estrutura que resulta em um sólido altamente poroso (GUO et al, 2009). Com a ativação do material carbonizado há a formação de mesoporos e macroporos (HERNÁNDEZ-MONTOYA, 2012) resultando em um maior número possível de distribuição de poros, variadas formas e tamanhos, dando origem a um produto com uma alta área superficial específica (BANSAL & GOYAL, 2005).

A ativação pode ser tanto física quanto química. Na ativação física as moléculas se ligam fracamente ao adsorvente, não alterando suas características físicas. O material é tratado termicamente em atmosfera levemente reativa como vapor de água e gás carbônico, ocorrendo simultaneamente a ativação e carbonização, onde são liberados umidade e

materiais indesejáveis como alcatrão monóxido e dióxido de carbono, hidrogênio e metano (GONÇALVES; NAKAMURA; VEIT, 2014).

Na ativação química, ocorre ligações de valências livres das moléculas do adsorvente no adsorbato. Nesse processo utiliza agentes ativantes, que atuam basicamente como agentes desidratantes e oxidantes (MAHAPATRAI; RAMTEKE; PALIWAL, 2012), como ácido fosfórico (H_3PO_4), cloreto de zinco ($ZnCl_2$), hidróxidos de metais alcalinos como o hidróxido de potássio (KOH) ou hidróxido de sódio (NaOH), ou ácido sulfúrico (H_2SO_4) (FOGLER, 1998; YORGUN e YILDIZ, 2015). Além disso, no estágio final no processo de ativação química ocorre a lavagem, onde o carvão ativado é lavado basicamente com ácido ou álcali, dependendo dos reagentes químicos utilizados na preparação, seguido de lavagem com água, para a eliminação da matéria inorgânica, afim de desenvolver a porosidade no carvão ativado (YAHYA; AL-QODAH e NGAH, 2015).

De modo geral, os processos de pirólise e ativação podem ser realizados tanto de forma conjunta como de forma separada. Na forma conjunta o precursor é misturado com agentes ativantes durante a pirólise. Neste caso, os ativadores químicos são usados em diferentes proporções, atuando de forma a desidratar, influenciando de forma direta a pirólise do precursor, evitando liberação de matéria orgânica volátil através da aromatização do esqueleto do carvão e maior fixação do carbono (TEIXEIRA, 2020). No caso da pirólise e ativação forem realizadas de forma separada, primeiramente é realizado a pirólise da amostra, e logo após é feita a impregnação com o agente ativante escolhido (GUO et al, 2009).

4. RESULTADOS E DISCUSSÕES

Os resultados obtidos neste estudo, juntamente com a discussão estão apresentados na forma de dois artigos científicos. O ARTIGO 1 está publicado na revista Molecules (ISSN: 1420-3049) com fator de impacto 4.927 classificada com Qualis A2 na área Engenharias II. O ARTIGO 2 está publicado na revista Environmental Science and Pollution Research (ISSN: 1614-7499) com fator de impacto 5.190 classificada com Qualis A2 na área Engenharias II.

**4.1. ARTIGO 1 - ADSORPTIVE FEATURES OF MAGNETIC ACTIVATED CARBONS
PREPARED BY A ONE-STEP PROCESS TOWARDS BRILLIANT BLUE DYE**

Victoria X. Nascimento¹, Carlos Schnorr², Sabrina F. Lütke¹, Maria C. F. da Silva¹, Fernando.
M. Machado³, Pascal S. Thue⁴, Éder C. Lima⁵, Julien Vieillard⁶, Luis F. O. Silva^{2*}, Guilherme
L. Dotto^{1,6**}

¹Research Group on Adsorptive and Catalytic Process Engineering (ENGEpac), Federal University of Santa Maria, Av. Roraima, 1000-7, 97105–900 Santa Maria, RS, Brazil.

²Universidad De La Costa, Calle 58 # 55-66, 080002 Barranquilla, Atlántico, Colombia.

³Technology Development Center, Federal University of Pelotas–UFPEL, Gomes Carneiro St., 96010-610, Pelotas, RS, Brazil.

⁴Environmental Science Graduate Program, Engineering Center, Federal University of Pelotas (UFPel), 989 Benjamin Constant St., 96010-020 Pelotas, RS, Brazil.

⁵Institute of Chemistry, Federal University of Rio Grande do Sul–UFRGS, Av. Bento Gonçalves 9500, P.O. Box 15003, 91501-970, Porto Alegre, RS, Brazil.

⁶Normandie Université, UNIROUEN, INSA Rouen, CNRS, COBRA (UMR 6014), 27000 Evreux, France.

* and **Corresponding authors: guilherme_dotto@yahoo.com.br; l Silva8@cuc.edu.co

Abstract

Water pollution by dyes has been a major environmental problem to be tackled, and magnetic adsorbents appear as promising alternatives to solve it. Herein, magnetic activated carbons were prepared by single-step method from Sapelli wood sawdust, properly characterized, and applied as adsorbents for brilliant blue dye removal. In particular, two magnetic activated carbons, MAC1105 and MAC111, were prepared using the proportion of biomass: KOH of 1:1 and varying the proportion of NiCl_2 of 0.5 and 1, respectively. The characterization results demonstrated that the different proportions of NiCl_2 mainly influenced the textural characteristics of the adsorbents. An increase in the surface area from 260.0 to $331.5 \text{ m}^2 \text{ g}^{-1}$ and in the total pore volume from 0.075 to $0.095 \text{ cm}^3 \text{ g}^{-1}$ was observed with the increase in the weight ratio of NiCl_2 . Both adsorbents exhibit ferromagnetic properties and the presence of nanostructured Ni particles. The different properties presented by the materials influenced the adsorption kinetics and equilibrium of brilliant blue dye. MAC111 showed faster kinetics, reaching the equilibrium in around 10 min, while for MAC1105 it took 60 minutes for the equilibrium to be reached. In addition, based on the Sips isotherm, the maximum adsorption capacity was 98.12 mg g^{-1} for MAC111, while for MAC1105 it was 60.73 mg g^{-1} . Furthermore, MAC111 presented the potential to be reused in more adsorption cycles than MAC1105, and the use of the adsorbents in the treatment of a simulated effluent exhibited high effectiveness, with removal efficiencies of up to 90%.

Keywords: Adsorption; Brilliant Blue; Kinetic; Sawdust; Simulated effluent

1. Introduction

The water crisis due to its pollution and scarcity has generated widespread concern worldwide. Several complex contaminants from industrial and domestic activities are indirectly or directly released into water bodies [1]. In this context, dyes are among the main organic contaminants [2]. These compounds are widely used in textile, leather, cosmetics, plastic, pharmaceutical, food processing, and various other industrial sectors [3]. Currently, there are more than 10,0000 commercial dyes available, and the estimated annual production of synthetic dyes is about 30,000 tons [2]. A large part of these dyes usually is discharged into water bodies through untreated wastewater, being a considerable source of pollution [4]. In general, dyes have a complex chemical construction which makes their degradation difficult and, consequently, they remain longer in the environment [2]. The presence of dyes in water bodies can affect the photosynthetic activity of aquatic life [5,6]. In addition, it can affect some conditions, such as the biological and chemical oxygen demands, dissolved oxygen concentration, and pH, as well as the life of aquatic animals and their predators [2]. Thus, the treatment of wastewater containing dyes is a very relevant issue.

Several technologies have been used to remove dyes from wastewater, such as advanced oxidation processes [7], flocculation/coagulation [8], biological treatments [9], ion-exchange [10], and adsorption [11]. Among these methods, adsorption is a promising technique for removing colored contaminants from wastewater [12,13]. Adsorption is promising since it has advantages such as applicability in different scenarios, ease of implementation, low space requirement, design simplicity, economic feasibility, and high efficiency [13,14].

In adsorption operations, activated carbon (AC) is widely used for removing inorganic and organic contaminants from aqueous solutions [15,16]. AC presents high surface area, pore volume, and abundant surface functional groups [17]. In parallel, the utilization of lignocellulosic wastes as precursor materials for AC production is a viable alternative due to

its low cost, availability, and ecological suitability [18-20]. In previous literature, several studies have been carried out on developing AC from different lignocellulosic wastes such as pecan nutshells [21], tangerine seed [22], banana peel [23], apple peel [24], pistachio wood wastes [25], and teak wood sawdust [26]. Specifically, sawdust, a lignocellulosic waste obtained from various woodworking operations is an accessible, abundant, and low-cost by-product, in addition to presenting disposal problems [27,28]. Thus, the conversion of sawdust into adsorbents is a good alternative for the management of this waste. In addition, the development of magnetic adsorbents has also been highlighted since it facilitates the separation of the solid from the liquid phase without requiring centrifugation [29-32]. Recently, different magnetic activated carbons (MAC) have been proposed to remove contaminants [33-37]. Generally, these magnetic activated carbons are prepared by co-precipitation, impregnation of the activated carbon, or impregnation of the precursor material followed by pyrolysis [37]. In the last procedure, carbonization, activation, and magnetization occur in a single step, an advantage from an economic and convenience perspective [38]. However, regardless of the preparation method, evaluating different experimental conditions to prepare AC is fundamental to finding a material with relevant features for adsorption [12].

Herein, MACs were produced from Sapelli wood sawdust, characterized, and applied in dye adsorption from an aqueous solution. The precursor was first impregnated with NiCl_2 and KOH and, then, the impregnated materials underwent pyrolysis. The effect of different weight ratios of NiCl_2 was investigated regarding their characteristics and performance on dye adsorption. Characterization was performed by scanning electron microscopy coupled with energy-dispersive X-ray spectroscopy (SEM/EDS), Fourier transform infrared spectroscopy (FTIR), N_2 adsorption/desorption isotherms, X-ray diffraction (XRD), thermogravimetric analysis (TGA/DTG), and vibrating sample magnetometer (VSM). Adsorption studies

involved kinetic and equilibrium experiments, regeneration/reuse tests, and tests with simulated industrial effluent.

2. Materials and methods

2.1. Materials

Sapelli wood sawdust (*E. cylindricum*), used as a precursor material for producing the magnetic activated carbons, was obtained from sawmills in Ngaoundere (Cameroon). The sawdust was milled, obtaining particle size lower than 250 µm. The anionic dye Brilliant Blue (BB, CI 42090, molar weight 792.8 g mol⁻¹, λ_{max} 630.0 nm) was supplied by Duas Rodas company (Brazil). Fig. 1S (supplementary material) shows the chemical structure of the BB dye obtained by the Chemsketch software. All other reagents used were of analytical grade.

2.2. Preparation of the magnetic activated carbons

In the MACs preparation, NiCl₂ produced magnetic features, and KOH was used as an activating agent to increase pore size and specific surface area. Initially, 100.0 g of the Sapelli wood sawdust was mixed with 100.0 g of KOH and 50.0 or 100.0 g of NiCl₂ (weight ratios of 1:1:0.5 and 1:1:1, respectively). Then, about 50 mL of distilled water were added to the mixtures, which were stirred with a magnetic stirrer at 90 °C for 2 h. The homogeneous pastes formed were subsequently oven-dried at 105 °C for 8 h and, after drying, each paste was introduced into a quartz reactor in a conventional furnace (Sanchis, Brazil). The heating was carried out from room temperature to 600 °C at a heating rate of 10 °C min⁻¹ and an inert gas (N₂) flow rate of 150 mL min⁻¹. After reaching the final temperature, it was maintained

for 30 min. Then, the furnace was turned off and kept under the inert gas flow until it reached a temperature below 200 °C. After cooling, the obtained materials were washed with a 0.1 mol L⁻¹ HCl solution under a reflux system at around 80 °C for 2 h. Subsequently, the materials were exhaustively washed with distilled water until the pH of the washing waters attains the pH of distilled water (pH 6–7). Finally, the materials were oven-dried at 105 °C for 8 h. The materials obtained were MAC1105 and MAC111, according to the weight ratios of Sapelli sawdust: KOH: NiCl₂ of 1:1:0.5 and 1:1:1, respectively.

2.3. MACs characterization

The textural properties (BET surface area, total pore volume, and average pore size) were obtained from N₂ adsorption/desorption isotherms at 77 K in a volumetric adsorption analyzer (Micromeritics, ASAP 2020, USA) using BET and BJH methods.

The surface morphologies of the materials were obtained by scanning electron microscopy (SEM) coupled with energy-dispersive X-ray spectroscopy (EDS) (Tescan, MIRA 3, Czech Republic). The working voltage was 12 kV and the magnifications were 5000× and 10000×.

Investigations concerning the surface functional groups were realized by Fourier transform infrared spectroscopy (FTIR) (Shimadzu, Prestige 21210045, Japan). The spectra were obtained with a resolution of 4 cm⁻¹ in the range from 4000 to 400 cm⁻¹ by diffuse reflectance technique with KBr.

Thermogravimetric (TGA) and derivative thermogravimetric (DTG) curves of the magnetic activated carbons were obtained in a TA instrument (Netzsch, STA 449 F3 Jupiter®, Germany). The analysis was carried out in the following conditions: temperature from 20 °C to 800 °C, a heating rate of 25 °C min⁻¹, and an N₂ flow rate of 50 mL min⁻¹.

The crystalline nature of the MACs was accessed by Powder X-Ray Diffraction (XRD) (Rigaku, Miniflex 300, Japan). The instrument was operated at 30 kV and 10 mA with Cu K α radiation ($\lambda = 1.541861 \text{ \AA}$). Measurements were done over the $10^\circ \leq 2\theta \leq 100^\circ$, using a scanning step of $0.06^\circ \text{ s}^{-1}$. The Scherrer's equation obtained the Ni particles' average crystallite size (D) in the magnetic activated carbons.

The magnetic properties were investigated at room temperature utilizing a vibrating-sample magnetometer (VSM) (MicroSense, EZ9, USA) performing from -20 kOe to $+20 \text{ kOe}$.

2.4. Kinetic and equilibrium adsorption experiments

Adsorption studies of BB dye from aqueous solutions were performed to evaluate the adsorption performance of the MACs. BB dye is extensively used in the food industry and can be found in various foods such as drink mixes, ice creams, candies, and gelatins.

For the adsorption assays, 20 mL of the BB dye solution at pH 4.0 (adjusted with 0.1 mol L $^{-1}$ HCl solution) were added in Erlenmeyer flasks with 0.02 g of the MAC (adsorbent dosage of 1 g L $^{-1}$). The flasks were stirred in a thermostatic agitator (Solab, SL222, Brazil) at 25 °C and 150 rpm. The kinetic study was performed with an initial BB dye concentration of 50 mg L $^{-1}$ at set intervals (0–240 min). The equilibrium study was carried out with initial BB dye concentrations from 0 to 200 mg L $^{-1}$ until it reached equilibrium. Afterward, the adsorbent was separated from the liquid phase using a magnet. The remaining BB concentration in the liquid was measured by spectrophotometry (Biospectro SP-22, Brazil) at 630 nm. The adsorption results were represented according to the standard of our group (supplementary material S1).

2.5. Kinetic and equilibrium models

See supplementary materials S2 and S3.

2.6 Regeneration and reuse experiments

Regeneration and reuse tests were conducted to verify the possibility of reusing the MACs. First, the MACs were loaded with BB dye at the following experimental conditions: initial dye concentration of 50 mg L^{-1} , pH 4.0, an adsorbent dosage of 1 g L^{-1} , 25°C , stirring rate of 150 rpm, and 2 h. After, the adsorbent was separated from the medium by a magnet and oven-dried at 105°C for 8 h.

In the regeneration step, four different regeneration agents, namely sodium chloride (NaCl), sodium hydroxide (NaOH), ammonium hydroxide (NH_4OH), and acetone ($\text{C}_3\text{H}_6\text{O}$) in the concentrations of 0.5 and 1.0 mol L^{-1} were tested to desorb the BB dye from the adsorbent. In this step, 20 mL of the regeneration agent were added in Erlenmeyer flasks with the magnetic activated carbon previously loaded with BB dye. The flasks were stirred for 2 h at 25°C and stirring rate 150 rpm. Subsequently, the regenerated adsorbent was separated from the medium using a magnet and oven-dried at 105°C for 8 h. After that, the regenerated magnetic activated carbons were used again for BB dye adsorption. The adsorption-regeneration cycle was realized several times using the regeneration agent that showed the best results.

2.7 Application in a simulated effluent

The simulated effluent was prepared using a grape drink mix obtained from local industry and presented a BB dye concentration of 52 mg L^{-1} and pH of 3.0. The matrix of the simulated effluent was composed of sugars, dehydrated grape juice, vitamin C, acidulant

(citric acid), acidity regulator (trisodium citrate), flavorings, sweeteners (potassium aspartame and acesulfame), anti-humectant (tricalcium phosphate), thickeners (sodium carboxymethylcellulose and xanthan gum) and dyes (brilliant blue, titanium dioxide derivatives, red 40, and indigotin blue). The experiments were carried out with 20 mL of the simulated effluent, a temperature of 25 °C, and a stirring rate of 150 rpm. Different adsorbent dosages (1, 5, and 10 g L⁻¹) and contact times (5–30 min) were tested. Before and after the adsorption tests, the spectra were obtained in a UV-vis spectrometer (Shimadzu, UV240, Japan). The spectra were recorded from 400 to 800 nm, and the areas under the absorption bands were used to obtain the removal efficiencies.

3. Results and discussion

3.1. features of the magnetic activated carbons

3.1.1. Scanning electron microscopy images

The SEM images of MAC1105 and MAC111, with magnifications of 5000× and 10000×, are shown in Fig. 1 (a, b) and (d, e), respectively. It is possible to observe that both materials had an irregular surface, the presence of roughness and some grains, and cavities along their surfaces. In addition, MAC111 seems to have a higher quantity of cavities than MAC1105, which is the main difference observed between the surface morphology of the produced MACs. These cavities are a favorable aspect for application in adsorption processes because they enable the BB molecules to penetrate the adsorbent until reaching the pores [39-40]. Such cavities can be formed by the decomposition induced by KOH [41]. In addition, since both MACs were prepared with the same weight ratio of KOH, the higher quantity of cavities observed for MAC111 can be attributed to the higher weight ratio of NiCl₂, which can cause the dehydration and decomposition of the lignocellulosic material [40]. This effect will be better explained further.

Fig. 1 (c) shows the EDS spectrum of MAC1105, and Fig. 1 (f) shows the EDS spectrum of MAC111. For both MACs, carbon (C), oxygen (O), and nickel (Ni) were the major elements. The appearance of Si comes from the precursor material (Sapelli wood sawdust) used in the production of the adsorbents. The presence of Ni indicates that the Ni compounds formed during the pyrolysis were not eliminated with the acid wash but remained embedded in the carbon matrix. This behavior is important since these Ni compounds generate magnetization in the samples.

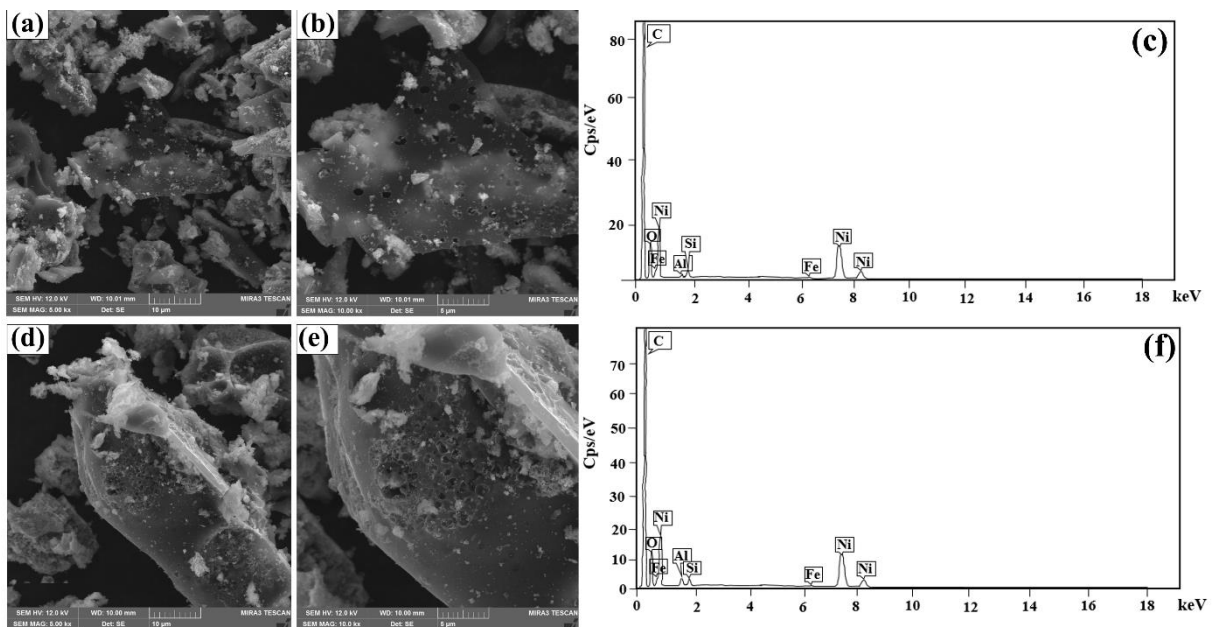


Figure 1. SEM images of (a) MAC1105 and (b) MAC111 and EDS spectra of (c) MAC1105 and (d) MAC111.

3.1.2. Functional groups on the magnetic activated carbons surface

Fig. 2 shows the FTIR spectra of MAC1105 (Fig. 2 (a)) and MAC111 (Fig. 2 (b)). Bands at 3431, 1625, and 1558 cm^{-1} can be observed for both materials. The bands at 3431 cm^{-1} can be ascribed to the stretching vibrations of O–H bonds from alcohols, phenols, or carboxylic acids present as functional groups on the surface of the MACs, or they can also be ascribed to the presence of adsorbed water [42]. The bands at 1625 cm^{-1} can be attributed to the C=O bonds [43]. At 1558 cm^{-1} , the bands observed can be attributed to the C=C stretching

vibrations of the aromatic rings of the activated carbons' structure [44]. Besides that, bands at 1034 e 1028 cm⁻¹ can be observed for MAC1105 and MAC111, respectively, and are due to the C–O stretching vibrations of hydroxyl in alcohols, phenols, or carboxyls [45].

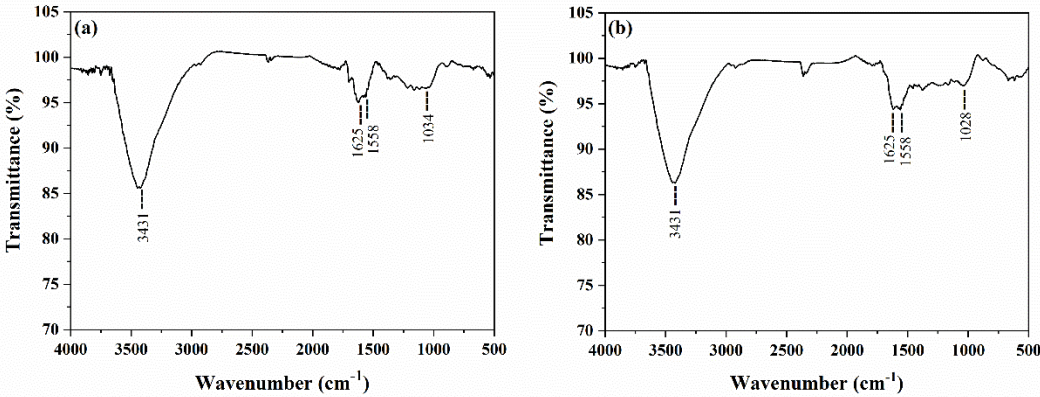


Figure 2. FTIR vibrational spectra of (a) MAC1105 and (b) MAC111.

3.1.3. Textural characteristics

Fig. 3 shows the N₂ adsorption/desorption isotherms and the BJH desorption pore size distributions for MAC1105 (Fig. 3 (a)) and MAC111 (Fig. 3 (b)). According to the IUPAC classification of adsorption isotherms, the adsorption isotherms of both materials were Type IV, accompanied by hysteresis [46]. Type IV isotherm is a characteristic of mesoporous materials. The adsorption hysteresis exhibited by both MACs was Type H4. This type of hysteresis loop is characteristic of micro/mesoporous carbonaceous materials [46]. From the pore size distribution, mesopores are observed for both materials.

Table 1 presents both materials' surface area, total pore volume, and average pore size. It can be observed that MAC111 presented a higher BET surface area and higher total pore volume than MAC1105. KOH used as the activating agent can react with the carbonaceous material leading to the formation of the porous structure and affecting the surface area and total pore volume [47]. Since both MAC1105 and MAC111 were prepared with the same

weight ratio of KOH, the superior features presented by MAC111 may be due to the higher weight ratio of NiCl₂ used to prepare this material. Therefore, in addition to generating magnetization, NiCl₂ can affect the textural characteristics of the samples. Similar behavior was observed by Thue et al. [37]. The authors prepared magnetic activated carbons from tucumã seed using ZnCl₂ and NiCl₂. They found out that the increase in the weight ratio of NiCl₂ led to an increase in the surface area and total pore volume of the obtained material. In addition, several other authors found that increasing the proportion of transition metal chlorides, such as ZnCl₂, FeCl₃, CoCl₂, and CuCl₂, led to improved textural properties [40,48-50]. The transition metals impregnated in the precursor material are cross-linked to the surface functional groups of the biomass, promoting the chemical dehydration and decomposition of the lignocellulosic material during the pyrolysis. After acid washes, the transition metals are removed, and the previously occupied spaces become free, forming the pores. Therefore, with higher weight ratios of these salts, more transition metal ions are available, improving the formation of the pore structure [40,48-50]. In the present work, although the presence of Ni in the carbon matrix was shown by the EDS spectra (Fig. 1), part of it may have been eliminated with the acid wash. Therefore, with a higher weight ratio of NiCl₂, more pores may have been created and, subsequently, become free with the acid wash. This may explain the higher surface area and total pore volume observed for MAC111.

Table 1. Textural characteristics of the magnetic activated carbons.

Activated carbon	BET surface área (m ² g ⁻¹)	Total pore volume (cm ³ g ⁻¹)	Average pore size (nm)
MAC1105	260.0	0.075	3.69
MAC111	331.5	0.095	3.60

Regarding the average pore sizes, values of 3.69 and 3.60 nm were found for MAC1105 and MAC111, respectively (Table 1). According to IUPAC, the pores of an

adsorbent can be classified as micropores (inner diameter < 2 nm), mesopores ($2 \text{ nm} \leq \text{inner diameter} \leq 50 \text{ nm}$), and macropores (inner diameter > 50 nm) [46]. Therefore, both MACs can be classified as mesoporous materials, corroborating the isotherms in Fig. 3.

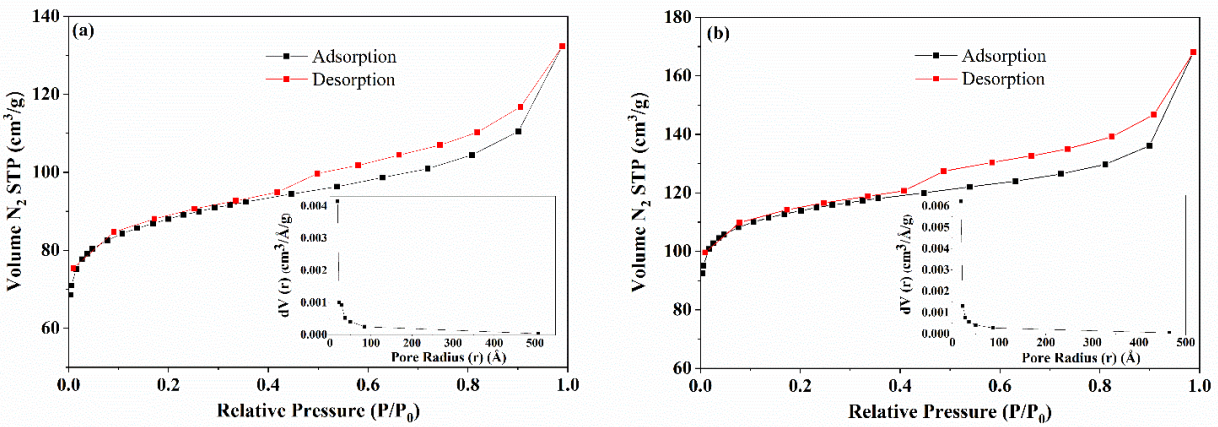


Figure 3. Nitrogen adsorption/desorption isotherms and the BJH pore size distribution of (a) MAC1105 and (b) MAC11.

3.1.4. Thermal analysis

Fig. 4 shows the thermal profile of the produced MACs. The thermal behavior was evaluated from room temperature to 800 °C under an N₂ atmosphere. The curve obtained for MAC1105 can be divided into four regions, while the curve obtained for MAC11 can be divided into five regions. The first region of weight loss was 21.4–98.9 °C and 19.9–104.9 °C for MAC1105 and MAC11, respectively, and can be attributed to the evaporation of moisture [37,51]. The temperature range for the second region of weight loss was 98.9–253.9 °C and 104.9–217.4 °C for MAC1105 and MAC11, respectively. This stage corresponds to the loss of water from the interstices and pores of the material [37,51]. The weight loss sum until these temperatures was 7.37% for MAC1105 and 9.60% for MAC11. The third region of weight loss varied from 253.9–463.9 °C for MAC1105. For MAC11, a third stage of weight loss occurred from 217.4–367.4 °C and a fourth stage occurred from 367.4–504.9 °C. These stages of weight loss can be assigned to the decomposition of oxygenated functional groups

present on the activated carbon surface [39]. The last stage for MAC1105 (fourth stage) was 763.9–798.9 °C and the last stage for MAC111 (fifth stage) was 504.9–793.3°C. These stages of weight loss correspond to the oxidation of the carbon matrix [51]. The total weight loss was 21.74% for MAC1105 and 24.80% for MAC111.

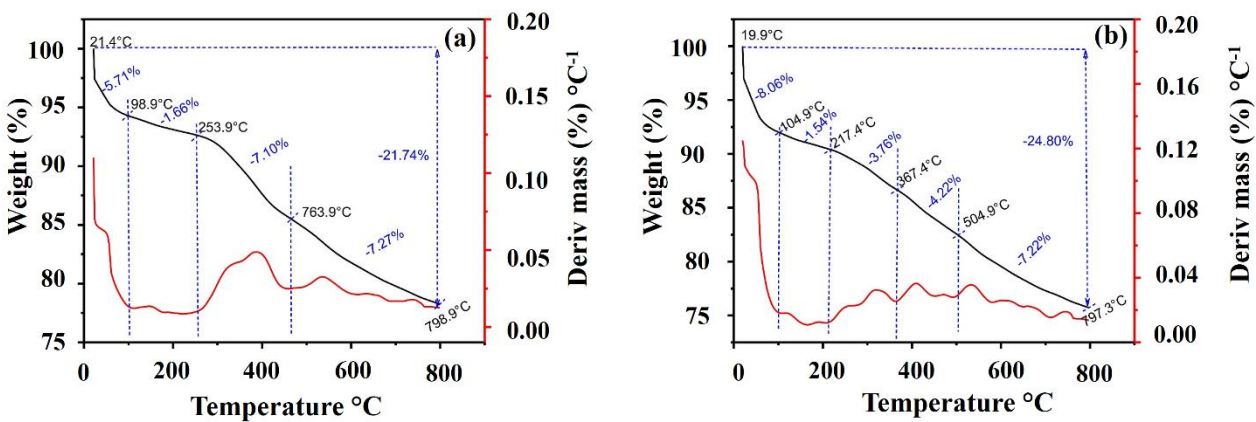


Figure 4. TGA curves of (a) MAC1105 and (b) MAC111.

3.1.5. X-ray diffraction

Fig. 5 shows the XRD diffractograms of MAC1105 and MAC111. Both samples show patterns of metallic Ni (crystalline system: cubic; JCPDS Card 00-004-0850). According to Thue et al. [37], the formation of metallic Ni occurs due to the reduction of the previously impregnated Ni^{2+} to Ni^0 . During pyrolysis, this reaction occurs at high temperatures and in the presence of reducing gases, such as H_2 and CH_4 . MAC1105 also shows patterns of nickel oxide (NiO ; crystalline system: rhombohedral; JCPDS Card 00-044-4459). These results also confirm that the Ni was not completely eliminated during the acid wash. Besides that, both MACs show patterns of silicon oxide (SiO_2 ; crystalline system: hexagonal; JCPDS Card 00-046-1045). The presence of SiO_2 in the samples comes from the Sapelli wood sawdust.

Nanostructured Ni particles with average crystallite sizes of 18.96 and 25.34 nm for MAC1105 and MAC111, respectively, were obtained (calculated using Scherrer's equation).

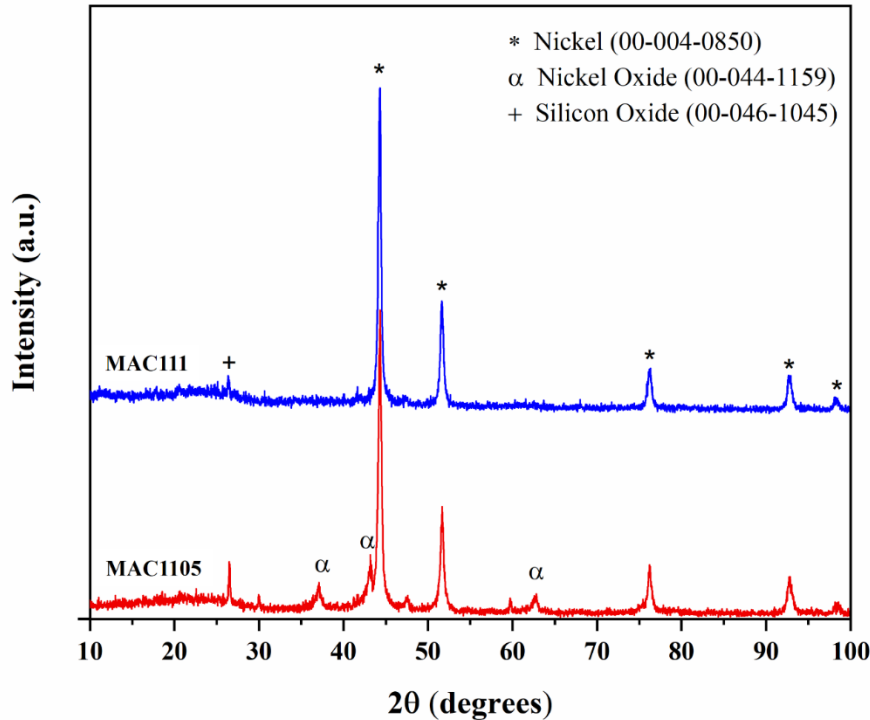


Figure 5. XRD patterns of MAC1105 and MAC111.

3.1.6. Magnetic features

Magnetization curves of the MACs are shown in Fig. 6 and the values of the hysteresis parameters are shown in Table 2. As can be seen, both exhibit ferromagnetic properties, with coercivity (H_C) values of 150.2 Oe and 200.2 Oe and remanence (M_R) values of 3.2 emu g⁻¹ and 4.1 emu g⁻¹ for MAC1105 and MAC111, respectively. These are interesting values for this kind of material [37,52,53]. On the other hand, the saturation magnetization (M_S) value, 13.6 emu g⁻¹ for both MACs, is slightly lower than the literature [37,52,53]. Despite the relatively low M_S value, the MACs produced can be easily moved and controlled in aqueous media by external magnetic fields.

Table 2. Magnetic properties of the magnetic activated carbons.

Sample	Coercivity (H_C , Oe)	Saturation magnetization (M_S , emu g ⁻¹)	Remanence (M_R , emu g ⁻¹)
MAC1105	150.2	13.6	3.2
MAC111	200.2	13.6	4.1

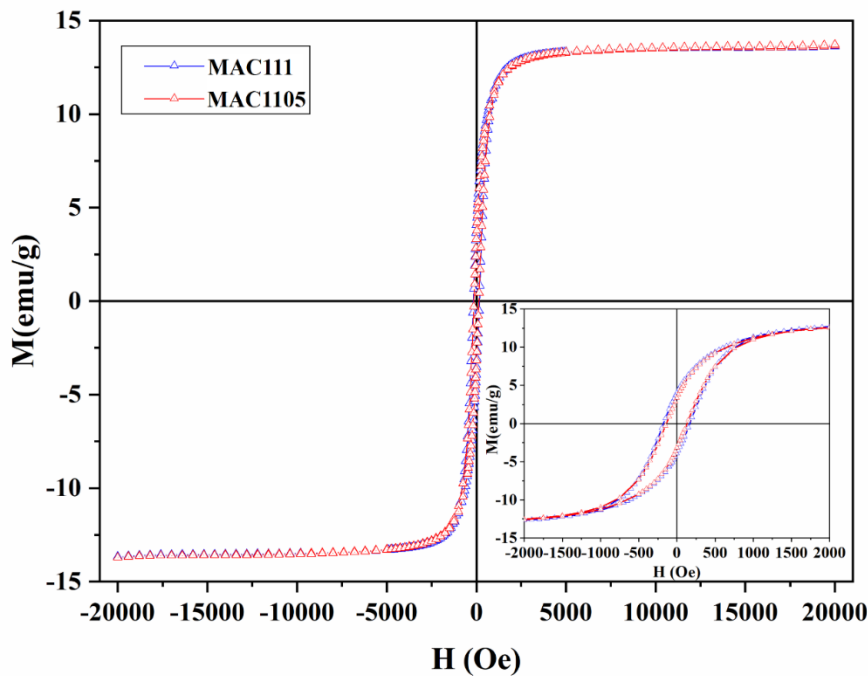


Figure 6. M-H hysteresis loops of MAC1105 and MAC111 at room temperature. The inset is a magnified view of the M-H curves.

3.2. Adsorption results

3.2.1. Kinetic profiles of BB adsorption

The kinetic behavior of BB dye adsorption was studied for both MACs with an initial adsorbate concentration of 50 mg L⁻¹ and pH 4. The adsorption capacity curves as a time function are shown in Fig. 7 (a) and (b) for MAC1105 and MAC111, respectively. It is possible to observe that the curve obtained for MAC111 was characterized by a faster adsorption rate. MAC111 reached equilibrium in around 10 minutes. For MAC1105, the equilibrium was reached in around 60 minutes. This behavior can be explained due to the higher total pore volume presented by MAC111 (Table 1). A high pore volume can enhance the kinetic of adsorption by allowing a faster diffusion rate of the dye molecules inside the pores to the adsorption sites [54].

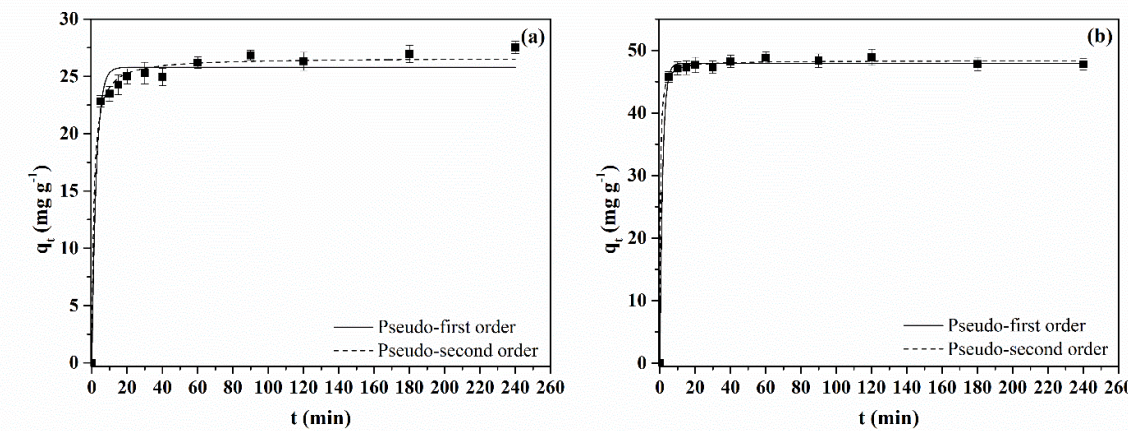


Figure 7. The kinetic curve of BB dye adsorption onto (a) MAC1105 and (b) MAC111.

The experimental kinetic data were fitted to the pseudo-first-order (PFO) and pseudo-second-order (PSO) models. The parameters of the models are depicted in Table 3. Based on the higher values of R^2 and R^2_{adj} , and the lower values of ARE , it can be concluded that the PSO model was the more suitable to represent the BB dye adsorption kinetic for both MACs. Furthermore, Table 3 confirms the faster kinetic and the higher adsorption capacity of MAC111 because k_2 and q_2 for this adsorbent were around two times higher concerning the same parameters for MAC1105. For comparison, several authors demonstrated that the PSO model was more suitable for representing the kinetic data of anionic dye adsorption [21,55-57].

Table 3. Kinetic parameters for the adsorption of BB dye.

Model	Activated carbon	
	MAC1105	MAC111
PFO		
q_1 (mg g ⁻¹)	25.79	47.93
k_1 (min ⁻¹)	0.396	0.612
R^2	0.9785	0.9983
R^2_{adj}	0.9480	0.9959
ARE (%)	3.83	1.00
PSO		
q_2 (mg g ⁻¹)	26.62	48.36
k_2 (g mg ⁻¹ min ⁻¹)	0.035	0.072

R^2	0.9931	0.9991
R^2_{adj}	0.9832	0.9977
ARE (%)	2.12	0.70

3.2.2. Adsorption isotherms

The equilibrium study for BB dye adsorption was carried out at 25 °C with initial adsorbate concentrations from 0 to 200 mg L⁻¹ and pH 4. Fig. 8 shows the equilibrium curves obtained for MAC1105 (Fig. 8 (a)) and for MAC111 (Fig. 8 (b)). According to Giles classification [58], the isotherms obtained for MAC1105 and MAC111 are typical type L1 and L2 isotherms, respectively. L-type isotherms indicate a high affinity between the adsorption sites of the adsorbent and the adsorbate molecules. Besides that, it is possible to observe (Fig. 8 (b)) that MAC111 presented a higher adsorption capacity than MAC1105. This result can also be explained due to the superior textural features exhibited by MAC111 (Table 1). The higher surface area presented by MAC111 makes a greater amount of surface active sites available to capture the adsorbate molecules.

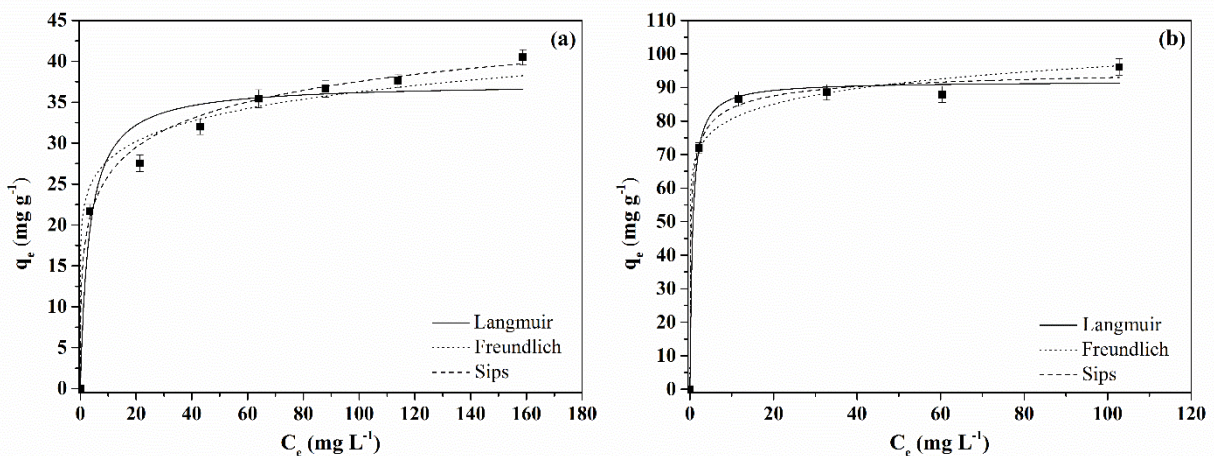


Figure 8. Equilibrium isotherms of BB blue dye adsorption onto (a) MAC1105 and (b) MAC111.

Langmuir, Freundlich, and Sips models were used to interpret the equilibrium curves. Table 4 shows the equilibrium parameters. Based on the R^2 , R^2_{adj} , and ARE values, it is possible to observe that only the Sips model was adequate to represent the equilibrium data for MAC1105. On the other hand, for MAC111, all three models presented a good fit. However, the Sips model presented slightly higher R^2 and R^2_{adj} values and a slightly lower ARE value. Therefore, it was established that the Sips model was more befittingly by the experimental equilibrium data for both MACs.

Table 4. Equilibrium parameters for the adsorption of BB dye.

Model	Activated carbon	
	MAC1105	MAC111
Langmuir		
q_m (mg g ⁻¹)	37.32	91.80
K_L (L mg ⁻¹)	0.314	1.655
R^2	0.9542	0.9946
R^2_{adj}	0.9359	0.9910
ARE (%)	7.58	2.28
Freundlich		
K_F ((mg g ⁻¹)(mg L ⁻¹) ^{-1/nF})	21.46	67.52
$1/nF$	0.114	0.077
R^2	0.9785	0.9927
R^2_{adj}	0.9699	0.9878
ARE (%)	5.79	2.44
Sips		
q_s (mg g ⁻¹)	60.73	98.12
K_S (L mg ⁻¹)	0.346	1.938
m_s	0.335	0.483
R^2	0.9937	0.9957
R^2_{adj}	0.9890	0.9894
ARE (%)	2.94	2.24

For comparison, table 5 shows the maximum adsorption capacity of different adsorbents for BB dye adsorption reported in the literature. It can be seen that the values

found in the present study are quite promising, and further studies on the adsorption conditions are required to increase the adsorption capacity.

Table 5. Adsorption capacities of different adsorbents for BB dye adsorption.

Adsorbent	Dosage (g L ⁻¹)	pH	T (°C)	Adsorption capacity (mg g ⁻¹)	Reference
MAC1105	1.0	4.0	25	60.7	This study
MAC111	1.0	4.0	25	98.1	This study
Chitosan vermiculite beads	5.0 ^a	10.2	25	181.6	[59]
Hen feather	0.4 ^a	2.0	30	317.0 ^b	[60]
Magnetic tungsten disulfide/carbon nanotubes nanocomposite	0.3 ^a	3.0	25	166.7	[61]
Bottom ash	4.0 ^a	3.0	50	6.9 ^b	[62]
De-oiled soya	2.0 ^a	3.0	50	18.2 ^b	[62]
Unmodified clay	10.0 ^a	5.4	30	6.2	[63]
Iron-modified clay	10.0 ^a	5.4	30	14.2	[63]

^aCalculated; ^bOriginal values converted to a mass base using the BB molar weight of 792.8 g mol⁻¹

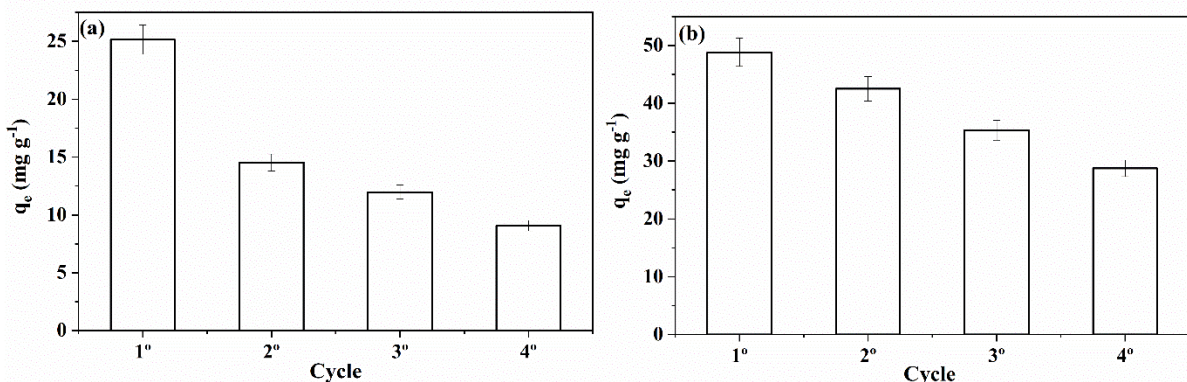
3.2.3. Regeneration and reuse study

Different chemical agents in different concentrations were tested for regenerating the MACs. Table 6 shows the equilibrium adsorption capacity for the second cycle of adsorption. It can be seen that the best results were obtained using NH₄OH in the concentration of 0.5 mol L⁻¹ for both MACs. Therefore, additional adsorption/regeneration cycles were performed using this regeneration condition to access the potential of reusing both materials. Fig. 9 shows the equilibrium adsorption capacity of BB dye for four cycles using MAC1105 (Fig. 9 (a)) and MAC111 (Fig. 9 (b)). It is possible to notice that the adsorption capacity gradually decreased over the cycles. This trend suggests that some BB dye molecules were not removed from the adsorbent surface upon regeneration. Therefore, the active sites occupied by these molecules become unavailable for adsorption in the next cycle.

Table 6. Regeneration test using different regeneration agents in different concentrations.

Activated carbon	Regenerating agent	Concentration of the regenerating agent (mol L^{-1})	q_e in the second cycle (mg g^{-1})^a
MAC1105	NaCl	0.5	6.05 ± 0.65
		1.0	5.80 ± 0.58
	NaOH	10.5	7.09 ± 0.74
		1.0	5.89 ± 0.63
	NH ₄ OH	0.5	10.78 ± 1.01
		1.0	5.72 ± 0.69
	$\text{C}_3\text{H}_6\text{O}$	0.5	8.58 ± 0.95
		1.0	7.35 ± 0.71
MAC111	NaCl	0.5	34.96 ± 0.87
		1.0	30.59 ± 1.23
	NaOH	10.5	29.21 ± 0.91
		1.0	22.52 ± 1.13
	NH ₄ OH	0.5	36.64 ± 0.87
		1.0	31.04 ± 0.92
	$\text{C}_3\text{H}_6\text{O}$	0.5	36.31 ± 1.04
		1.0	30.91 ± 0.98
	NaCl	0.5	34.96 ± 0.87

^a Mean \pm standard deviation ($n = 3$).

**Figure 9.** Reuse cycles of (a) MAC1105 and (b) MAC111.

It also can be observed that MAC111 showed a smaller decrease in adsorption capacity over the cycles than MAC1105 (Fig. 9). In addition, the adsorption capacity observed for MAC111 at the end of the fifth cycle (around 29 mg g^{-1}) is higher than the adsorption capacity observed for MAC1105 even in the first cycle (around 25 mg g^{-1}).

Overall, the results showed that MAC111 has a higher potential to be reused in more adsorption cycles, directly affecting the operating costs.

3.2.4. Application of MACs to treat a simulated effluent

A simulated effluent was prepared from a grape drink mix to verify the applicability of the MACs for removing BB dye in a complex matrix. The MACs were evaluated regarding the removal efficiency using different adsorbent dosages (1, 5, and 10 g L⁻¹) and contact times (5–30 min). The visible spectra (400–800 nm) of the simulated effluent before and after the adsorption tests are shown in Fig. 10. It was observed that the adsorption was fast since the removal efficiencies were virtually the same for all contact times studied. The removal efficiency obtained using a dosage of 1 g L⁻¹ was below 40%. The active sites are easily saturated with low adsorbent dosage since the simulated effluent contains several compounds other than the BB dye. However, using higher adsorbent dosages, high removal efficiencies were obtained. In 30 minutes, MAC1105 and MAC111 were capable of removing, respectively, 73% and 88% using the adsorbent dosage of 5 g L⁻¹, and 93% and 95% using the adsorbent dosage of 10 g L⁻¹. These results indicated that the MACs are promising adsorbents for treating effluents from the food industry containing the BB dye.

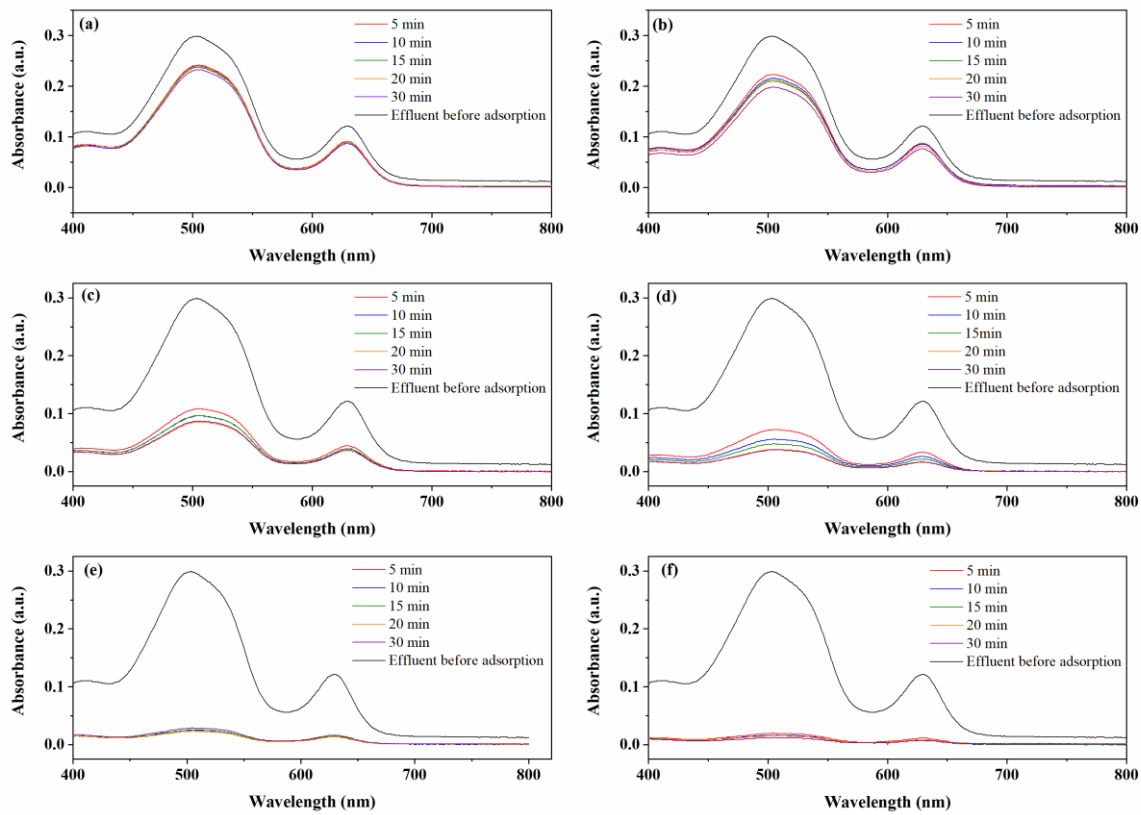


Figure 10. Absorption spectra of simulated effluent before and after adsorption with 1 g L^{-1} : (a) MAC1105 and (b) MAC111; 5 g L^{-1} ; (c) MAC1105 and (d) MAC111; 10 g L^{-1} ; (e) MAC1105 and (d) MAC111.

4. Conclusion

In this work, magnetic activated carbons from Sapelli wood sawdust were successfully prepared, characterized, and applied in the adsorption of BB dye from an aqueous solution. The different weight ratios of NiCl_2 influenced mainly the textural properties of the materials. The increase in the weight ratio of NiCl_2 led to an increase in the surface area from $260.0 \text{ m}^2 \text{ g}^{-1}$ (MAC1105) to $331.5 \text{ m}^2 \text{ g}^{-1}$ (MAC111) and in the total pore volume from $0.075 \text{ cm}^3 \text{ g}^{-1}$ (MAC1105) to $0.095 \text{ cm}^3 \text{ g}^{-1}$ (MAC111). The average pore size remained virtually the same, around 3.6 nm , regardless of the weight ratio of NiCl_2 . Both MACs exhibit ferromagnetic properties at room temperature. The presence of nanostructured Ni particles with average

crystallite sizes of 18.96 nm (MAC1105) and 25.34 nm (MAC111) was observed. According to the FTIR spectra, very similar surface chemistry was obtained for both MACs, both exhibiting hydroxyl and carboxyl groups. Furthermore, a very similar thermal behavior was also observed for both materials.

From the adsorption study, important differences between the MACs were observed. MAC111 exhibited faster kinetics and reach the equilibrium in around 10 minutes. For MAC1105, on the other hand, the equilibrium was reached only in 60 minutes. For both adsorbents, the pseudo-second-order model well represented the kinetic data. Regarding the adsorption isotherms, the Sips model satisfactorily represented the data. In addition, MAC111 showed a higher maximum adsorption capacity ($q_s = 98.12 \text{ mg g}^{-1}$) than MAC1105 ($q_s = 60.73 \text{ mg g}^{-1}$). The regeneration and reuse study showed that MAC111 had a higher potential to be reused in more adsorption cycles. Finally, MAC1105 and MAC111 were promising for treating a simulated effluent containing the BB dye, achieving removal efficiencies of 93% and 95%, respectively. These results demonstrated that the MACs were promising adsorbents for BB dye removal from an aqueous solution with good efficiency and easy magnetic separation. Besides that, it is noteworthy that MAC111 showed the best results due to its best features arising from the higher weight ratio of NiCl_2 used in its production. Nevertheless, further and more complete studies, such as the effect of the adsorbent dosage, pH and temperature, and the adsorption thermodynamics, are required for application purposes.

Declarations: The authors declare that they have no known competing financial interests or personal relationships that could have appeared to influence the work reported in this paper.

References

- [1] Patra BR, Mukherjee A, Nanda S, Dalai AK (2021) Biochar production, activation and adsorptive applications: a review. *Environ Chem Lett* 19:2237–2259. <https://doi.org/10.1007/s10311-020-01165-9>
- [2] Haleem A, Shafiq A, Chen SQ, Nazar M (2023) A Comprehensive Review on Adsorption, Photocatalytic and Chemical Degradation of Dyes and Nitro-Compounds over Different Kinds of Porous and Composite Materials. *Molecules* 28:1081. <https://doi.org/10.3390/molecules28031081>
- [3] Alias SS, Harun Z, Azhar FH, Ibrahim SA, Johar B (2020) Comparison between commercial and synthesised nano flower-like rutile TiO₂ immobilised on green super adsorbent towards dye wastewater treatment. *J Clean Prod* 251:119448. <https://doi.org/10.1016/j.jclepro.2019.119448>
- [4] Shah LA, Malik T, Siddiq M, Haleem A, Sayed M, Naeem A (2019) TiO₂ nanotubes doped poly (vinylidene fluoride) polymer membranes (PVDF/TNT) for efficient photocatalytic degradation of brilliant green dye. *J Environ Chem Eng* 7:103291. <https://doi.org/10.1016/j.jece.2019.103291>
- [5] Bhatti HN, Safa Y, Yakout SM, Shair OH, Iqbal M, Nazir A (2020) Efficient removal of dyes using carboxymethyl cellulose/alginate/polyvinyl alcohol/rice husk composite: Adsorption/desorption, kinetics and recycling studies. *Int J Biol Macromol* 150:861–870. <https://doi.org/10.1016/j.ijbiomac.2020.02.093>
- [6] Wekoye JN, Wanyonyi WC, Wangila PT, Tonui MK (2020) Kinetic and equilibrium studies of Congo red dye adsorption on cabbage waste powder. *Environ Chem Ecotoxicol* 2:24–31. <https://doi.org/10.1016/j.enceco.2020.01.004>
- [7] Ortiz-Martínez AK, Godínez LA, Martínez-Sánchez C, García-Espinoza JD, Robles I (2021) Preparation of modified carbon paste electrodes from orange peel and used

- coffee ground. New materials for the treatment of dye-contaminated solutions using electro-Fenton processes. *Electrochim Acta* 390:138861. <https://doi.org/10.1016/j.electacta.2021.138861>
- [8] Dotto J, Fagundes-Klen MR, Veit MT, Palácio SM, Bergamasco R (2019). Performance of different coagulants in the coagulation/flocculation process of textile wastewater. *J Clean Prod* 208:656–665. <https://doi.org/10.1016/j.jclepro.2018.10.112>
- [9] Arunprasath T, Sudalai S, Meenatchi RS, Jeyavishnu K, Arumugam A (2019) Biodegradation of triphenylmethane dye malachite green by a newly isolated fungus strain. *Biocatal Agric Biotechnol* 17:672–679. <https://doi.org/10.1016/j.bcab.2019.01.030>
- [10] Hassan MM, Carr CM (2018) A critical review on recent advancements of the removal of reactive dyes from dyehouse effluent by ion-exchange adsorbents. *Chemosphere* 209:201–219. <https://doi.org/10.1016/j.chemosphere.2018.06.043>
- [11] de Salomón YLO, Georgin J, Franco DSP, Netto MS, Foletto EL, Allasia D, Dotto GL (2021) Application of seed residues from Anadenanthera macrocarpa and Cedrela fissilis as alternative adsorbents for remarkable removal of methylene blue dye in aqueous solutions. *Environ Sci Pollut Res* 28:2342–2354. <https://doi.org/10.1007/s11356-020-10635-0>
- [12] Dotto GL, McKay G (2020) Current scenario and challenges in adsorption for water treatment. *J Environ Chem Eng* 8:103988. <https://doi.org/10.1016/j.jece.2020.103988>
- [13] Tahir MA, Bhatti HN, Iqbal M (2016) Solar red and brittle blue direct dyes adsorption onto Eucalyptus angophoroides bark: Equilibrium, kinetics and thermodynamic studies. *J Environ Chem Eng* 4:2431–2439. <https://doi.org/10.1016/j.jece.2016.04.020>
- [14] Jawad AH, Abdulhameed AS, Reghioua A, Yaseen ZM (2020) Zwitterion composite chitosan-epichlorohydrin/zeolite for adsorption of methylene blue and reactive red 120

- dyes. Int J Biol Macromol 163: 756–765.
<https://doi.org/10.1016/j.ijbiomac.2020.07.014>
- [15] Puchana-Rosero MJ, Adebayo MA, Lima EC, Machado FM, Thue PS, Vaghetti JCP, Umpierrez CS, Gutterres M (2016) Microwave-assisted activated carbon obtained from the sludge of tannery-treatment effluent plant for removal of leather dyes. *Colloids Surfaces A Physicochem Eng Asp* 504:105–115.
<https://doi.org/10.1016/j.colsurfa.2016.05.059>
- [16] Yunus ZM, Al-Gheethi A, Othman N, Hamdan R, Ruslan NN (2020) Removal of heavy metals from mining effluents in tile and electroplating industries using honeydew peel activated carbon: A microstructure and techno-economic analysis. *J Clean Prod* 251:119738. <https://doi.org/10.1016/j.jclepro.2019.119738>
- [17] Rashid J, Tehreem F, Rehman A, Kumar R (2019) Synthesis using natural functionalization of activated carbon from pumpkin peels for decolorization of aqueous methylene blue. *Sci Total Environ* 671:369–376.
<https://doi.org/10.1016/j.scitotenv.2019.03.363>
- [18] Kang K, Nanda S, Lam SS, Zhang T, Huo L, Zhao L (2020) Enhanced fuel characteristics and physical chemistry of microwave hydrochar for sustainable fuel pellet production via co-densification. *Environ Res* 186:109480.
<https://doi.org/10.1016/j.envres.2020.109480>
- [19] Sarker TR, Pattnaik F, Nanda S, Dalai AK, Meda V, Naik S (2021) Hydrothermal pretreatment technologies for lignocellulosic biomass: A review of steam explosion and subcritical water hydrolysis. *Chemosphere* 284:131372.
<https://doi.org/10.1016/j.chemosphere.2021.131372>
- [20] Supong A, Bhomick PC, Baruah M, Pongener C, Sinha UB, Sinha D (2019) Adsorptive removal of Bisphenol A by biomass activated carbon and insights into the adsorption

- mechanism through density functional theory calculations. *Sustain Chem Pharm* 13: 100159. <https://doi.org/10.1016/j.scp.2019.100159>
- [21] Zazycki MA, Godinho M, Perondi D, Foletto EL, Collazzo GC, Dotto GL (2018) New biochar from pecan nutshells as an alternative adsorbent for removing reactive red 141 from aqueous solutions. *J Clean Prod* 171:57–65. <https://doi.org/10.1016/j.jclepro.2017.10.007>
- [22] Wang Y, Wang S, Xie T, Cao J (2020) Activated carbon derived from waste tangerine seed for the high-performance adsorption of carbamate pesticides from water and plant. *Bioresour Technol* 316:123929. <https://doi.org/10.1016/j.biortech.2020.123929>
- [23] Van Thuan T, Quynh BTP, Nguyen TD, Ho VTT, Bach LG (2017) Response surface methodology approach for optimization of Cu²⁺, Ni²⁺ and Pb²⁺ adsorption using KOH-activated carbon from banana peel. *Surfaces and Interfaces* 6:209–217. <https://doi.org/10.1016/j.surfin.2016.10.007>
- [24] Enniya I, Rghioui L, Jourani A (2018) Adsorption of hexavalent chromium in aqueous solution on activated carbon prepared from apple peels. *Sustain Chem Pharm* 7:9–16. <https://doi.org/10.1016/j.scp.2017.11.003>
- [25] Sajjadi S-A, Meknati A, Lima EC, Dotto GL, Mendoza-Castillo DI, Anastopoulos I, Alakhras F, Unuabonah EI, Singh P, Hosseini-Bandegharaei A (2019) A novel route for preparation of chemically activated carbon from pistachio wood for highly efficient Pb (II) sorption. *J Environ Manage* 236:34–44. <https://doi.org/10.1016/j.jenvman.2019.01.087>
- [26] Kumar A, Gupta H (2020) Activated carbon from sawdust for naphthalene removal from contaminated water. *Environ Technol Innov* 20:101080. <https://doi.org/10.1016/j.eti.2020.101080>

- [27] Chikri R, Elhadiri N, Benchanaa M, Maguana Y (2020) Efficiency of sawdust as low-cost adsorbent for dyes removal. *J Chem* 2020:1–17. <https://doi.org/10.1155/2020/8813420>
- [28] Mallakpour S, Sirous F, Hussain CM (2021) Sawdust, a versatile, inexpensive, readily available bio-waste: From mother earth to valuable materials for sustainable remediation technologies. *Adv Colloid Interface Sci* 295:102492. <https://doi.org/10.1016/j.cis.2021.102492>
- [29] Vieira LHS, Sabino CMS, Soares Júnior FH, Rocha JS, Castro MO, Alencar RS, da Costa LS, Viana BC, de Paula AJ, Soares JM, Souza Filho AG, Otubo L, Fechine PBA, Ghosh A, Ferreira OP (2020) Strategic design of magnetic carbonaceous nanocomposites and its application as multifunctional adsorbent. *Carbon* 161:758–771. <https://doi.org/10.1016/j.carbon.2020.01.089>
- [30] Liu X, Wang Y, Zhang TC, Xiang G, Wang X, Yuan S (2021) One-Pot Synthesis of a Magnetic TiO₂/PTh/γ-Fe₂O₃ Heterojunction Nanocomposite for Removing Trace Arsenite via Simultaneous Photocatalytic Oxidation and Adsorption. *Ind Eng Chem Res* 60:528–540. <https://doi.org/10.1021/acs.iecr.0c04262>
- [31] Moosavi S, Lai CW, Gan S, Zamiri G, Pivehzhani OA, Johan MR (2020) Application of efficient magnetic particles and activated carbon for dye removal from wastewater. *ACS Omega*, 5:20684–20697. <https://doi.org/10.1021/acsomega.0c01905>
- [32] Wang Y, Zhang Y, Zhang TC, Xiang G, Wang X, Yuan S (2020) Removal of trace arsenite through simultaneous photocatalytic oxidation and adsorption by magnetic Fe₃O₄@PpPDA@TiO₂ core–shell nanoparticles. *ACS Appl Nano Mater* 3:8495–8504. <https://pubs.acs.org/doi/10.1021/acsanm.0c02083>

- [33] Du Q, Zhang S, Song J, Zhao Y, Yang F (2020). Activation of porous magnetized biochar by artificial humic acid for effective removal of lead ions. *J Hazard Mater* 389:122115. <https://doi.org/10.1016/j.jhazmat.2020.122115>
- [34] Feng Z, Chen H, Li H, Yuan R, Wang F, Chen Z, Zhou B (2020) Preparation, characterization, and application of magnetic activated carbon for treatment of biologically treated papermaking wastewater. *Sci Total Environ* 713:136423. <https://doi.org/10.1016/j.scitotenv.2019.136423>
- [35] Pereira D, Rocha LS, Gil MV, Otero M, Silva NJO, Esteves VI, Calisto V (2021) In situ functionalization of a cellulosic-based activated carbon with magnetic iron oxides for the removal of carbamazepine from wastewater. *Environ Sci Pollut Res* 28: 18314–18327. <https://doi.org/10.1007/s11356-020-09314-x>
- [36] Salem S, Teimouri Z, Salem A (2020) Fabrication of magnetic activated carbon by carbothermal functionalization of agriculture waste via microwave-assisted technique for cationic dye adsorption. *Adv Powder Technol* 31:4301–4309. <https://doi.org/10.1016/j.apt.2020.09.007>
- [37] Thue PS, Umpierres CS, Lima EC, Lima DR, Machado FM, Reis GS, Silva RS, Pavan FA, Tran HN (2020) Single-step pyrolysis for producing magnetic activated carbon from tucum (*Astrocaryum aculeatum*) seed and nickel(II) chloride and zinc(II) chloride. Application for removal of nicotinamide and propanolol. *J Hazard Mater* 398:122903. <https://doi.org/10.1016/j.jhazmat.2020.122903>
- [38] Bai X, Yu L, Hua Z, Tang Z, Zhang J (2015) Synthesis and characterization of superparamagnetic activated carbon adsorbents based on cyanobacteria. *Mater Chem Phys* 163:407–415. <https://doi.org/10.1016/j.matchemphys.2015.07.058>
- [39] Lütke SF, Igansi AV, Pegoraro L, Dotto GL, Pinto LAA, Cadaval TRS (2019) Preparation of activated carbon from black wattle bark waste and its application for

phenol adsorption. J Environ Chem Eng 7:103396.

<https://doi.org/10.1016/j.jece.2019.103396>

[40] Thue PS, Lima EC, Sieliechi JM, Saucier C, Dias SLP, Vaghetti JCP, Rodembusch FS, Pavan FA (2017). Effects of first-row transition metals and impregnation ratios on the physicochemical properties of microwave-assisted activated carbons from wood biomass. J Colloid Interface Sci 486:163–175.

<http://dx.doi.org/10.1016/j.jcis.2016.09.070>

[41] Muniandy L, Adam F, Rahman A, Mohamed AR, Ng EP (2014) The synthesis and characterization of high purity mixed microporous/mesoporous activated carbon from rice husk using chemical activation with NaOH and KOH. Microporous Mesoporous Mater 197:316–323. <https://doi.org/10.1016/j.micromeso.2014.06.020>

[42] Ogungbenro AE, Quang DV, Al-Ali KA, Vega LF, Abu-Zahra MRM (2020) Synthesis and characterization of activated carbon from biomass date seeds for carbon dioxide adsorption. J Environ Chem Eng 8:104257. <https://doi.org/10.1016/j.jece.2020.104257>

[43] Ferreira SD, Altafini CR, Perondi D, Godinho M (2015) Pyrolysis of Medium Density Fiberboard (MDF) wastes in a screw reactor. Energy Convers Manag 92:223–233. <https://doi.org/10.1016/j.enconman.2014.12.032>

[44] Duan S, Ma W, Pan Y, Meng F, Yu S, Wu L (2017) Synthesis of magnetic biochar from iron sludge for the enhancement of Cr(VI) removal from solution. J Taiwan Inst Chem Eng 80:835–841. <https://doi.org/10.1016/j.jtice.2017.07.002>

[45] Fontana KB, Chaves ES, Sanchez JDS, Watanabe ERLR, Pietrobelli JMTA, Lenzi GG (2016) Textile dye removal from aqueous solutions by malt bagasse: Isotherm, kinetic and thermodynamic studies. Ecotoxicol Environ Saf 124:329–336. <https://doi.org/10.1016/j.ecoenv.2015.11.012>

- [46] Thommes M, Kaneko K, Neimark AV, Olivier JP, Rodriguez-Reinoso F, Rouquerol J, Sing KSW (2015) Physisorption of gases, with special reference to the evaluation of surface area and pore size distribution (IUPAC Technical Report), Pure and Applied Chemistry. <https://doi.org/10.1515/pac-2014-1117>
- [47] da Silva MCF, Schnorr C, Lütke SF, Knani S, Nascimento VX, Lima EC, Thue, PS, Vieillard J, Silva, LFO, Dotto, GL (2022) KOH activated carbons from Brazil nut shell: Preparation, characterization, and their application in phenol adsorption. *Chem Eng Res Des* 187:387–396. <https://doi.org/10.1016/j.cherd.2022.09.012>
- [48] Li Y, Li Y, Li L, Shi X, Wang Z (2016) Preparation and analysis of activated carbon from sewage sludge and corn stalk. *Adv Powder Technol* 27:684–691. <https://doi.org/10.1016/j.apt.2016.02.029>
- [49] Yu F, Zhu X, Jin W, Fan J, Clark JH, Zhang S (2020) Optimized synthesis of granular fuel and granular activated carbon from sawdust hydrochar without binder. *J Clean Prod* 276:122711. <https://doi.org/10.1016/j.jclepro.2020.122711>
- [50] Yuan Y, Huang L, Zhang TC, Ouyang L, Yuan S (2021) One-step synthesis of ZnFe₂O₄-loaded biochar derived from leftover rice for high-performance H₂S removal. *Sep Purif Technol* 279:119686. <https://doi.org/10.1016/j.seppur.2021.119686>
- [51] Cunha MR, Lima EC, Lima DR, da Silva RS, Thue PS, Seliem MK, Sher F, dos Reis GS, Larsson SH (2020) Removal of captopril pharmaceutical from synthetic pharmaceutical-industry wastewaters: Use of activated carbon derived from *Butia catarinensis*. *J Environ Chem Eng* 8:104506. <https://doi.org/10.1016/j.jece.2020.104506>
- [52] Cazetta AL, Pezoti O, Bedin KC, Silva TL, Junior AP, Asefa T, Almeida VC (2016) Magnetic Activated Carbon Derived from Biomass Waste by Concurrent Synthesis: Efficient Adsorbent for Toxic Dyes. *ACS Sustain Chem Eng* 4:1058–1068. <https://doi.org/10.1021/acssuschemeng.5b01141>

- [53] Zhou L, Shao Y, Liu J, Ye Z, Zhang H, Ma J, Jia Y, Gao W, Li Y (2014) Preparation and Characterization of Magnetic Porous Carbon Microspheres for Removal of Methylene Blue by a Heterogeneous Fenton Reaction. *Appl Mater Interfaces* 6:7275–7285. <https://doi.org/10.1021/am500576p>
- [54] Lawtae P, Tangsathitkulchai C (2021) The Use of High Surface Area Mesoporous-Activated Carbon from Longan Seed Biomass for Increasing Capacity and Kinetics of Methylene Blue Adsorption from Aqueous Solution. *Molecules* 26:6521.
- [55] Lyu W, Yu M, Li J, Feng J, Yan W (2022) Adsorption of anionic acid red G dye on polyaniline nanofibers synthesized by FeCl₃ oxidant: Unravelling the role of synthetic conditions. *Colloids Surfaces A Physicochem Eng Asp* 647:129203. <https://doi.org/10.1016/j.colsurfa.2022.129203>
- [56] Patra C, Gupta R, Bedadeep D, Narayanasamy S (2020) Surface treated acid-activated carbon for adsorption of anionic azo dyes from single and binary adsorptive systems: A detail insight. *Environ Pollut* 266:115102. <https://doi.org/10.1016/j.envpol.2020.115102>
- [57] Wang Q, Luo C, Lai Z, Chen S, He D, Mu J (2022) Honeycomb-like cork activated carbon with ultra-high adsorption capacity for anionic, cationic and mixed dye: Preparation, performance and mechanism. *Bioresour Technol* 357:127363. <https://doi.org/10.1016/j.biortech.2022.127363>
- [58] Giles CH, Smith D, Huitson A (1974) A general treatment and classification of the solute adsorption isotherm. *J Colloid Interface Sci* 47:755–765. [https://doi.org/10.1016/0021-9797\(74\)90252-5](https://doi.org/10.1016/0021-9797(74)90252-5)
- [59] Şenol ZM, Gürsoy N, Şimşek S, Özer A, Karakuş N (2020) Removal of food dyes from aqueous solution by chitosan- vermiculite beads. *Int J Biol Macromol* 148:635–646. <https://doi.org/10.1016/j.ijbiomac.2020.01.166>

- [60] Mittal A (2006) Use of hen feathers as potential adsorbent for the removal of a hazardous dye, Brilliant Blue FCF, from wastewater. *J Hazard Mater* 128:233–239. <https://doi.org/10.1016/j.jhazmat.2005.08.043>
- [61] Arabkhani P, Javadian H, Asfaram A, Sadeghfar F, Sadegh F (2021) Synthesis of magnetic tungsten disulfide/carbon nanotubes nanocomposite (WS₂/Fe₃O₄/CNTs-NC) for highly efficient ultrasound-assisted rapid removal of amaranth and brilliant blue FCF hazardous dyes. *J Hazard Mater* 420:126644. <https://doi.org/10.1016/j.jhazmat.2021.126644>
- [62] Gupta VK, Mittal A, Krishnan L, Mittal J (2006) Adsorption treatment and recovery of the hazardous dye, Brilliant Blue FCF, over bottom ash and de-oiled soya. *J Colloid Interface Sci* 293:16–26. <https://doi.org/10.1016/j.jcis.2005.06.021>
- [63] Hernández-Hernández KA, Solache-Ríos M, Díaz-Nava MC (2013) Removal of Brilliant Blue FCF from Aqueous Solutions Using an Unmodified and Iron-Modified Bentonite and the Thermodynamic Parameters of the Process. *Water, Air, Soil Pollut* 224:1562. <https://doi.org/10.1007/s11270-013-1562-9>

Supplementary Material

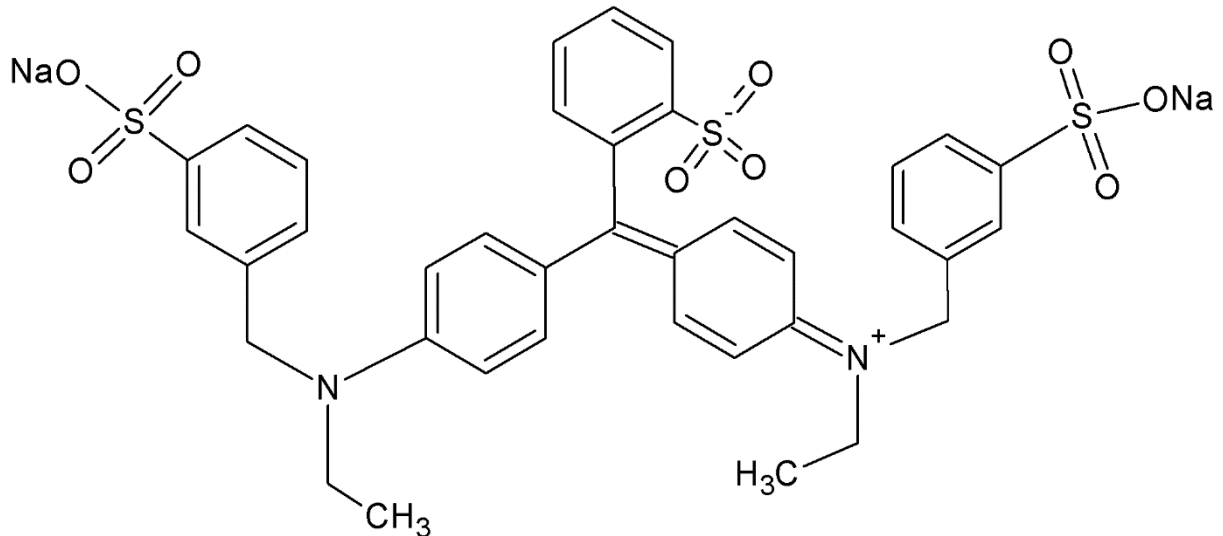


Fig. 1S. Chemical structure of the brilliant blue dye.

S1. Adsorption quantification

All assays were performed in replicate ($n = 3$), and blank tests were also realized. The adsorption capacity at time t (q_t) and the equilibrium adsorption capacity (q_e) were determined by Eq. (1) and (2), respectively:

$$q_t = \frac{V(C_0 - C_t)}{m} \quad (1)$$

$$q_e = \frac{V(C_0 - C_e)}{m} \quad (2)$$

Where C_0 is the initial BB dye concentration (mg L^{-1}), C_t is the BB dye concentration in the liquid phase at time t (mg L^{-1}), C_e is the equilibrium BB dye concentration in the liquid phase (mg L^{-1}), m is adsorbent mass (g), and V is the volume of the solution (L).

S2. Kinetic models

The adsorption kinetic behavior onto the MACs was evaluated by the pseudo-first-order (PFO) and pseudo-second-order (PSO) models [1]. The mathematical equations of these models are shown in Eq. (3) and (4), respectively:

$$q_t = q_I(1 - \exp(-k_1 t)) \quad (3)$$

$$q_t = \frac{t}{(1/k_2 q_2^2) + (t/q_2)} \quad (4)$$

Where q_t is the adsorption capacity at time t (mg g^{-1}), q_I is the adsorption capacity predicted by the pseudo-first-order model (mg g^{-1}), q_2 is the adsorption capacity predicted by the pseudo-second-order model (mg g^{-1}), k_1 is the pseudo-first-order rate constant (min^{-1}), and k_2 is the pseudo-second-order rate constant ($\text{g mg}^{-1} \text{ min}^{-1}$).

S3. Isotherm models

The adsorption equilibrium data were fitted to the Langmuir [2], Freundlich [3], and Sips [4] models, which are presented in the Eq. (5), (6), and (7), respectively:

$$q_e = \frac{q_m K_L C_e}{1 + K_L C_e} \quad (5)$$

$$q_e = K_F C_e^{1/nF} \quad (6)$$

$$q_e = q_s \frac{K_S C_e^{m_s}}{1 + K_S C_e^{m_s}} \quad (7)$$

Where q_e is equilibrium adsorption capacity (mg g^{-1}), C_e is the equilibrium BB dye concentration in the liquid phase (mg L^{-1}), q_m is the maximum adsorption capacity of the Langmuir model (mg g^{-1}); K_L is the Langmuir equilibrium constant (L mg^{-1}); K_F is the

Freundlich equilibrium constant ($(\text{mg g}^{-1}) (\text{mg L}^{-1})^{-1/nF}$), $1/nF$ is the heterogeneity factor, q_s is the maximum adsorption capacity of the Sips model (mg g^{-1}), K_s is the Sips equilibrium constant (L mg^{-1}) and m_s the exponent of the Sips model.

The parameters of the models were estimated through nonlinear regression using the Quasi-Newton estimation method. Statistica 7.0 software (Statsoft, USA) was used in the calculations. The fit quality was evaluated by determination coefficient (R^2), adjusted determination coefficient (R^2_{adj}), and average relative error (ARE).

References

- [1] Ho YS, McKay G (1998) A comparison of chemisorption kinetic models applied to pollutant removal on various sorbents. *Process Saf Environ Prot* 76:332–340.
<https://doi.org/10.1205/095758298529696>
- [2] Langmuir I (1918) The adsorption of gases on plane surfaces of glass, mica and platinum. *J Am Chem Soc* 40:1361–1403. <https://doi.org/10.1021/ja02242a004>
- [3] Freundlich H (1907) Über die Adsorption in Lösungen. *Zeitschrift für Phys Chemie* 57U: 385–470. <https://doi.org/10.1515/zpch-1907-5723>
- [4] Sips R (1948) On the Structure of a Catalyst Surface. *J Chem Phys* 16:490–495.
<https://doi.org/doi.org/10.1063/1.1746922>

4.2. ARTIGO 2 – BRILLIANT BLUE FCF DYE ADSORPTION USING MAGNETIC ACTIVATED CARBON FROM SAPELLI WOOD SAWDUST

Victoria X. Nascimento¹, Sabrina F. Lütke¹, Maria C. F. da Silva¹, Fernando. M. Machado²,
Éder. C. Lima³, Guilherme L. Dotto^{1*}

¹Research Group on Adsorptive and Catalytic Process Engineering (ENGEpac), Federal University of Santa Maria, Av. Roraima, 1000-7, 97105–900 Santa Maria, RS, Brazil

²Technology Development Center, Federal University of Pelotas–UFPEL, Gomes Carneiro St., 96010-610, Pelotas, RS, Brazil

³Institute of Chemistry, Federal University of Rio Grande do Sul–UFRGS, Av. Bento Gonçalves 9500, P.O. Box 15003, 91501-970, Porto Alegre, RS, Brazil

*Corresponding author: Research Group on Adsorptive and Catalytic Process Engineering (ENGEpac), Federal University of Santa Maria, Av. Roraima, 1000-7, 97105–900 Santa Maria, RS, Brazil. Email: guilherme_dotto@yahoo.com.br

**Brilliant blue FCF dye adsorption using magnetic activated carbon from Sapelli wood
sawdust**

Victoria X. Nascimento¹, Diana Pinto², Sabrina F. Lütke¹, Maria C. F. da Silva¹, Fernando.

M. Machado³, Éder. C. Lima⁴, Luis F. O. Silva², Guilherme L. Dotto^{1*}

¹Research Group on Adsorptive and Catalytic Process Engineering (ENGEPAC), Federal University of Santa Maria, Av. Roraima, 1000-7, 97105–900 Santa Maria, RS, Brazil.

²Universidad de La Costa, CUC, Calle 58 # 55-56, 080002 Barranquilla, Atlántico, Colombia.

³Technology Development Center, Federal University of Pelotas–UFPEL, Gomes Carneiro St., 96010-610, Pelotas, RS, Brazil.

⁴Institute of Chemistry, Federal University of Rio Grande do Sul–UFRGS, Av. Bento Gonçalves 9500, P.O. Box 15003, 91501-970, Porto Alegre, RS, Brazil

*Corresponding author: Email: guilherme_dotto@yahoo.com.br

Abstract

Sapelli wood sawdust-derived magnetic activated carbon (SWSMAC) was produced by the single-step pyrolysis method using KOH and NiCl₂ as activating and magnetization agents. SWSMAC was characterized by several techniques (SEM/EDS, N₂ adsorption/desorption isotherms, FTIR, XRD, VSM, and pHpz) and applied in the brilliant blue FCF dye adsorption from an aqueous medium. The obtained SWSMAC was a mesoporous material and showed good textural properties. Metallic nanostructured Ni particles were observed. Also, SWSMAC exhibited ferromagnetic properties. In the adsorption experiments, the most adequate conditions were an adsorbent dosage of 0.75 g L⁻¹ and a solution pH of 4. The adsorption was fast, and the pseudo-second-order demonstrated greater suitability to the kinetic data. The equilibrium data were well fitted by the Sips model, and the maximum adsorption capacity predicted by this model was 111.50 mg g⁻¹ (at 55 °C). The thermodynamic study revealed that the adsorption was spontaneous, favorable, and endothermic. Besides, the mechanistic elucidation suggested that electrostatic interactions, hydrogen bonding, π–π interactions, and n–π interactions were involved in the brilliant blue FCF dye adsorption onto SWSMAC. In summary, an advanced adsorbent material was developed from waste by single-step pyrolysis, and this material effectively adsorbs brilliant blue FCF dye.

Keywords Adsorption mechanism; Anionic dye; Magnetic adsorbent; Low-cost biomass; Single-step pyrolysis.

Introduction

In the face of industrial advances, the water resources pollution has turned into a huge and challenging problem. Dyes are among the main water pollutants as they come from several industries, such as food, tannery, paper and pulp, textile, chemical, among others (Katheresan et al. 2018; Sultana et al. 2022). In the last years, wastewater containing dyes has become an important issue since they can cause deleterious impacts on the environment and human beings (Chikri et al. 2020). Synthetic dyes from the triphenylmethane class, such as brilliant blue FCF, malachite green, methyl violet, fast green, and patent blue V are widely used in the industry, accounting for about 30–40% (Adenan et al. 2022; Lucová et al. 2013; Mishra and Maiti 2018; Selvamani et al. 2021). Among the above-mentioned dyes, brilliant blue FCF dye is extensively used in the food and textile industries. This dye has high mobility in soil and groundwater. The dominantly anionic properties and the three sulfonic acid groups present in the dye molecule make it highly ionic and easily soluble in the aqueous medium (Germán-Heins and Flury 2000; Wang et al. 2020). The facile transport of this dye in soil and water can cause risks to the environment (Wang et al. 2020). In the aquatic ecosystem, the presence of a minimum amount of synthetic dyes can affect the transparency and gaseous solubility, causing effects on the photosynthetic activity and the food source of organisms (Pereira et al. 2021). Therefore, removing dyes from wastewater is a relevant issue regarding environment protection.

Literature reports different technologies for the removal of dyes from aqueous medium, such as flocculation/coagulation (Chenna et al. 2022), ion exchange (Cseri et al. 2021), biological treatments (Ruscasso et al. 2022), advanced oxidation processes (Nawaz et al. 2022), and adsorption (Wang et al. 2021). However, adsorption is a method that stands out since it has low cost, simple operation, high efficiency, and the possibility of regeneration of the adsorbent (Sultana et al. 2022). Activated carbon (AC) is the most well-known and used

adsorbent, since it has good textural characteristics and the presence of surface functional groups that can interact with the adsorbate molecules (Feiqiang et al. 2018; Illingworth et al. 2019). AC can be prepared from many different precursor materials, such as waste from agroindustries (Ramatshatsha-Makhwedzha et al. 2022), tire waste (Ali et al. 2021), and sawdust (Chikri et al. 2020), among others. Sawdust is an abundant and low-cost biomass with disposal problems (Chikri et al. 2020; Mallakpour et al. 2021), and is obtained from woodworking operations (Mallakpour et al. 2021). In Central Africa, the estimated annual production of the Sapelli species is 1.44 million m³ of round wood, making it the second most exploited species (RSR 2018). Consequently, high amounts of Sapelli wood sawdust are generated, having great potential to be used for AC production.

One of the issues related to the use of AC relies on the fact that when powdered AC is used, a high-performance centrifuge is frequently required for separation due to its small particle (Thue et al. 2020). Therefore, the introduction of magnetism into AC has gained attention (Feiqiang et al. 2018; Moosavi et al. 2020), since the simple use of an external magnetic field allows the adsorbent to be separated from the aqueous medium (Feiqiang et al. 2018; Moosavi et al. 2020). Regarding the available production methods of magnetic activated carbon (MAC), the single-step pyrolysis, in which the precursor material is impregnated with activating and magnetization agents and subsequently subjected to pyrolysis, stands out. In this method, carbonization, activation, and magnetization occur simultaneously, providing lower energy costs when compared to other methods, such as co-precipitation and impregnation of the AC and further pyrolysis (Thue et al. 2020).

In this research, MAC was produced from Sapelli wood sawdust using single-step pyrolysis and applied for the brilliant blue FCF dye adsorption from an aqueous medium. KOH was used to increase the textural properties, and NiCl₂ to produce the magnetic features. The material was characterized by different techniques. In addition, brilliant blue FCF dye

adsorption studies (kinetics, equilibrium, and thermodynamics) were carried out, and the possible adsorption mechanisms were proposed.

Materials and methods

Materials

Sapelli wood sawdust was obtained from sawmills in Ngaoundere (Cameroon). The brilliant blue FCF dye (C.I. 42090, molar weight 792.8 g mol⁻¹, λ_{max} 630.0 nm) was supplied by Duas Rodas company (Brazil). Other reagents used were of analytical grade.

Magnetic activated carbon preparation

Sapelli wood sawdust-derived magnetic activated carbon (SWSMAC) was prepared by a single-step pyrolysis method. The sample was first impregnated with KOH and NiCl₂ and, posteriorly, it was pyrolyzed in a conventional furnace (Sanchis, Brazil) at 600 °C. After the pyrolysis, the sample was cooled, acid-washed, and dried. More detail about the preparation process can be found in the Supplementary Material (S1).

Characterization

SWSMAC was characterized by the following techniques: Scanning Electron Microscopy coupled with Energy Dispersive X-Ray Spectroscopy, N₂ adsorption/desorption isotherms, Fourier Transform Infrared Spectroscopy, Vibrating Sample Magnetometer, X-ray powder diffraction, and point of zero charge. For more details, see Supplementary Material (S2).

Adsorption experiments

In the brilliant blue FCF dye adsorption experiments, firstly, dosage ($0.25\text{--}1.5 \text{ g L}^{-1}$) and pH (2–10) testes were performed. After defining the most adequate conditions, the adsorption kinetic curves were obtained using different initial dye concentrations (25–200 mg L^{-1}) at set time intervals (0–180 min). Finally, the equilibrium isotherms were also obtained using different initial dye concentrations (50–200 mg L^{-1}) and temperatures (25–55 °C). For more details on the adsorption experiments, see Supplementary Material (S3).

Kinetic, equilibrium, and thermodynamic modeling

See Supplementary Material (S4).

Results and Discussion

SWSMAC features

The SEM image of SWSMAC with a magnification of 5000 \times is shown in Fig. 1(a). It was observed that SWSMAC exhibited a porous structure with an irregular surface, some cavities, and roughness. The EDS spectrum of SWSMAC is shown in Fig. 1(b). The main elements of SWSMAC, as expected, are carbon (C), oxygen (O), and nickel (Ni). Ni indicates that, during the acid wash, the compounds formed by the decomposition of NiCl_2 were not eliminated. The Ni present in the sample is an important aspect because it generates magnetization.

The N_2 adsorption/desorption isotherms and the BJH pore size distributions obtained for SWSMAC are demonstrated in Fig. 2. The adsorption isotherm profile obtained (Fig. 2(a)) is Type IV, being representative of mesoporous materials (Thommes et al. 2015). The isotherm was accompanied by a Type H4 hysteresis loop, which is frequently related to

narrow slit-shaped pores (Thommes et al. 2015). The BET surface area was $331.54 \text{ m}^2 \text{ g}^{-1}$ and total pore volume was $0.095 \text{ cm}^3 \text{ g}^{-1}$. In addition, the average pore diameter was 3.60 nm. Therefore, according to IUPAC, SWSMAC is a mesoporous material because it presents an inner diameter between 2 nm and 50 nm (Thommes et al. 2015). The average pore diameter is an important feature since it shows whether or not the adsorbate molecules are able to penetrate the adsorbent particle. Since the brilliant blue FCF dye has molecular dimensions of $1.07 \text{ nm} \times 1.47 \text{ nm} \times 1.88 \text{ nm}$ (Tamai et al. 1999), it can be concluded that SWSMAC is suitable for its adsorption because it presents a pore diameter larger than the dimensions of the brilliant blue FCF dye molecule.

Fig. 3 shows the XRD pattern of SWSMAC. Patterns of metallic Ni (crystalline system: cubic; JCPDS Card 00-004-0850) and silicon oxide (SiO_2 ; crystalline system: hexagonal; JCPDS Card 00-046-1045) can be observed. Metallic Ni is formed from the reduction of Ni^{2+} previously impregnated, which occurs due to the high temperature and reducing gases that are present during the pyrolysis (Thue et al. 2020). From Scherrer's equation, it was possible to verify that the obtained nanostructured Ni particles had an average crystallite size of 25.34 nm. The presence of SiO_2 in the sample comes from the Sapelli wood sawdust.

Fig. 4 shows the magnetization curve of SWSMAC. It is possible to observe a S-shaped hysteresis loop, which indicates that the material shows ferromagnetism (Kaur et al. 2021). Furthermore, the value of coercivity was 200.2 Oe, saturation magnetization was 13.6 emu g^{-1} , and remanence was 4.1 emu g^{-1} .

Fig. 5 shows the FTIR spectrum of SWSMAC before and after the dye adsorption. In the spectra before the adsorption (Fig. 5(a)), the band observed at 3448 cm^{-1} indicates the stretching of $-\text{OH}$ bonds from oxygenated surface functional groups, such as alcohols, phenols, or carboxyls or it can also refer to adsorbed water (Ogungbenro et al. 2020). The

band at 1619 cm^{-1} is attributed to the stretching of C=O bonds from carboxylic acids or esters (Thue et al. 2020). In 1562 cm^{-1} , the observed band is due to the stretching of C=C bonds of the aromatic rings of the material (Nizam et al. 2021). Finally, the band at 1039 cm^{-1} is related to the stretching of C–O bonds (Thue et al. 2020). After the adsorption, it is possible to observe small changes in some bands (Fig. 5(b)). These changes can indicate the participation of some functional groups in the brilliant blue FCF dye adsorption and possible interaction mechanisms. These interactions will be scrutinized in subsection 3.5.

The determination of point of zero charge (pH_{PZC}) of SWSMAC is presented in Fig. 6. The pH_{PZC} value indicates the surface charge of the adsorbent material at a given pH, whether it is positive or negative, making it possible to know the adequate pH region for the removal of anionic or cationic adsorbates. Under conditions where $\text{pH} < \text{pH}_{\text{PZC}}$, the adsorbent acquires a positive surface charge, promoting the adsorption of anionic species. On the other hand, when $\text{pH} > \text{pH}_{\text{PZC}}$, the adsorbent material takes on a negative surface charge, being more suitable for the adsorption of cationic species (Machado et al. 2020). Then, considering the estimated pH_{PZC} for SWSMAC ($\text{pH}_{\text{PZC}} = 7.0$), it can be assumed that the material has positive surface charge at the acidic pH region and a negative surface charge at the alkaline pH region.

Adsorbent dosage and pH effects on brilliant blue FCF dye adsorption

The effect of the SWMAC dosage on the brilliant blue FCF dye adsorption is shown in Fig. 7. It was observed a typical tendency of increasing removal percentage with increasing SWSMAC dosage. The removal percentage abruptly increased to the dosage of 1.00 g L^{-1} , which is due to the increased amount of adsorption sites with higher adsorbent masses. From 1.00 g L^{-1} , there was no remarkable increase in the removal percentage, and at the dosage of 1.75 g L^{-1} , the removal percentage was almost 100%. Regarding the adsorption capacity, an inverse behavior was observed. A decrease from around 57 mg g^{-1} to around 32 mg g^{-1} was

observed with the increasing adsorbent dosage from 0.25 to 1.50 g L⁻¹. This behavior is possible due to some adsorption sites remaining unoccupied when using high SWMAC dosages, resulting in an overdosage (Netto et al. 2022). Thus, considering the intersection value, the adsorbent dosage of 0.75 g L⁻¹ was selected for further experiments. In this dosage, an adsorption capacity value of around 53 mg g⁻¹ and a removal percentage of around 82% were obtained.

The control of pH of the solution is a very relevant in an adsorption process since it affects the ionization of the surface functional groups, affecting the surface charge of the adsorbent, and also affects the ionic form of the adsorbate (Bonilla-Petriciolet et al. 2019). Fig. 8 shows the effect of the pH of the solution on the adsorption capacity of the brilliant blue FCF dye. The higher adsorption capacity value (around 58 mg g⁻¹) was obtained at pH 4. With increasing pH from 4 to 10, the adsorption capacity decreased. Likewise, with decreasing pH from 4 to 2, there was also a decrease in the adsorption capacity. These trends can be explained based on the pH_{PZC} of SWMAC, established as 7.0 (Fig. 6). At pH 4, SWMAC has a positive surface charge, which favors the adsorption of the anionic brilliant blue FCF dye molecules. As the pH of the solution increases, the amount of positively charged surface functional groups decreases until, from pH 7, the surface of the adsorbent becomes negatively charged due to the deprotonation of some surface functional groups. This behavior results in the electrostatic repulsion with the anionic brilliant blue FCF dye and, consequently, in the decrease of the adsorption capacity. At a very low pH value (pH = 2), despite the positive surface charge of SWMAC, there was a decrease in the adsorption capacity. This decrease can be explained due to the excess of H₃O⁺ (hydronium ions) and the consequent neutralization of the -SO₃⁻ groups of the brilliant blue FCF dye molecule (Heydari et al. 2016; Lim et al. 2021; Mittal et al. 2009). Since the best adsorption capacity

was found at pH 4, this condition was selected for carrying out the subsequent adsorption studies.

Kinetic results

In the adsorption kinetic study, experiments were carried out in different contact times (0–180 min) using different initial dye concentrations (25, 50, 100, 150, and 200 mg L⁻¹). Pertinent information about the adsorption process, such as the adsorption rate, the time taken to reach the equilibrium, and the mass transfer parameters, can be obtained from the kinetic study. Therefore, it is very important to carry out adsorption kinetic studies (Bonilla-Petriciolet et al. 2019, 2017). The kinetic curves obtained for the brilliant blue FCF dye adsorption onto SWSMAC are shown in Fig. 9. The adsorption was very fast in the first 20 minutes for all initial concentrations. Afterward, there was no significant change in the brilliant blue FCF dye adsorption capacity, that is, the system reached the equilibrium. The behavior described above is due to the SWSMAC presenting fully available adsorption sites at the beginning of the process, filling over time until reaching equilibrium (Diel et al. 2021). In addition, an increase in the adsorption capacity was observed with increasing initial dye concentration. However, this increase was less pronounced when considering the initial dye concentrations of 100, 150, and 200 mg L⁻¹. Therefore, it can be concluded that with an initial concentration of 100 mg L⁻¹, the available adsorption sites are almost completely occupied and close to saturation.

The kinetic models of pseudo-first-order (PFO) and pseudo-second-order (PSO) models were used for fitting the experimental data. The estimated kinetic parameters are depicted in Table 1. With the highest values of R^2 and R^2_{adj} and lowest values of ARE, the PSO model proved to be the most adequate to represent the kinetic data of the brilliant blue FCF dye adsorption onto SWSMAC, suggesting that the adsorption occurs through external

and internal mass transfer mechanisms (Ho and Mckay 1998; Qiu et al. 2009). Furthermore, Arabkhani et al. (2021) and Şenol et al. (2020) also found that the PSO model was the best model to represent the kinetic data of the brilliant blue FCF dye adsorption onto magnetic tungsten disulfide/carbon nanotubes nanocomposite and chitosan-vermiculite beads, respectively. Besides, as shown in Table 1, the theoretical adsorption capacities predicted by the PSO model (q_2) are very close to the experimental values (q_{exp}), corroborating with the suitability of this model.

Isotherms and thermodynamics results

Adsorption equilibrium isotherms are of fundamental importance since they indicate the quality of the adsorbent by determining the maximum adsorption capacity, giving information regarding the adsorption mechanism, and providing the necessary information for estimating the thermodynamic parameters (Bonilla-Petriciolet et al. 2019, 2017). Fig. 10 shows the equilibrium curves obtained for the brilliant blue FCF dye adsorption onto SWSMAC at different temperatures with initial dye concentrations from 50 to 200 mg L⁻¹. According to the Giles classification, the obtained adsorption isotherms are L2 type (Langmuir type) (Giles et al. 1974). The plateau in the curve identifies the maximum adsorption capacity, as indicated by subclass "2". Besides, the L-type isotherm also suggests a high affinity between the adsorbate molecules and the adsorption sites of the adsorbent (Giles et al. 1974).

It was possible to observe that the increase in temperature positively affected the brilliant blue FCF dye adsorption onto SWSMAC. When the temperature was increased from 25 °C to 55 °C, there was an increase in the adsorption capacity from around 70 mg g⁻¹ to around 90 mg g⁻¹ (considering the initial dye concentration of 200 mg L⁻¹). This behavior suggests that the brilliant blue FCF dye adsorption was endothermic.

Langmuir, Freundlich, and Sips' models were adjusted to the experimental data. Table 2 shows the equilibrium parameters obtained. Due to the higher R^2 and R^2_{adj} values and the lower ARE values, the Sips model was proved to be the most suitable to represent the experimental equilibrium data. Besides, it is worth mentioning that the q_s and k_s values increased with increasing temperature, corroborating the information that there was a favoring of the adsorption process at higher temperatures. At 55 °C, the q_s value was 111.50 mg g⁻¹. Arabkhani et al. (2021), for instance, synthesized a magnetic tungsten disulfide/carbon nanotubes nanocomposite and found a maximum adsorption capacity value of the brilliant blue FCF dye of 166.7 mg g⁻¹. Şenol et al. (2020), using chitosan-vermiculite beads to remove the brilliant blue FCF dye, found a maximum adsorption capacity of 181.6 mg g⁻¹. Hernández-Hernández et al. (2013), on the other hand, found maximum adsorption capacity values of 6.16 mg g⁻¹ and 14.22 mg g⁻¹ in the brilliant blue FCF dye adsorption using unmodified clay and iron-modified clay, respectively. Therefore, based on the above comparison, SWSMAC exhibited a satisfactory adsorption capacity, showing to be a promising candidate for the removal of the brilliant blue FCF dye from aqueous solution.

The thermodynamic parameters (ΔG° , ΔS° , and ΔH°) of the brilliant blue FCF dye adsorption onto SWSMAC are shown in Table 3. Since it was verified that the Sips model was the most adequate isotherm model, the Sips equilibrium constant (k_s) was used to calculate the thermodynamic equilibrium constant (K_D). The R^2 value of the Van't Hoff graph was 0.9759 (see Fig. S1 in the Supplementary Material).

The negative ΔG° values (-33.42 to -40.15 kJ mol⁻¹) indicated that the brilliant blue FCF dye adsorption onto SWSMAC was a thermodynamically favorable process. Besides, it can be stated that the adsorption under study was more spontaneous at higher temperatures since more negative ΔG° values were obtained with increasing temperature. The positive ΔH° value asserted that the brilliant blue FCF dye adsorption was endothermic, agreeing with the

previously observed temperature dependence. In addition, the magnitude of the ΔH° value (33.40 kJ mol⁻¹) corroborates with the occurrence of physisorption (Bonilla-Petriciolet et al. 2017). The positive ΔS° value indicated that the disorder at the solid-liquid interface increased during the adsorption. This is due to displacement of the coordinated water molecules by the adsorbate molecules during adsorption. The water molecules acquire more translational entropy than is lost by the adsorbate molecules, resulting in greater randomness in the adsorbate-adsorbent interaction (Kyzas et al. 2012). In addition, since only the ΔS° contributed to obtaining negative ΔG° values, it was possible to conclude that the brilliant blue FCF dye adsorption onto SWSMAC was an entropy-controlled phenomenon (Lütke et al. 2019). Arabkhani et al. (2021) and Gupta et al. (2006) found similar thermodynamic results for the brilliant blue FCF dye adsorption.

Adsorption mechanism elucidation

The adsorption mechanism of the brilliant blue FCF onto SWSMAC was elucidated from changes verified on the FTIR spectra of SWSMAC before and after the adsorption and the characteristics of the molecular structure of the brilliant blue FCF dye. In addition, different interaction mechanisms were here considered, such as electrostatic interactions, hydrogen bonding interactions, $\pi-\pi$ interactions, and $n-\pi$ interactions (Nizam et al. 2021; Tran et al. 2017; Ullah et al. 2022; Wang et al. 2022).

Firstly, as previously discussed, at pH 4.0, the SWSMAC's surface becomes positively charged since some surface functional groups, such as hydroxyl groups, are protonated. Therefore, electrostatic interactions can occur due to attraction between these surface functional groups with positive charges and the sulfonate groups (SO_3^-) of the brilliant blue FCF dye molecule, which are negatively charged. Furthermore, since the adsorption capacity was highly influenced by the pH of the solution (Fig. 8), the important role of the electrostatic

interactions in the brilliant blue FCF dye adsorption onto SWSMAC is suggested. However, other types of interactions must be considered.

Another possible adsorption interaction is the hydrogen bonding interaction. In this type of interaction, the hydrogen atoms from hydroxyl groups of the adsorbent tend to interact with electronegative atoms of the adsorbent's structure (Nizam et al. 2021; Tran et al. 2017; Ullah et al. 2022). In the case reported here, interactions can be formed between the hydrogen of the –OH groups from the SWSMAC's surface and the electronegative nitrogen and oxygen atoms of the brilliant blue FCF dye molecule. Fig. 5 shows that, after the adsorption, the band at 3448 cm^{-1} (assigned to the hydroxyl functional groups), becomes more intense. This trend indicates that, possibly, there were hydrogen bonding interactions between the brilliant blue FCF dye molecule and the SWSMAC.

$\pi-\pi$ interactions involve the aromatic rings present in the adsorbate and activated carbon structure (Nizam et al. 2021; Tran et al. 2017). Regarding this type of interaction, in Fig. 5, it is possible to notice a change in the band assigned to the C=C bonds (1562 cm^{-1} in the FTIR spectra before the adsorption and 1564 cm^{-1} in the FTIR spectra after the adsorption). This observation can be related to the occurrence of $\pi-\pi$ interactions.

Finally, in $n-\pi$ interactions, lone pairs of electrons (n) from the adsorbent's oxygen functional groups interact with the aromatic rings (π) of the adsorbate molecules (Tran et al. 2017). The FTIR spectra (Fig. 5) showed an abrupt decrease in the intensity of the C–O bonds (1039 cm^{-1} in the FTIR spectra before the adsorption and 1035 cm^{-1} in the FTIR spectra after the adsorption) after adsorption, suggesting that this groups possibly participate in $n-\pi$ interactions.

The proposed interaction mechanisms between the brilliant blue FCF dye molecules and the SWSMAC are illustrated in Fig. 11.

Conclusion

In the present study, Sapelli wood sawdust-derived magnetic activated carbon was produced by the single-step pyrolysis method, characterized, and applied in the brilliant blue FCF dye adsorption. The detailed characterization of the material showed a successful synthesis. SWSMAC exhibited mesoporous structure, good BET surface area ($331.54\text{ m}^2\text{ g}^{-1}$) and total pore volume ($0.095\text{ cm}^3\text{ g}^{-1}$), nanostructured Ni particles with average crystallite size of 25.34 nm, and ferromagnetic properties. Regarding the adsorption experiments, the best results were obtained with a dosage of 0.75 g L^{-1} and pH 4.0. The kinetic study showed that the adsorption was very fast, and the equilibrium was reached in around 20 minutes. Pseudo-second-order model provided the best fit for the experimental kinetic data. From the equilibrium study, it was verified that the Sips model was the most adequate, and the maximum adsorption capacity was 111.50 mg g^{-1} (at $55\text{ }^\circ\text{C}$). The thermodynamic investigation indicated favorable, spontaneous, and endothermic adsorption. Moreover, it was proposed that the adsorption mechanism of the brilliant blue FCF dye onto SWSMAC involved electrostatic interactions, hydrogen bonding, $\pi-\pi$ interactions, and n– π interactions.

Thereby, the results found in this work demonstrated the possibility of using Sapelli wood sawdust-derived magnetic activated carbon as an alternative adsorbent for the brilliant blue FCF dye, with good efficiency and easy magnetic separation, contributing both to the management of waste generated in high amounts and the treatment of wastewater containing dyes.

References

Adenan NH, Lim YY, Ting ASY (2022) Removal of triphenylmethane dyes by Streptomyces bacillaris: A study on decolorization, enzymatic reactions and toxicity of treated dye

solutions. J Environ Manage 318:115520.

<https://doi.org/10.1016/j.jenvman.2022.115520>

Ali UFM, Hussin F, Gopinath SCB, Aroua MK, Khamidun MH, Jusoh N, Ibrahim N, Ahmad SFK (2021) Advancement in recycling waste tire activated carbon to potential adsorbents. *Environ Eng Res* 27:210452–0. <https://doi.org/10.4491/eer.2021.452>

Arabkhani P, Javadian H, Asfaram A, Sadeghfar F, Sadegh F (2021) Synthesis of magnetic tungsten disulfide/carbon nanotubes nanocomposite (WS₂/Fe₃O₄/CNTs-NC) for highly efficient ultrasound-assisted rapid removal of amaranth and brilliant blue FCF hazardous dyes. *J Hazard Mater* 420:126644. <https://doi.org/10.1016/j.jhazmat.2021.126644>

Bonilla-Petriciolet A, Mendoza-Castillo DI, Dotto GL, Duran-Valle CJ (2019) Adsorption in Water Treatment. *Chem Mol Sci Chem Eng* 1–19. <https://doi.org/10.1016/b978-0-12-409547-2.14390-2>

Bonilla-Petriciolet A, Mendoza-Castillo DI, Reynel-Ávila HE (2017) Adsorption Processes for Water Treatment and Purification. Springer International Publishing, Switzerland. <https://doi.org/https://doi.org/10.1007/978-3-319-58136-1>.

Chenna M, Kebaili M, Lardjane N, Drouiche N, Lounici H (2022) Modeling and Optimization by RSM for the Removal of the Dye "Palanil blue R" by Coagulation-Flocculation Process. *Int J Environ Res* 16:1–12. <https://doi.org/10.1007/s41742-022-00413-w>

Chikri R, Elhadiri N, Benchanaa M, El maguana Y (2020) Efficiency of sawdust as low-cost adsorbent for dyes removal. *J Chem* 2020:1–17. <https://doi.org/10.1155/2020/8813420>

Cseri L, Topuz F, Abdulhamid MA, Alammar A, Budd PM, Szekely G (2021) Electrospun Adsorptive Nanofibrous Membranes from Ion Exchange Polymers to Snare Textile Dyes from Wastewater. *Adv Mater Technol* 6:2000955. <https://doi.org/10.1002/admt.202000955>

- Diel JC, Franco DSP, Nunes IS, Pereira HA, Moreira KS, Burgo TAL, Foletto EL, Dotto GL (2021) Carbon nanotubes impregnated with metallic nanoparticles and their application as an adsorbent for the glyphosate removal in an aqueous matrix. *J Environ Chem Eng* 9:105178. <https://doi.org/10.1016/j.jece.2021.105178>
- Feiqiang G, Xiaolei L, Xiaochen J, Xingmin Z, Chenglong G, Zhonghao R (2018) Characteristics and toxic dye adsorption of magnetic activated carbon prepared from biomass waste by modified one-step synthesis. *Colloids Surfaces A Physicochem Eng Asp* 555:43–54. <https://doi.org/10.1016/j.colsurfa.2018.06.061>
- Freundlich H (1907) Über die Adsorption in Lösungen. *Zeitschrift für Phys Chemie* 57U:385–470. <https://doi.org/10.1515/zpch-1907-5723>
- Germán-Heins J, Flury M (2000) Sorption of Brilliant Blue FCF in soils as affected by pH and ionic strength. *Geoderma* 97:87–101. [https://doi.org/10.1016/S0016-7061\(00\)00027-6](https://doi.org/10.1016/S0016-7061(00)00027-6)
- Giles CH, Smith D, Huitson A (1974) A general treatment and classification of the solute adsorption isotherm. *J Colloid Interface Sci* 47:755–765. [https://doi.org/10.1016/0021-9797\(74\)90252-5](https://doi.org/10.1016/0021-9797(74)90252-5)
- Gupta VK, Mittal A, Krishnan L, Mittal J (2006) Adsorption treatment and recovery of the hazardous dye, Brilliant Blue FCF, over bottom ash and de-oiled soya. *J Colloid Interface Sci* 293:16–26. <https://doi.org/10.1016/j.jcis.2005.06.021>
- Hernández-Hernández KA, Solache-Ríos M, Díaz-Nava MC (2013) Removal of Brilliant Blue FCF from Aqueous Solutions Using an Unmodified and Iron-Modified Bentonite and the Thermodynamic Parameters of the Process. *Water, Air, Soil Pollut* 224:1562. <https://doi.org/10.1007/s11270-013-1562-9>
- Heydari R, Hosseini M, Alimoradi M, Zarabi S (2016) A Simple Method for Simultaneous Spectrophotometric Determination of Brilliant Blue FCF and Sunset Yellow FCF in

- Food Samples after Cloud Point Extraction. *J Chem Soc Pakistan* 38:438–445.
- Ho YS, Mckay G (1998) Kinetic models for the sorption of dye from aqueous solution by wood. *Process Saf Environ Prot* 76:183–191. <https://doi.org/10.1205/095758298529326>
- Illingworth JM, Rand B, Williams PT (2019) Non-woven fabric activated carbon produced from fibrous waste biomass for sulphur dioxide control. *Process Saf Environ Prot* 122:209–220. <https://doi.org/10.1016/j.psep.2018.12.010>
- Katheresan V, Kansedo J, Lau SY (2018) Efficiency of various recent wastewater dye removal methods: A review. *J Environ Chem Eng* 6:4676–4697. <https://doi.org/10.1016/j.jece.2018.06.060>
- Kaur J, Kaur M, Ubhi MK, Kaur N, Greneche JM (2021) Composition optimization of activated carbon-iron oxide nanocomposite for effective removal of Cr(VI)ions. *Mater Chem Phys* 258:124002. <https://doi.org/10.1016/j.matchemphys.2020.124002>
- Kyzas GZ, Lazaridis NK, Mitropoulos AC (2012) Removal of dyes from aqueous solutions with untreated coffee residues as potential low-cost adsorbents: Equilibrium , reuse and thermodynamic approach. *Chem Eng J* 189–190:148–159. <https://doi.org/10.1016/j.cej.2012.02.045>
- Langmuir I (1918) The adsorption of gases on plane surfaces of glass, mica and platinum. *J Am Chem Soc* 40:1361–1403. <https://doi.org/10.1021/ja02242a004>
- Lim S, Kim JH, Park H, Kwak C, Yang J, Kim J, Ryu SY, Lee J (2021) Role of electrostatic interactions in the adsorption of dye molecules by Ti₃C₂-MXenes. *RSC Adv* 11:6201–6211. <https://doi.org/10.1039/d0ra10876f>
- Lucová M, Hojerová J, PaŽoureková S, Klimová Z (2013) Absorption of triphenylmethane dyes Brilliant Blue and Patent Blue through intact skin, shaven skin and lingual mucosa from daily life products. *Food Chem Toxicol* 52:19–27. <https://doi.org/10.1016/j.fct.2012.10.027>

- Lütke SF, Igansi AV, Pegoraro L, Dotto GL, Pinto,LAA, Cadaval TRS (2019) Preparation of activated carbon from black wattle bark waste and its application for phenol adsorption. *J Environ Chem Eng* 7:103396. <https://doi.org/10.1016/j.jece.2019.103396>
- Machado LMM, Lütke SF, Perondi D, Godinho M, Oliveira MLS, Collazzo GC, Dotto GL (2020) Treatment of effluents containing 2-chlorophenol by adsorption onto chemically and physically activated biochars. *J Environ Chem Eng* 8:104473. <https://doi.org/10.1016/j.jece.2020.104473>
- Mallakpour S, Sirous F, Hussain CM (2021) Sawdust, a versatile, inexpensive, readily available bio-waste: From mother earth to valuable materials for sustainable remediation technologies. *Adv Colloid Interface Sci* 295:102492. <https://doi.org/10.1016/j.cis.2021.102492>
- Mishra S, Maiti A (2018) The efficacy of bacterial species to decolourise reactive azo, anthroquinone and triphenylmethane dyes from wastewater: a review. *Environ Sci Pollut Res* 25:8286–8314. <https://doi.org/10.1007/s11356-018-1273-2>
- Mittal A, Mittal J, Malviya A, Gupta V.K (2009) Adsorptive removal of hazardous anionic dye "Congo red" from wastewater using waste materials and recovery by desorption. *J Colloid Interface Sci* 340:16–26. <https://doi.org/10.1016/j.jcis.2009.08.019>
- Moosavi S, Lai CW, Gan S, Zamiri G, Akbarzadeh Pivehzhani O, Johan MR (2020) Application of efficient magnetic particles and activated carbon for dye removal from wastewater. *ACS Omega* 5:20684–20697. <https://doi.org/10.1021/acsomega.0c01905>
- Nawaz S, Siddique M, Khan R, Riaz N, Waheed U, Shahzadi I, Ali A (2022) Ultrasound-Assisted Hydrogen Peroxide and Iron Sulfate Mediated Fenton Process as an Efficient Advanced Oxidation Process for the Removal of Congo Red Dye. *Polish J Environ Stud* 31:2749–2761. <https://doi.org/10.15244/pjoes/144298>
- Netto MS, Georgin J, Franco DSP, Mallmann ES, Foletto EL, Godinho M, Pinto D, Dotto GL

- (2022) Effective adsorptive removal of atrazine herbicide in river waters by a novel hydrochar derived from *Prunus serrulata* bark. *Environ Sci Pollut Res* 29, 3672–3685. <https://doi.org/https://doi.org/10.1007/s11356-021-15366-4>
- Nizam NUM, Hanafiah MM, Mahmoudi E, Halim AA, Mohammad AW (2021) The removal of anionic and cationic dyes from an aqueous solution using biomass-based activated carbon. *Sci Rep* 11:8623. <https://doi.org/10.1038/s41598-021-88084-z>
- Ogungbenro AE, Quang DV, Al-Ali KA, Vega LF, Abu-Zahra MRM (2020) Synthesis and characterization of activated carbon from biomass date seeds for carbon dioxide adsorption. *J Environ Chem Eng* 8:104257. <https://doi.org/10.1016/j.jece.2020.104257>
- Pereira AGB, Rodrigues FHA, Paulino AT, Martins AF, Fajardo AR (2021) Recent advances on composite hydrogels designed for the remediation of dye-contaminated water and wastewater: A review. *J Clean Prod* 284:124703 Contents. <https://doi.org/10.1016/j.jclepro.2020.124703>
- Qiu H, Lv L, Pan BC, Zhang QJ, Zhang WM, Zhang QX (2009) Critical review in adsorption kinetic models. *J Zhejiang Univ Sci A* 10:716–724. <https://doi.org/10.1631/jzus.A0820524>
- Ramutshatsha-Makhwedzha D, Mavhungu A, Moropeng ML, Mbaya R (2022) Activated carbon derived from waste orange and lemon peels for the adsorption of methyl orange and methylene blue dyes from wastewater. *Heliyon* 8, e09930. <https://doi.org/10.1016/j.heliyon.2022.e09930>
- RSR, 2018. Vision Stratégique et Industrialisation de la Filière Bois dans les 6 pays du Bassin du Congo Horizon 2030. FRM Ingénierie.
- Ruscasso F, Cavello I, Curutchet G, Cavalitto S (2022) Antarctic yeasts: potential use in a biologic treatment of textile azo dyes. *Bioresour Bioprocess* 9:1–12. <https://doi.org/10.1186/s40643-022-00507-5>

- Selvamani T, Anandan S, Asiri AM, Maruthamuthu P, Ashokkumar M (2021) Preparation of MgTi₂O₅ nanoparticles for sonophotocatalytic degradation of triphenylmethane dyes. Ultrason Sonochem 75:105585. <https://doi.org/10.1016/j.ultsonch.2021.105585>
- Şenol ZM, Gürsoy N, Şimşek S, Özer A, Karakuş N (2020) Removal of food dyes from aqueous solution by chitosan- vermiculite beads. Int J Biol Macromol 148:635–646. <https://doi.org/10.1016/j.ijbiomac.2020.01.166>
- Sips R (1948) On the Structure of a Catalyst Surface. J Chem Phys 16:490–495. <https://doi.org/doi.org/10.1063/1.1746922>
- Sultana M, Rownok MH, Sabrin M, Rahaman MH, Alam SMN (2022) A review on experimental chemically modified activated carbon to enhance dye and heavy metals adsorption. Clean Eng Technol 6:100382. <https://doi.org/10.1016/j.clet.2021.100382>
- Tamai H, Yoshida T, Sasaki M, Yasuda H (1999) Dye adsorption on mesoporous activated carbon fiber obtained from pitch containing yttrium complex. Carbon 37:983–989. [https://doi.org/10.1016/S0008-6223\(98\)00294-2](https://doi.org/10.1016/S0008-6223(98)00294-2)
- Thommes M, Kaneko K, Neimark AV, Olivier JP, Rodriguez-Reinoso F, Rouquerol J, Sing KSW (2015) Physisorption of gases, with special reference to the evaluation of surface area and pore size distribution (IUPAC Technical Report), Pure and Applied Chemistry. <https://doi.org/10.1515/pac-2014-1117>
- Thue PS, Umpierres CS, Lima EC, Lima DR, Machado FM, dos Reis GS, da Silva RS, Pavan FA, Tran HN (2020) Single-step pyrolysis for producing magnetic activated carbon from tucum (*Astrocaryum aculeatum*) seed and nickel(II) chloride and zinc(II) chloride. Application for removal of nicotinamide and propanolol. J Hazard Mater 398:122903. <https://doi.org/10.1016/j.jhazmat.2020.122903>
- Tran HN, Wang YF, Youb SJ, Chao HP (2017) Insights into the mechanism of cationic dye adsorption on activated charcoal: The importance of π–π interactions. Process Saf

Environ Prot 107:168–180. <https://doi.org/10.1016/j.psep.2017.02.010>

Ullah F, Ji G, Irfan M, Gao Y, Shafiq F, Sun Y, Ain QU, Li A (2022) Adsorption performance and mechanism of cationic and anionic dyes by KOH activated biochar derived from medical waste pyrolysis. Environ Pollut 314:120271. <https://doi.org/10.1016/j.envpol.2022.120271>

Wang H, Li Z, Yahyaoui S, Hanafy H, Seliem MK, Bonilla-Petriciolet A, Dotto GL, Sellaoui L, Li Q (2021) Effective adsorption of dyes on an activated carbon prepared from carboxymethyl cellulose: Experiments, characterization and advanced modelling. Chem Eng J 417:128116. <https://doi.org/10.1016/j.cej.2020.128116>

Wang Q, Luo C, Lai Z, Chen S, He D, Mu J (2022) Honeycomb-like cork activated carbon with ultra-high adsorption capacity for anionic, cationic and mixed dye: Preparation, performance and mechanism. Bioresour Technol 357:127363. <https://doi.org/10.1016/j.biortech.2022.127363>

Wang Y, Li Y, Zhang Y, Wei W (2020) Enhanced brilliant blue FCF adsorption using microwave-hydrothermal synthesized hydroxyapatite nanoparticles. J Dispers Sci Technol 41:1346–1355. <https://doi.org/10.1080/01932691.2019.1623695>

Figure captions

Fig. 1 (a) SEM image and (b) EDS spectrum of SWSMAC.

Fig. 2 (a) Nitrogen adsorption/desorption isotherms and (b) BJH pore size distribution of SWSMAC.

Fig. 3 XRD pattern of SWSMAC.

Fig. 4 M-H hysteresis loop of SWSMAC at room temperature. The inset is a magnified view of the M-H curve.

Fig. 5 FTIR vibrational spectra of SWSMAC (a) before and (b) after the brilliant blue FCF dye adsorption.

Fig. 6 Determination of the pH_{PZC} of SWSMAC.

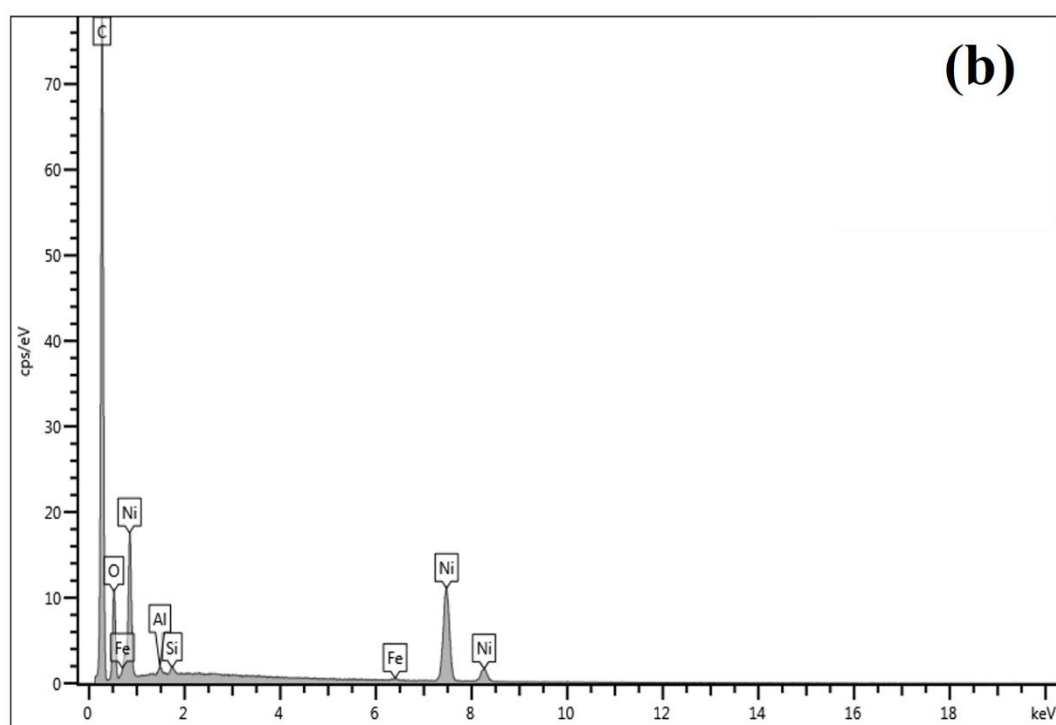
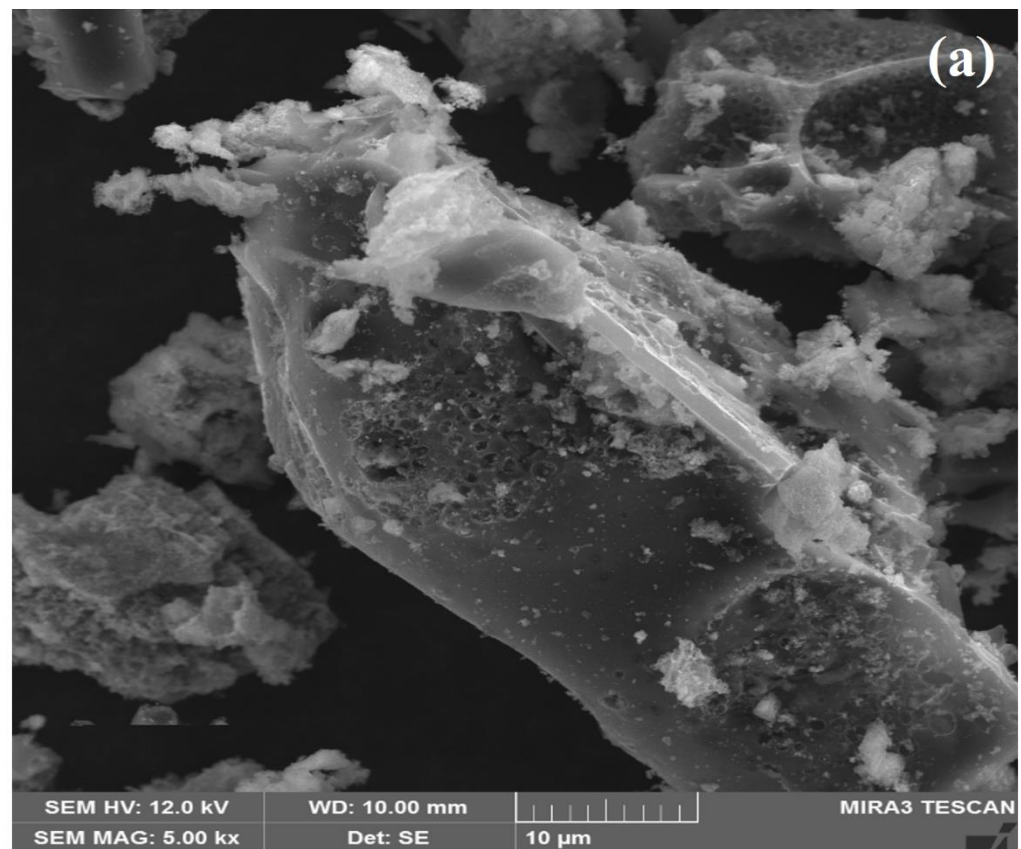
Fig. 7 Effect of SWSMAC dosage in the brilliant blue FCF dye adsorption.

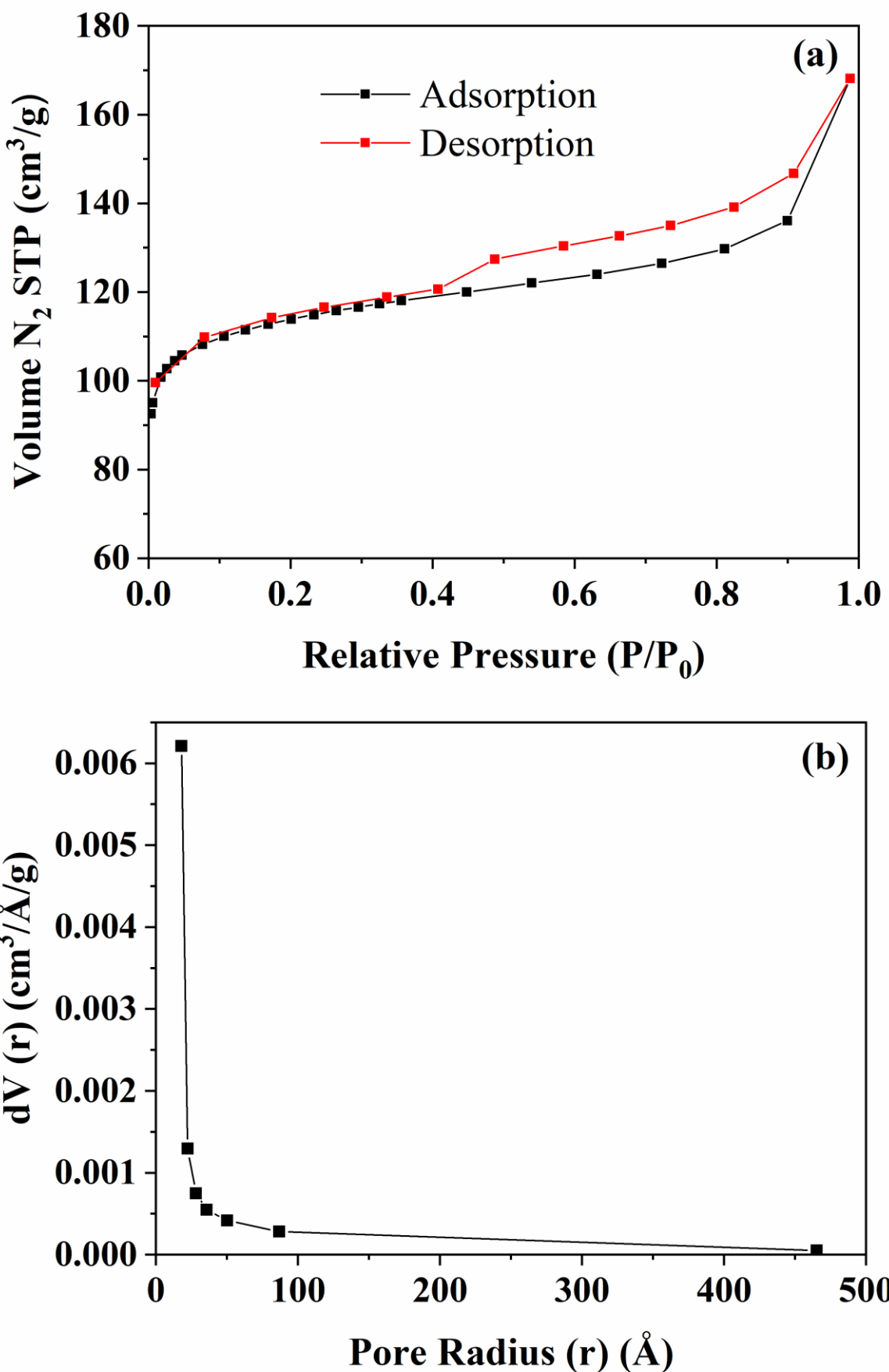
Fig. 8 Effect of the pH of the solution in the brilliant blue FCF dye adsorption.

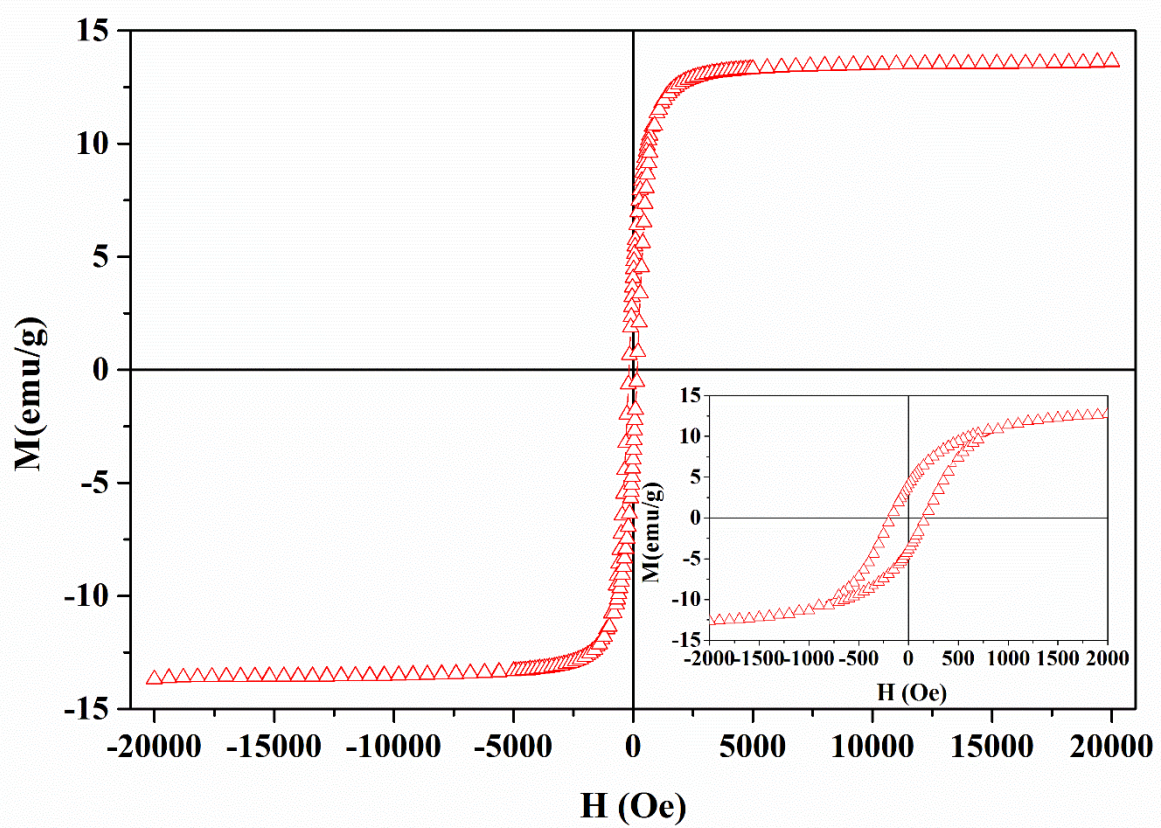
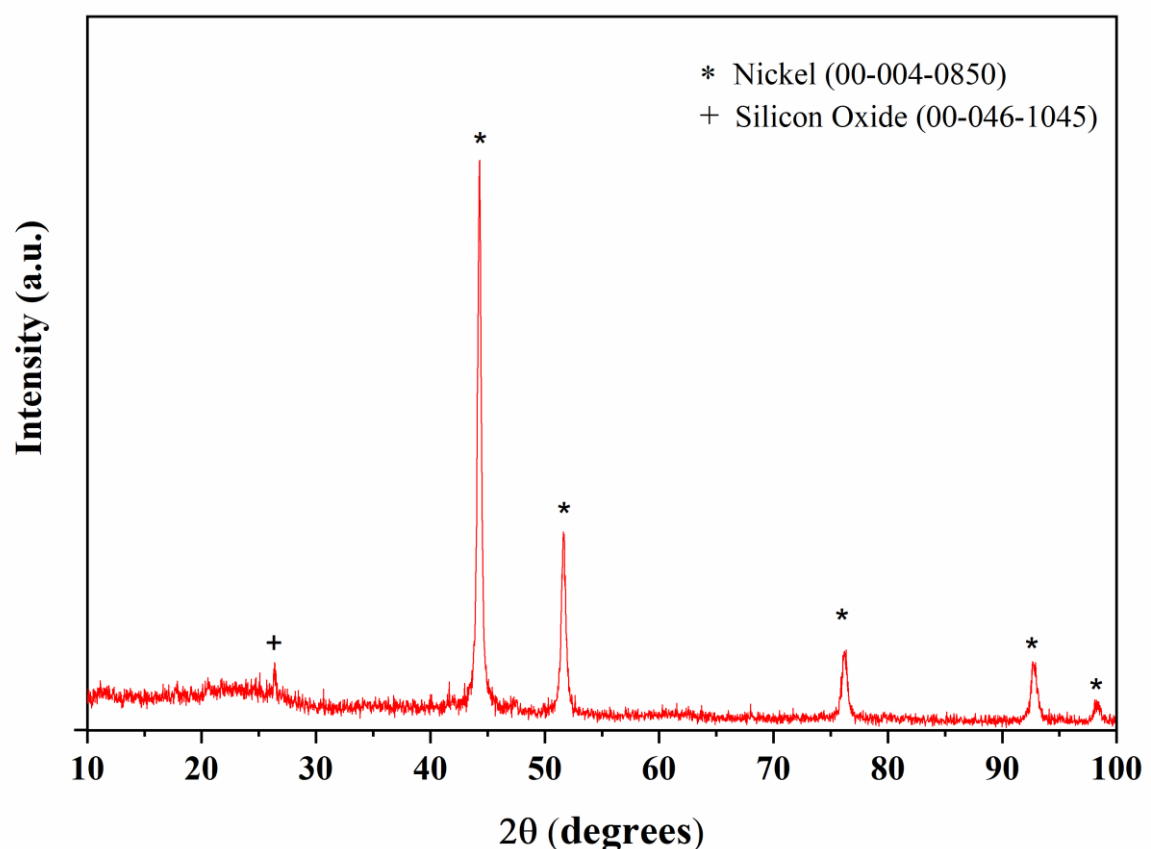
Fig. 9 Kinetic curve of the brilliant blue FCF dye adsorption onto SWSMAC.

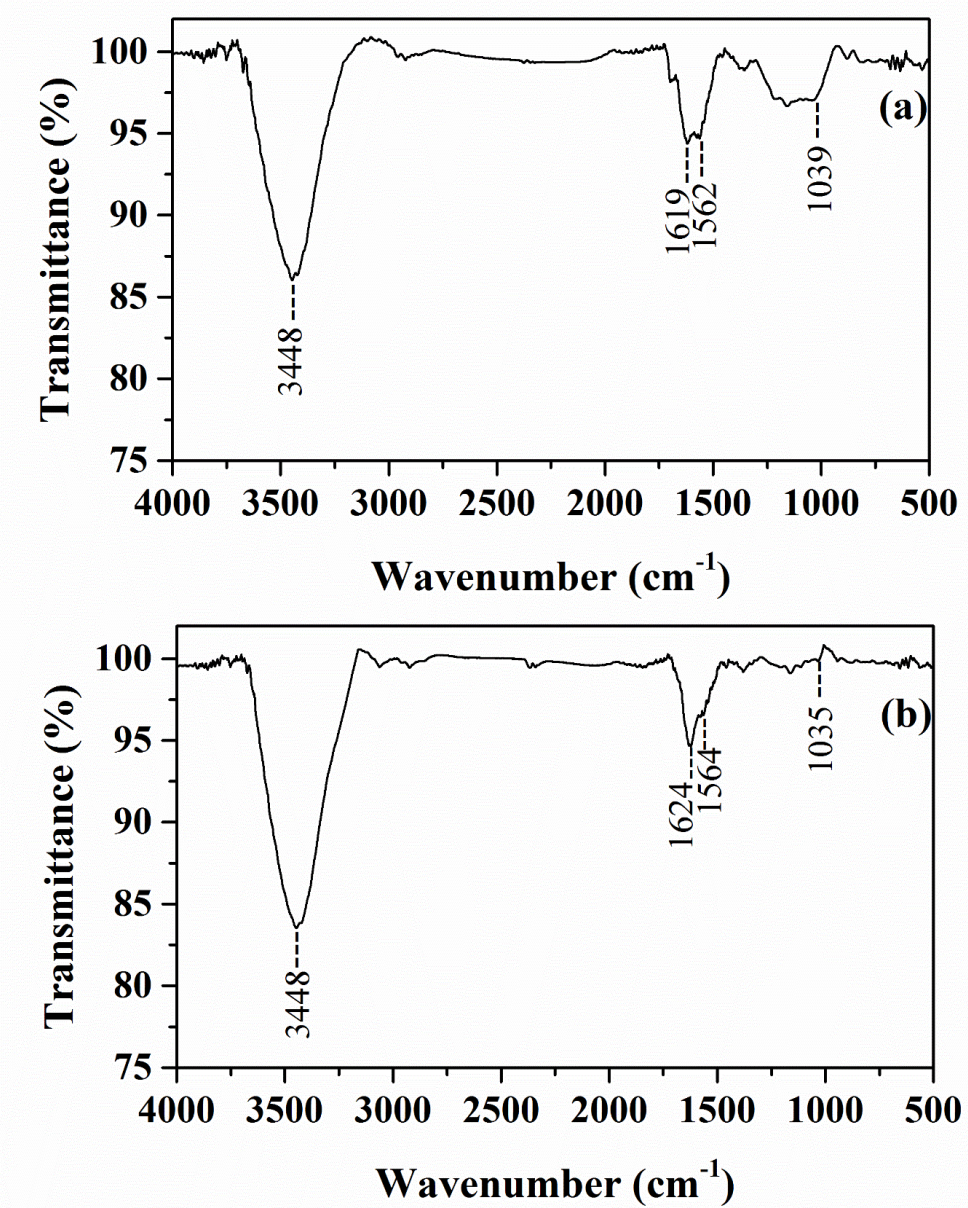
Fig. 10 Equilibrium isotherms of the brilliant blue FCF dye adsorption onto SWSMAC.

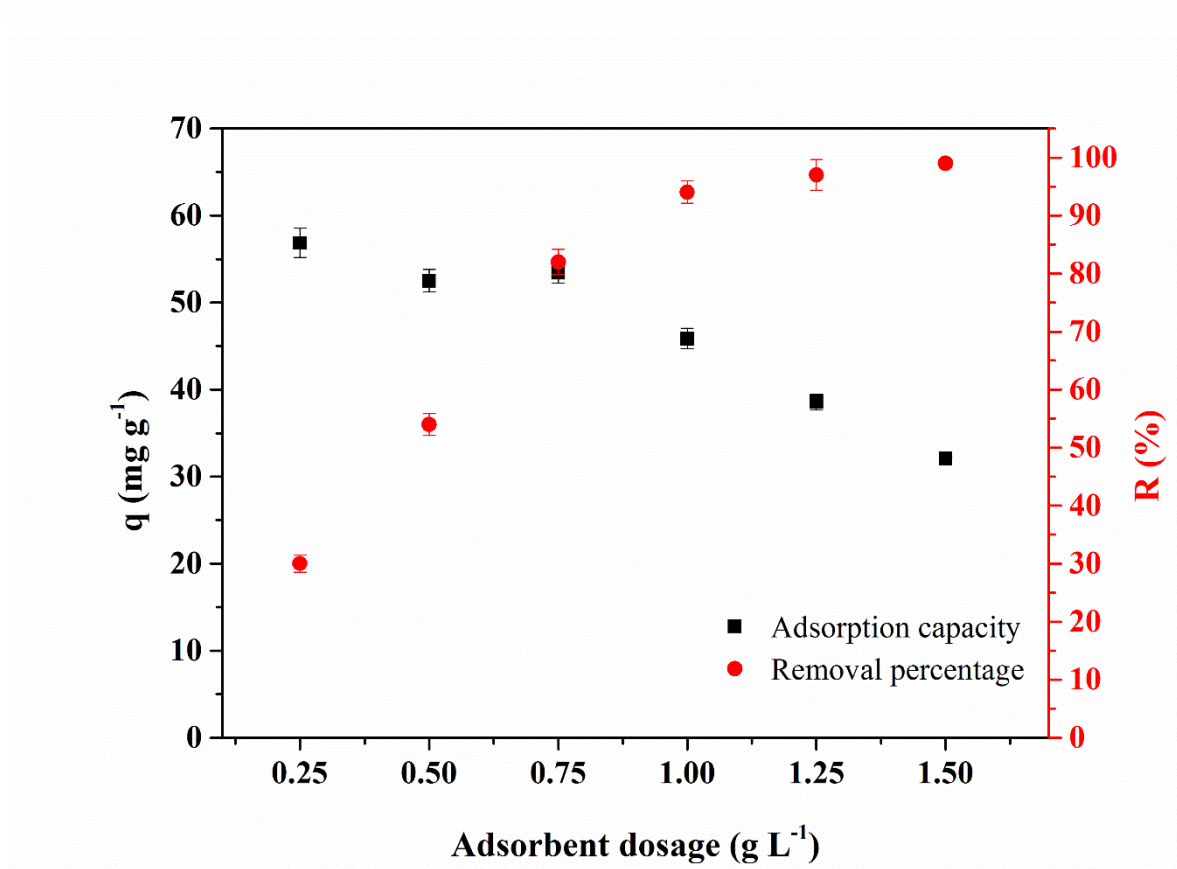
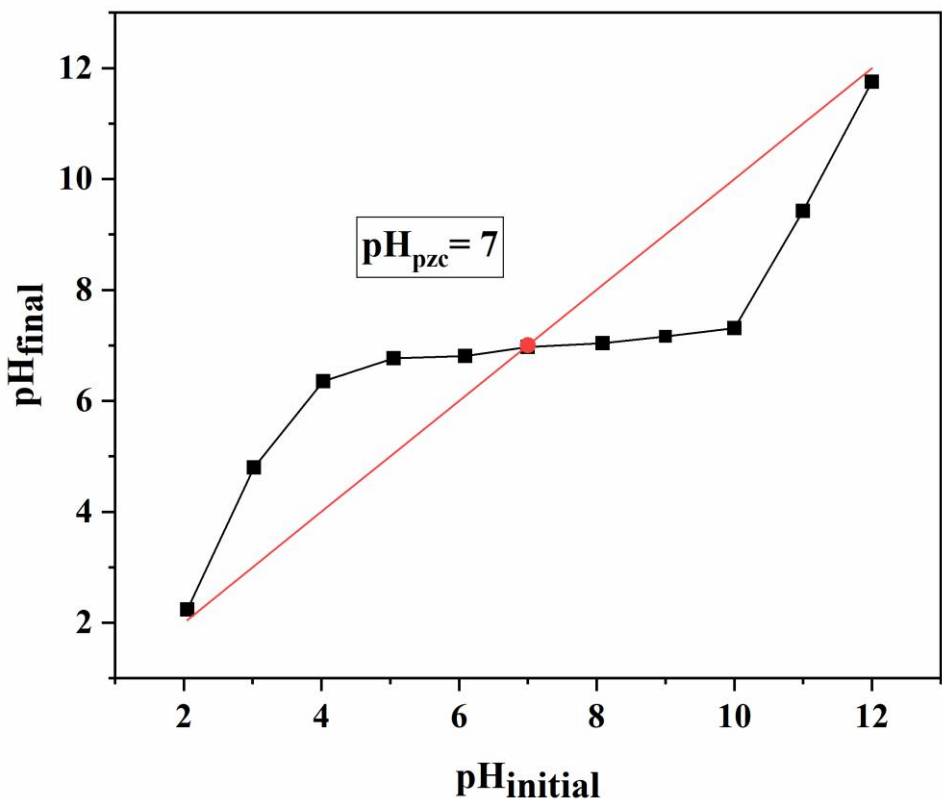
Fig. 11 Proposed adsorption interactions of the brilliant blue FCF dye onto SWSMAC.

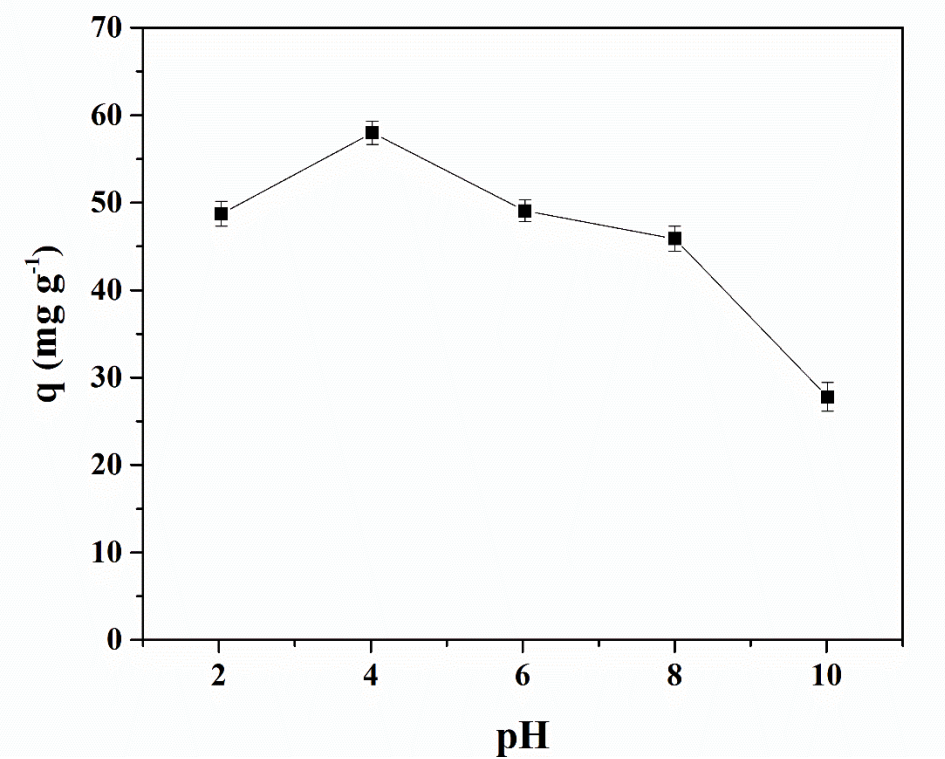


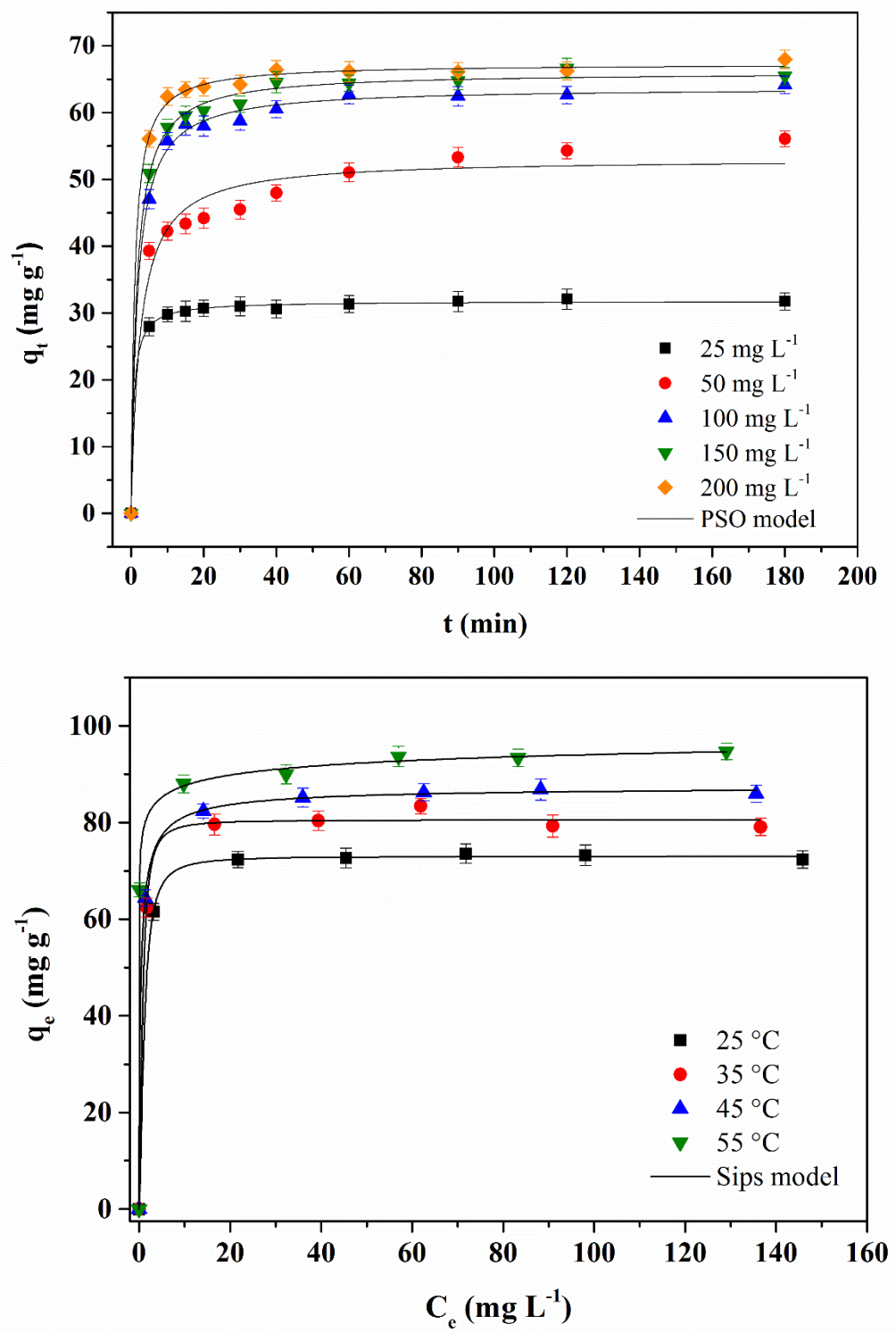












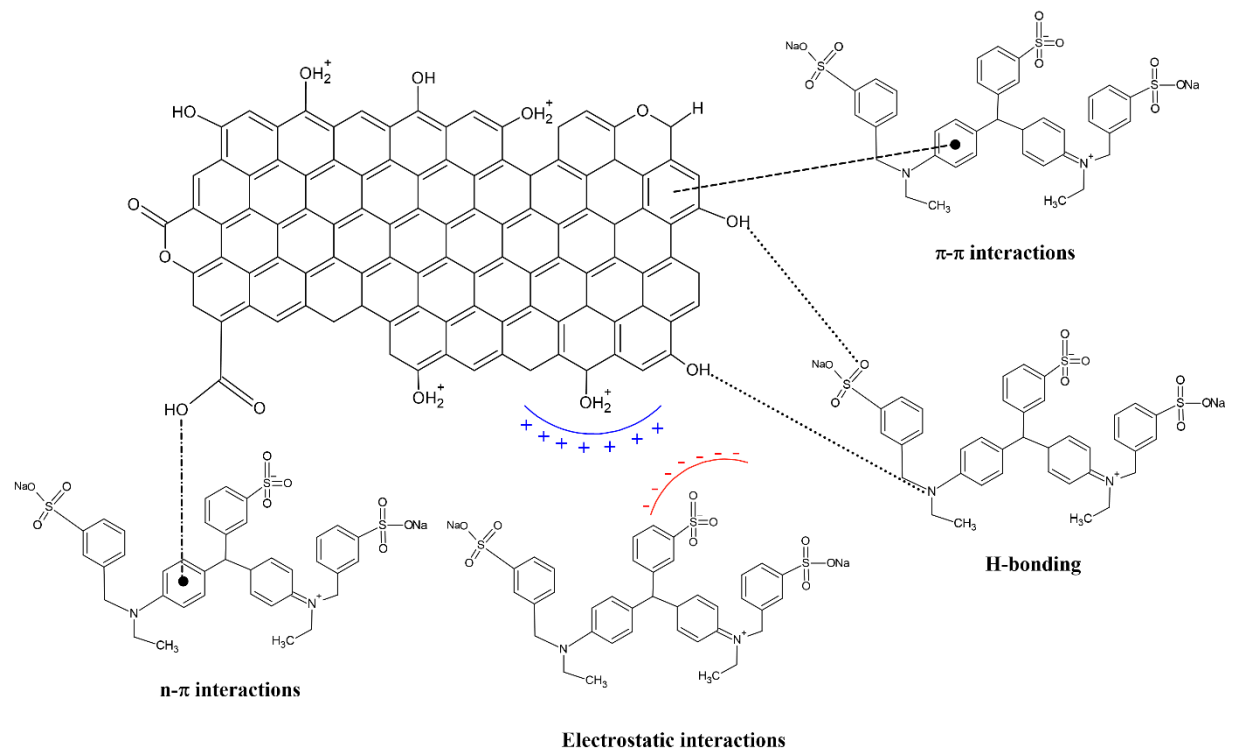


Table captions

Table 1. Kinetic parameters of the brilliant blue FCF dye adsorption

Table 2. Equilibrium parameters of the brilliant blue FCF dye adsorption.

Table 3. Thermodynamic parameters of the brilliant blue FCF dye adsorption

Table 1. Kinetic parameters of the brilliant blue FCF dye adsorption.

Model	Initial brilliant blue dye concentration (mg L^{-1})				
	25	50	100	150	200
Pseudo-first-order					
$q_1 (\text{mg g}^{-1})$	31.09	49.60	61.03	63.36	65.46
$k_1 (\text{min}^{-1})$	0.4456	0.2537	0.2769	0.3000	0.3757
R^2	0.9957	0.9253	0.9890	0.9861	0.9952
R^2_{adj}	0.9946	0.9066	0.9862	0.9826	0.9940
$ARE (\%)$	1.60	7.56	2.76	3.15	1.73
Pseudo-second-order					
$q_2 (\text{mg g}^{-1})$	31.78	53.10	63.76	66.06	67.30
$k_2 (\text{g mg}^{-1} \text{ min}^{-1})$	0.0453	0.0076	0.0092	0.0099	0.0155
R^2	0.9992	0.9717	0.9977	0.9981	0.9989
R^2_{adj}	0.9990	0.9646	0.9971	0.9976	0.9986
$ARE (\%)$	0.53	4.40	1.22	0.96	0.81
$q_{exp} (\text{mg g}^{-1})$	31.73	56.07	64.15	65.44	67.97

Table 2. Equilibrium parameters of the brilliant blue FCF dye adsorption.

Model	Temperature (°C)			
	25	35	45	55
Langmuir				
q_m (mg g ⁻¹)	73.70	81.30	86.39	92.08
k_L (L mg ⁻¹)	1.6140	2.0154	2.1783	32.0456
R^2	0.9996	0.9974	0.9996	0.9958
R^2_{adj}	0.9994	0.9961	0.9994	0.9925
ARE (%)	0.48	1.28	0.54	1.80
Freundlich				
$k_F((\text{mg g}^{-1})(\text{L mg}^{-1})^{-1/nF})$	60.7806	64.5233	66.5827	76.1925
$1/nF$	0.0420	0.0523	0.0606	0.0483
R^2	0.9944	0.9854	0.9919	0.9979
R^2_{adj}	0.9770	0.9706	0.9762	0.9968
ARE (%)	2.19	3.94	2.70	1.33
Sips				
q_S (mg g ⁻¹)	73.04	80.55	87.65	105.88
k_S (L mg ⁻¹)	0.8415	1.5312	2.2318	2.8989
m_S	1.6012	1.6016	0.7532	0.2197
R^2	0.9998	0.9977	0.9998	0.9996
R^2_{adj}	0.9996	0.9954	0.9996	0.9992
ARE (%)	0.33	1.04	0.31	0.46
q_{exp} (mg g ⁻¹)	72.37	79.12	85.96	94.74

Table 3. Thermodynamic parameters of the brilliant blue FCF dye adsorption.

Temperature (°C)	K_D	ΔG° (kJ mol ⁻¹)	ΔH° (kJ mol ⁻¹)	ΔS° (kJ mol ⁻¹ K ⁻¹)
25	667191.69	-33.42		
35	1214027.23	-35.67	33.40	0.224
45	1769504.95	-37.91		
55	2298421.85	-40.15		

Supplementary Material

S1. Magnetic activated carbon preparation

Sapelli wood sawdust-derived magnetic activated carbon (SWSMAC) was prepared by a single-step pyrolysis process in which carbonization, activation, and magnetization occur simultaneously. The procedure was carried out according to the literature (Thue et al., 2020). Initially, 100 g of Sapelli wood sawdust was mixed with 100 g of KOH and 100 g of NiCl₂ and dissolved in approximately 50 mL of distilled water. Next, the mixture was mechanically stirred using a magnetic stirrer at 90 °C for 2 h to form a paste. Then, the paste was oven-dried (105 °C, 8 h) and pyrolyzed in a quartz reactor in a conventional furnace (Sanchis, Brazil). First, the furnace was heated from 25 to 600 °C at 10 °C min⁻¹, under an N₂ flow rate of 150 mL min⁻¹. Next, the temperature of the furnace was kept fixed at 600 °C for 30 min. After this time, the furnace was shut down and kept under the N₂ flow until it attained a temperature lower than 200 °C. Then, the inorganic compounds in the carbonaceous matrix were partially leached out to maintain the Ni compounds and eliminate the K compounds. This leaching was carried out using a 0.1 mol L⁻¹ HCl solution under a reflux system at around 80 °C for 2 h. After the leaching, the material was exhaustively washed with distilled water until the pH of the washing waters attained a value of around 6–7. Finally, the material was oven-dried (105 °C, 8 h).

S2. Characterization

The morphological structure of the magnetic activated carbon was identified by Scanning Electron Microscopy (SEM) (Tescan, MIRA 3, Czech Republic). The apparatus was operated with a working voltage of 12 kV and magnification of 5000×. The basic element components were determined by energy-dispersive X-ray spectroscopy (EDS). The textural properties were determined based on nitrogen adsorption/desorption isotherms at 77 K using a volumetric adsorption analyzer (Micromeritics, ASAP 2020, USA). Brunauer-Emmett-Teller (BET) and Barrett-Joyner-Halenda (BJH) methods were used to obtain the BET surface area, total pore volume, and average pore size. The surface functional groups of the magnetic activated carbon were identified by Fourier transform infrared spectroscopy (FTIR) (Shimadzu, Prestige 21210045, Japan). Spectra were recorded before and after the adsorption to identify the possible interactions between the adsorbent's surface functional groups and the brilliant blue FCF dye molecule. The analysis was performed using the diffuse reflectance

technique with KBr (resolution of 4 cm⁻¹, range of 4000–400 cm⁻¹). The magnetic properties were investigated using a vibrating-sample magnetometer (VSM) (MicroSense, EZ9, USA) at room temperature over the range of -20 kOe to +20 kOe. Furthermore, powder X-ray diffraction (XRD) investigations were done to access the material's crystalline nature. The instrument (Rigaku, Miniflex 300, Japan) was operated at 30 kV and 10 mA with Cu K α radiation ($\lambda = 1.541861 \text{ \AA}$), over the range of $10^\circ \leq 2\theta \leq 100^\circ$, using a scanning step of 0.060 s⁻¹. Scherrer's equation (Eq. 1) was used to obtain the average crystallite size (D) of the Ni particles present in the adsorbent material (Thue et al. 2020):

$$D = \frac{0.9\lambda}{\beta \cos(\theta)} \quad (1)$$

Where: λ is the wavelength of the Cu K α radiation, β is the full width at half maximum (FWHM) of the patterns, and θ is the diffraction angle.

For the point of zero charge (pH_{PZC}) determination, a NaCl solution (0.1 mol L⁻¹) was prepared, and the pH of this solution was adjusted from 2 to 12, with HCl or NaOH (0.1 mol L⁻¹). Then, 20 mL of the pH-adjusted NaCl solution and 0.02 g of SWSMAC were added to Erlenmeyer flasks and kept under constant stirring at 150 rpm (Solab, SL 222, Brazil) at 25 °C for 24 h. After, the adsorbent was separated from the solution by filtration, and the final pH was measured. The pH_{PZC} was determined from the initial pH versus the final pH plot (Netto et al. 2021).

S3. Adsorption experiments

In all adsorption tests, 20 mL of the brilliant blue FCF dye solution was added to Erlenmeyer flasks with a pre-determined amount of SWSMAC and stirred in a thermostatic shaker at 150 rpm (Solab, SL 222, Brazil). The dosage and pH effect on the brilliant blue FCF dye adsorption was first evaluated. The experiments were carried out using a brilliant blue FCF dye solution of initial concentration 50 mg L⁻¹ and a temperature of 25 °C. The adsorbent dosage from 0.25 to 1.5 g L⁻¹ was used to evaluate the impact of SWSMAC dosage on dye adsorption. The dosage experiments were performed using a dye solution of pH 4.0 (adjusted by adding HCl). The pH test was realized by varying the pH of the brilliant blue FCF dye solution (2, 4, 6, 8, and 10, adjusted with HCl or NaOH) using the adequate adsorbent dosage previously defined. After determining an adequate adsorbent dosage and

pH, the adsorption kinetic study was carried out using brilliant blue FCF dye solutions of different initial concentrations (25, 50, 100, 150, and 200 mg L⁻¹) at set time intervals (0–180 min) and temperature of 25 °C. Finally, the equilibrium study was also carried out using brilliant blue FCF dye solutions of different initial concentrations (50, 75, 100, 125, 150, and 200 mg L⁻¹) and different temperatures (25, 35, 45, and 55 °C).

All experiments were carried out in triplicate ($n = 3$), and blank tests were performed. After the experiments, the solid phase was separated using a magnet, and the remaining brilliant blue FCF dye concentration in the liquid phase was determined by spectrophotometry at the maximum absorption wavelength ($\lambda_{max} = 630$ nm) using a UV-Vis spectrophotometer (Biospectro SP-22, Brazil). The adsorption capacity at time t (q_t), equilibrium adsorption capacity (q_e), and removal percentage (R , %) were determined by Eq. (2), (3), and (4), respectively:

$$q_t = \frac{V(C_0 - C_t)}{m} \quad (2)$$

$$q_e = \frac{V(C_0 - C_e)}{m} \quad (3)$$

$$R(\%) = \frac{(C_0 - C_e)}{C_0} \times 100 \quad (4)$$

Where: C_0 is the initial brilliant blue FCF dye concentration (mg L⁻¹), C_t is the brilliant blue FCF dye concentration in the liquid phase at time t (mg L⁻¹), C_e is the equilibrium brilliant blue FCF dye concentration in the liquid phase (mg L⁻¹), m is the adsorbent mass (g), and V is the volume of the solution (L).

S4. Kinetic, equilibrium, and thermodynamic modeling

The mathematical equations of the pseudo-first-order (PFO) and pseudo-second-order (PSO) models (Ho and McKay 1998) are shown in Eq. (5) and (6), respectively:

$$q_t = q_1(1 - \exp(-k_1 t)) \quad (5)$$

$$q_t = \frac{t}{\left(1/k_2 q_2^2\right) + t/q_2} \quad (6)$$

Where: q_t is the adsorption capacity at time t (mg g^{-1}), q_1 is the adsorption capacity predicted by the pseudo-first model (mg g^{-1}), q_2 is the adsorption capacity predicted by the pseudo-second model (mg g^{-1}), k_1 is the pseudo-first order rate constant (min^{-1}), and k_2 is the pseudo-second order rate constant ($\text{g mg}^{-1} \text{ min}^{-1}$).

Langmuir (Langmuir 1918), Freundlich (Freundlich 1907), and Sips (Sips 1948) models are presented by the Eq. (7), (8), and (9), respectively:

$$q_e = \frac{q_m k_L C_e}{1 + k_L C_e} \quad (7)$$

$$q_e = k_F C_e^{1/n_F} \quad (8)$$

$$q_e = \frac{q_s k_s (C_e)^{m_s}}{1 + k_s (C_e)^{m_s}} \quad (9)$$

Where: q_e is the equilibrium adsorption capacity (mg g^{-1}), C_e is the equilibrium concentration in the liquid phase (mg L^{-1}), q_m is the maximum adsorption capacity of the Langmuir model (mg g^{-1}), k_L is the Langmuir equilibrium constant (L mg^{-1}), k_F is the Freundlich equilibrium constant ($(\text{mg g}^{-1}) (\text{mg L}^{-1})^{-1/n_F}$), $1/n_F$ is the heterogeneity factor, q_s is the maximum adsorption capacity of the Sips model (mg g^{-1}), k_s is the Sips equilibrium constant (L mg^{-1}), and m_s is the exponent of the Sips model.

The validity of the kinetic and isotherm models was assessed by determination coefficient (R^2), adjusted determination coefficient (R^2_{adj}), and average relative error (ARE). R^2 , R^2_{adj} and ARE , were calculated according to Eq. (10), (11), and (12), respectively:

$$R^2 = \left(\frac{\sum_i^n (q_{i,exp} - \bar{q}_{exp})^2 - \sum_i^n (q_{i,exp} - q_{i,model})^2}{\sum_i^n (q_{i,exp} - \bar{q}_{exp})^2} \right) \quad (10)$$

$$R^2_{adj} = 1 - \left(1 - R^2 \right) \left(\frac{n-1}{n-p-1} \right) \quad (11)$$

$$ARE = \frac{100}{n} \sum_i^n \left| \frac{q_{i,exp} - q_{i,model}}{q_{i,model}} \right| \quad (12)$$

Where: $q_{i,model}$ is the individual theoretical adsorption capacity value predicted by the model, $q_{i,exp}$ is the individual experimental adsorption capacity value, \bar{q}_{exp} is the average of all experimental adsorption capacity values measured; n is the number of experimental points, and p is the number of parameters in the fitting model.

The thermodynamic parameters Gibb's free energy change (ΔG° , kJ mol^{-1}), enthalpy change (ΔH° , kJ mol^{-1}), and entropy change (ΔS° , $\text{J mol}^{-1} \text{K}^{-1}$) were calculated according to Eq. (13), (14), and (15) (Lima et al. 2019, Wang et al. 2019):

$$\Delta G^\circ = -RT \ln(K_D) \quad (13)$$

$$\ln(K_D) = \frac{\Delta S^\circ}{R} - \frac{\Delta H^\circ}{RT}$$

(14)

$$K_D = \frac{(1000 \cdot K_s \cdot M_w) \cdot [\text{adsorbate}]^p}{\gamma} \quad (15)$$

Where: T is the absolute temperature (K), R is the universal gas constant ($8.31 \times 10^{-3} \text{ kJ mol}^{-1} \text{ K}^{-1}$), K_D is the thermodynamic equilibrium constant, K_s is the equilibrium constant of the best isotherm model (in the case here, is the Sips equilibrium constant), $[\text{adsorbate}]^\circ$ is the standard concentration of the adsorbate (1 mol L^{-1}), and γ is the coefficient of activity (dimensionless).

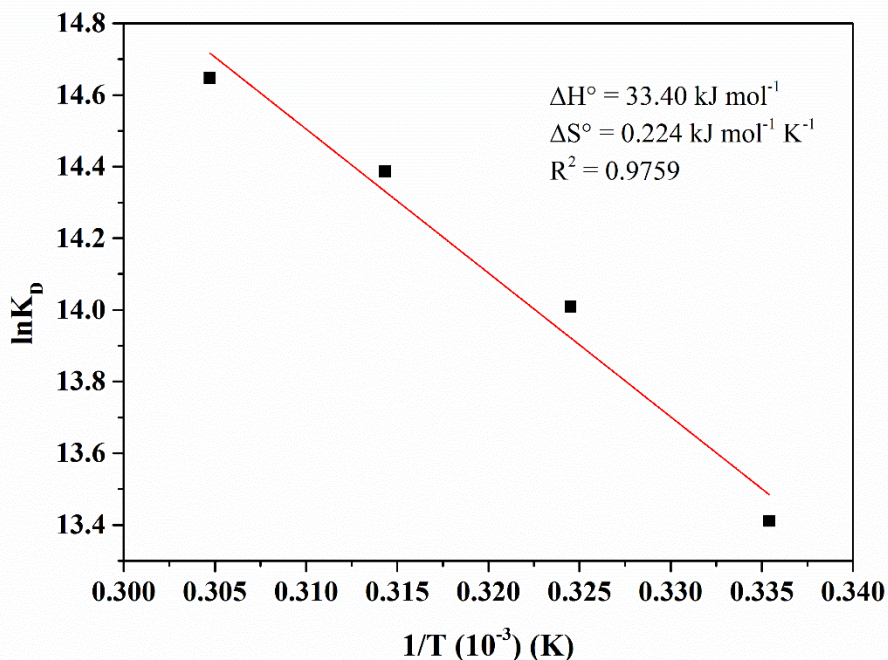


Fig. S1 Fitting of Van't Hoff equation for the calculation of the adsorption thermodynamic parameters.

References

- Freundlich H (1907) Über die Adsorption in Lösungen. Zeitschrift für Phys Chemie 57U: 385–470z. <https://doi.org/10.1515/zpch-1907-5723>
- Ho YS, McKay G (1998) A comparison of chemisorption kinetic models applied to pollutant removal on various sorbents. Process Saf Environ Prot 76:332–340. <https://doi.org/10.1205/095758298529696>
- Langmuir I (1918) The adsorption of gases on plane surfaces of glass, mica and platinum. J Am Chem Soc 40:1361–1403. <https://doi.org/10.1021/ja02242a004>
- Lima EC, Hosseini-Bandegharaei A, Moreno-Piraján JC, Anastopoulos I (2019) A critical review of the estimation of the thermodynamic parameters on adsorption equilibria. Wrong use of equilibrium constant in the Van't Hoff equation for calculation of thermodynamic parameters of adsorption. J Mol Liq 273:425–434. <https://doi.org/10.1016/j.molliq.2018.10.048>
- Netto MS, Oliveira JS, Salau NPG, Dotto GL (2021) Analysis of adsorption isotherms of Ag+, Co+2, and Cu+2 onto zeolites using computational intelligence models. J Environ Chem Eng 9:104960. <https://doi.org/10.1016/j.jece.2020.104960>
- Sips R (1948) On the Structure of a Catalyst Surface. J Chem Phys 16:490–495. <https://doi.org/doi.org/10.1063/1.1746922>

Thue PS, Umpierres CS, Lima EC, Lima DR, Machado FM, Reis GS, Silva RS, Pavan FA, Tran HN (2020) Single-step pyrolysis for producing magnetic activated carbon from tucum (*Astrocaryum aculeatum*) seed and nickel(II) chloride and zinc(II) chloride. Application for removal of nicotinamide and propanolol. *J Hazard Mater* 398:122903. <https://doi.org/10.1016/j.jhazmat.2020.122903>

Wang Y, Li Y, Zhang Y, Wei W (2019) Enhanced brilliant blue FCF adsorption using microwave-hydrothermal synthesized hydroxyapatite nanoparticles. *J Dispers Sci Technol* 41:1346–1355. <https://doi.org/10.1080/01932691.2019.1623695>

5. DISCUSSÕES

Dois carvões ativados magnéticos chamados CAM1105 e CA111 foram preparados a partir da serragem de madeira ativados e magnetizados com KOH e NiCl₂ respectivamente. Os adsorventes foram caracterizados usando as técnicas de MEV/EDS, FTIR, BET, TGA, DRX, VSM e experimentos de adsorção foram realizados na remoção do corante azul brilhante. O estudo dividiu-se em duas etapas, Artigo 1 e Artigo 2.

De modo geral, na primeira etapa (Artigo 1) do estudo foi demonstrado que os CAMs foram adsorventes promissores para remoção do corante azul brilhante de soluções aquosas, com boa eficiência e fácil separação magnética. Nesta etapa, foi evidente que a diferença na proporção de NiCl₂ influenciou nas características texturais dos carvões. Assim, o CAM111 apresentou os melhores resultados, mostrando-se mais eficiente que o CAM1105. Nas imagens MEV foi possível observar que o CAM111 mostrou ter maior quantidade de cavidades do que CAM1105, fato que foi confirmado com as análises BET/ BJH, onde CA111 apresentou maior área superficial e volume total de poros. Ou seja, a razão de peso de NiCl₂ levou ao aumento da área superficial e do volume total de poros do material obtido. E apesar dos espectros de EDS demonstrarem a presença de Ni na matriz de carbono, parte dele pode ter sido eliminado com a lavagem ácida, contribuindo assim pela formação de poros. Ambos os adsorventes exibiram propriedades ferromagnéticas e a presença de partículas nanoestruturadas de Ni. Além disso, estudos preliminares sobre o equilíbrio de adsorção mostrou que a cinética de adsorção do CAM111 foi mais rápida do que a CAM1105 e capacidade de adsorção do CAM111 foi mais alta, em torno de 96 mg g⁻¹ enquanto a do CAM1105 foi em torno de 40 mg g⁻¹. Nesta etapa, também foi demonstrado que os carvões magnéticos ativados apresentam potencial para serem reutilizados em mais ciclos de adsorção e que o emprego dos adsorventes no tratamento de um efluente simulado pode ter eficiências de remoção de mais de 90%.

Sendo assim, por apresentar resultados mais satisfatórios e promissores apenas o CAM111 foi objeto de estudo na segunda etapa (Artigo 2). Aqui, além dos experimentos anteriores, foi investigado o ponto de carga zero, dosagem do carvão, pH da solução, temperatura, termodinâmica e mecanismo de adsorção envolvidos na adsorção do corante azul brilhante. Nos experimentos de adsorção do corante primeiramente foram realizados testes de dosagem e pH e os melhores resultados foram obtidos com dosagem de 0,75 g L⁻¹ e pH 4,0. Após estabelecer as condições mais adequadas do pH e dosagem, as curvas cinéticas de adsorção foram obtidas usando diferentes concentrações iniciais de corante (25–200 mg L⁻¹)

em intervalos de tempo definidos (0–180 min). O estudo cinético mostrou que a adsorção foi rápida independente das concentrações iniciais o equilíbrio foi alcançado em cerca de 20 min. Vale ressaltar, que uma cinética rápida é uma vantagem importante em um processo de adsorção. Além disso, com base nos valores mais elevados do coeficiente de determinação (R_2) e menores valores do erro relativo médio (ARE) o modelo de PSO foi mais adequado para representar os dados experimentais, sugerindo que a adsorção ocorre através de mecanismos externos e internos de transferência de massa.

As isotermas de equilíbrio foram obtidas usando diferentes concentrações iniciais de corante (50–200 mg L⁻¹) e temperaturas (25–55 °C). O estudo do equilíbrio de adsorção mostrou que o processo de adsorção é favorecido pelo aumento da temperatura, chegando a uma capacidade máxima de adsorção de 111,50 mg g⁻¹ á 55 °C. Os altos valores do coeficiente de determinação (R_2) e os baixos valores do erro relativo médio (ARE) mostraram que o modelo de Sips foi o mais adequado para representar os dados de equilíbrio. O modelo indicou que o parâmetro k_S aumentou com o aumento da temperatura, confirmando que a adsorção foi favorecida em 55°C. A partir dos valores da variação da energia livre de Gibbis, entalpia e entropia (ΔG° , ΔH° e ΔS°), os estudos termodinâmicos indicaram uma adsorção favorável, espontânea e endotérmica.

O mecanismo de adsorção do corante azul brilhante no CAM111 foi explicado a partir das mudanças verificadas nos espectros de FTIR do CAM111 antes e depois da adsorção, e das características da estrutura molecular do corante. Dessa forma, verificou-se que o mecanismo de adsorção entre o carvão ativado magnético e o corante azul brilhante envolveu interações eletrostáticas, interações de ligações de hidrogênio, interações $\pi-\pi$ e $n-\pi$.

Por fim os resultados encontrados neste trabalho demonstraram a possibilidade de utilizar o carvão ativado magnético derivado da serragem da madeira Sapelli como adsorvente alternativo para a remoção corante azul brilhante em meio aquoso, com boa eficiência e fácil separação magnética, contribuindo tanto para o gerenciamento de um resíduo gerado em quantidades elevadas quanto para o tratamento de águas residuais contendo corantes.

6. CONCLUSÃO GERAL

Neste estudo, carvões ativados magnéticos, derivado da serragem da madeira Sapelli foram preparados por pirólise de etapa única, com diferentes proporções em peso de cloreto de níquel (NiCl_2), caracterizados e aplicados na adsorção do corante azul brilhante. A caracterização detalhada do material mostrou uma síntese bem-sucedida. As diferentes proporções de peso de NiCl_2 influenciaram nas propriedades dos adsorventes. Uma maior razão de peso de NiCl_2 levou a um aumento na área de superfície de $260,023 \text{ m}^2 \text{ g}^{-1}$ (CAM1105) para $331,543 \text{ m}^2 \text{ g}^{-1}$ (CAM111) e no volume total de poros de $0,075 \text{ cm}^3 \text{ g}^{-1}$ (CAM1105) para $0,095 \text{ cm}^3 \text{ g}^{-1}$ (CAM111). O tamanho médio dos poros permaneceu em torno de 3,6 nm, independentemente da relação de peso. Os CAMs exibiram propriedades ferromagnéticas à temperatura ambiente. Além disso, ambos os CAMs mostraram a presença de partículas nanoestruturadas de Ni com tamanho médio de cristalito de 18,96 nm (CAM1105) e 25,34 nm (CAM111). A partir do estudo de adsorção, foi possível observar que o CAM111 atingiu o equilíbrio mais rapidamente que o CA1105. Além disso, a capacidade de adsorção do CAM 111 foi maior (96 mg g^{-1}) do que o CAM1105 (40 mg g^{-1}). O estudo de regeneração e reutilização mostrou que o CAM111 tinha maior potencial para ser reutilizado em mais ciclos de adsorção. Por fim, ambos adsorventes foram promissores para o tratamento de um simulado contendo o corante azul brilhante, alcançando percentuais de remoção de até 90%.

Diante desses resultados, o CAM111 foi escolhido dentre os carvões ativados por apresentar resultados superiores como, área superficial, volume de poros e capacidade de adsorção. Dessa forma, experimentos de adsorção mais detalhados foram realizados do ponto de vista cinético, de equilíbrio e termodinâmico. Com base nos experimentos de adsorção, os melhores resultados foram obtidos com dosagem de $0,75 \text{ g L}^{-1}$ e pH 4,0. O estudo cinético mostrou que a adsorção foi rápida, e o equilíbrio foi alcançado em cerca de 20 minutos. O modelo de pseudo-segunda ordem forneceu o melhor ajuste para os dados cinéticos experimentais. A partir do estudo do equilíbrio, verificou-se que o modelo Sips foi o mais adequado, e o processo de adsorção foi favorecido com o aumento da temperatura, atingindo capacidade máxima de adsorção de $111,50 \text{ mg g}^{-1}$ á 55°C . A investigação termodinâmica indicou uma adsorção favorável, espontânea e endotérmica. Além disso, foi proposto que o mecanismo de adsorção do corante azul brilhante no CAM111 envolveu interações eletrostáticas, interações de ligações de hidrogênio, interações $\pi-\pi$ e $n-\pi$.

Em geral, pode-se concluir que os carvões ativados magnéticos foram preparados com sucesso. O NiCl₂, além de servir como agente magnetizante pode influenciar nas características texturais dos carvões, alterando sua eficiência no processo de adsorção. O CAM111 apresentou resultados promissores, afirmando que pode ser utilizado como adsorvente na remoção do corante aniônico azul brilhante, visto que, é preparado por um método simples utilizando material precursor acessível e de baixo custo. Ainda, vale ressaltar, que o uso da serragem como material precursor na síntese de adsorventes aplicados na remoção de águas residuais coloridas pode representar dois ótimos benefícios ambientais: a destinação adequada de resíduos e a eficiência no tratamento dos efluentes.

7. REFERENCIAS

- ABDEL-GHANI, Nour T. *et al.* Magnetic activated carbon nanocomposite from *Nigella sativa* L. waste (MNSA) for the removal of Coomassie brilliant blue dye from aqueous solution: Statistical design of experiments for optimization of the adsorption conditions. **Journal of Advanced Research**, v. 17, p. 55-63, 2019.
- ADEGOKE, Kayode Adesina; BELLO, Olugbenga Solomon. Dye sequestration using agricultural wastes as adsorbents. **Water Resources and Industry**, v. 12, p. 8-24, 2015.
- ALLIED MARKET RESEARCH. Textile dyes market by dye type (direct, reactive, vat, basic, acid, disperse, and others), and fiber type (wool, polyester, acrylic and others): **Global opportunity analysis and industry forecast**, 2019 <<http://www.alliedmarketresearch.com/textile-dyes-market>> Acesso: 31 de março de 2022.
- ALTINTIG, Esra *et al.* Effective removal of methylene blue from aqueous solutions using magnetic loaded activated carbon as novel adsorbent. **Chemical Engineering Research and Design**, v. 122, p. 151-163, 2017.
- AMCHOVA, Petra; KOTOLOVA, Hana; RUDA-KUCEROVA, Jana. Health safety issues of synthetic food colorants. **Regulatory toxicology and pharmacology**, v. 73, n. 3, p. 914-922, 2015.
- AGÊNCIA NACIONAL DE ÁGUAS (ANA). Panorama das Águas: Água no Mundo, 2018.
- ANAS, Muhammad *et al.* Photocatalytic degradation of organic dye using titanium dioxide modified with metal and non-metal deposition. **Materials Science in Semiconductor Processing**, v. 41, p. 209-218, 2016.
- ANVISA. Agência Nacional de Vigilância Sanitária, 2005. Resolução – RDC nº 218. Diário Oficial da República Federativa do Brasil.
- ARGUN, Mehmet Emin *et al.* Activation of pine cone using Fenton oxidation for Cd (II) and Pb (II) removal. **Bioresource technology**, v. 99, n. 18, p. 8691-8698, 2008.
- ARUNPRASATH, T. *et al.* Biodegradation of triphenylmethane dye malachite green by a newly isolated fungus strain. **Biocatalysis and Agricultural Biotechnology**, v. 17, p. 672-679, 2019.

BADAWY, Abdelrahman A.; IBRAHIM, Shaimaa M.; ESSAWY, Hisham A. Enhancing the textile dye removal from aqueous solution using cobalt ferrite nanoparticles prepared in presence of fulvic acid. **Journal of Inorganic and Organometallic Polymers and Materials**, v. 30, n. 5, p. 1798-1813, 2020.

BADI, Mojtaba Yegane *et al.* Modification of activated carbon with magnetic Fe₃O₄ nanoparticle composite for removal of ceftriaxone from aquatic solutions. **Journal of Molecular Liquids**, v. 261, p. 146-154, 2018.

BAYOL, Nicolas et al. Forest management and the timber sector in Central Africa. **The Forests of the Congo Basin-State of the Forest 2010**, p. 43-61, 2012.

BELUCI, Natália de Camargo Lima *et al.* Facile filtration system to remove Diuron in aqueous solutions. **Journal of Hazardous Materials**, v. 404, p. 124163, 2021.

BENKHAYA, Said; M'RABET, Souad; EL HARFI, Ahmed. Classifications, properties, recent synthesis and applications of azo dyes. **Heliyon**, v. 6, n. 1, p. e03271, 2020.

BENHABILES, Sadjia; RIDA, Kamel. Production of efficient activated carbon from sawdust for the removal of dyes in single and binary systems—a full factorial design. **Particulate Science and Technology**, v. 39, n. 2, p. 237-251, 2021.

BHATTI, Haq N. *et al.* Efficient removal of dyes using carboxymethyl cellulose/alginate/polyvinyl alcohol/rice husk composite: adsorption/desorption, kinetics and recycling studies. **International journal of biological macromolecules**, v. 150, p. 861-870, 2020.

BONCIU, Elena; ROSCULETE, Elena; ROSCULETE, C. A. The clastogenic effect of tartrazine, a synthetic yellow dye, in plant meristematic tissues. **Annals of the University of Craiova-Agriculture, Montanology, Cadastre Series**, v. 49, n. 1, p. 32-35, 2019.

BONILLA-PETRICIOLET, Adrián; MENDOZA-CASTILLO, Didilia Ileana; REYNEL-ÁVILA, Hilda Elizabeth (Ed.). Adsorption Processes for Water Treatment and Purification. 1. Ed., Springer International Publishing, 2017.

BULUT, Yasemin; AYDIN, Haluk. A kinetics and thermodynamics study of methylene blue adsorption on wheat shells. **Desalination**, v. 194, n. 1-3, p. 259-267, 2006.

CAZETTA, André Luiz et al. **Síntese e caracterização de carvões ativados magnéticos (CAMs) da casca do coco (*Cocos nucifera*): estudos de adsorção do corante amarelo crepúsculo.** 2014. Dissertação de Mestrado. Universidade Estadual de Maringá.

CHEN, Dong-Hwang; HSIEH, Chih-Hsuan. Synthesis of nickel nanoparticles in aqueous cationic surfactant solutions. **Journal of Materials Chemistry**, v. 12, n. 8, p. 2412-2415, 2002.

CHIKRI, R. *et al.* Efficiency of sawdust as low-cost adsorbent for dyes removal. **Journal of Chemistry**, v. 2020, 2020.

CLARKE, E. A; ANLIKER, R. Handbook of environmental chemistry. **Organic Dyes and Pigments, Springer-Verlag, Heidelberg**, p. 181-215, 1980.

COLLIVIGNARELLI, Maria Cristina *et al.* H₂O₂ based oxidation processes for the treatment of real high strength aqueous wastes. **Sustainability**, v. 9, n. 2, p. 244, 2017.

COONEY, David O. Adsorption Design for Wastewater Treatment. Florida: CRC Press, 1999

COLPANI, Gustavo Lopes. **Preparação e caracterização de adsorventes para a remoção de surfactantes aniônicos em águas residuárias.** Dissertação (Mestrado em Engenharia Química) – Universidade Federal de Santa Catarina, Florianópolis, SC, 2012.

CUSIOLI, Luís Fernando *et al.* Soybean hulls as a low-cost biosorbent for removal of methylene blue contaminant. **Environmental Progress & Sustainable Energy**, v. 39, n. 2, p. e13328, 2019.

DAMDIB, Sakonsupa *et al.* Removal of reactive black dye in water by magnetic mesoporous carbon from macadamia nutshell. **Adsorption Science & Technology**, v. 2022, 2022.

DAMODARAN, Srinivasan; PARKIN, Kirk L. **Química de alimentos de Fennema.** Artmed editora, 2018.

DAS, Ananya; DEY, Apurba. P-Nitrophenol-Bioremediation using potent *Pseudomonas* strain from the textile dye industry effluent. **Journal of Environmental Chemical Engineering**, v. 8, n. 4, p.

- DASTGHEIB, Seyed A. et al. Preparation of functionalized and metal-impregnated activated carbon by a single-step activation method. **Applied surface science**, v. 290, p. 92-101, 2014.
- DE VIDALES, María J. Martín *et al.* 3D printed floating photocatalysts for wastewater treatment. **Catalysis Today**, v. 328, p. 157-163, 2019.
- DINÇER, Ali Rıza *et al.* Comparison of activated carbon and bottom ash for removal of reactive dye from aqueous solution. **Bioresource Technology**, v. 98, n. 4, p. 834-839, 2007.
- DOTTO, Guilherme Luiz; PINTO, LA de A. Adsorption of food dyes onto chitosan: Optimization process and kinetic. **Carbohydrate Polymers**, v. 84, n. 1, p. 231-238, 2011.
- DOTTO, Juliana *et al.* Performance of different coagulants in the coagulation/flocculation process of textile wastewater. **Journal of cleaner production**, v. 208, p. 656-665, 2019.
- EREN, Zeynep; ACAR, Filiz Nuran. Adsorption of Reactive Black 5 from an aqueous solution: equilibrium and kinetic studies. **Desalination**, v. 194, n. 1-3, p. 1-10, 2006.
- FREUNDLICH, H. Z. **Journal of Physical Chemistry**, v. 57, p. 385, 1907.
- FEIQIANG, Guo *et al.* Characteristics and toxic dye adsorption of magnetic activated carbon prepared from biomass waste by modified one-step synthesis. **Colloids and Surfaces A: Physicochemical and Engineering Aspects**, v. 555, p. 43-54, 2018.
- FOTEINIS, Spyros *et al.* Environmental sustainability of the solar photo-Fenton process for wastewater treatment and pharmaceuticals mineralization at semi-industrial scale. **Science of the Total Environment**, v. 612, p. 605-612, 2018.
- GARG, V. K. *et al.* Dye removal from aqueous solution by adsorption on treated sawdust. **Bioresource technology**, v. 89, n. 2, p. 121-124, 2003.
- GERMAN-HEINS, Judit; FLURY, Markus. Sorption of Brilliant Blue FCF in soils as affected by pH and ionic strength. **Geoderma**, v. 97, n. 1-2, p. 87-101, 2000.
- GILES, C. H.; SMITH, D.; HUITSON, A. A general treatment and classification of the solute: part I. theoretical. **J. Colloid Interface Sci**, v. 47, p. 755-765, 1974.

GOMES, Keiva Maria Silva *et al.* Citotoxicity of food dyes sunset yellow (E-110), bordeaux red (E-123), and tatrazine yellow (E-102) on Allium cepa L. root meristematic cells. **Food Science and Technology**, v. 33, p. 218-223, 2013.

GUARATINI, Cláudia CI; ZANONI, Maria Valnice B. Corantes têxteis. **Química nova**, v. 23, p. 71-78, 2000.

GUPTA, V. K. e SUHAS. Application of low-cost adsorbents for dye removal—a review. **Journal of environmental management**, v. 90, n. 8, p. 2313-2342, 2009.

GUPTA, Tripti *et al.* Adsorption of Indigo Carmine Dye by Acacia nilotica sawdust activated carbon in fixed bed column. **Scientific Reports**, v. 12, n. 1, p. 1-14, 2022.

HAN, Zhantao *et al.* Magnetite impregnation effects on the sorbent properties of activated carbons and biochars. **Water research**, v. 70, p. 394-403, 2015

HASSAN, Mohammad M.; CARR, Christopher M. A critical review on recent advancements of the removal of reactive dyes from dye house effluent by ion-exchange adsorbents. **Chemosphere**, v. 209, p. 201-219, 2018.

HAMEED, B. H.; AHMAD, A. A.; AZIZ, N. Isotherms, kinetics and thermodynamics of acid dye adsorption on activated palm ash. **Chemical Engineering Journal**, v. 133, n. 1-3, p. 195-203, 2007.

HOMAGAI, Puspa Lal *et al.* Adsorption and removal of crystal violet dye from aqueous solution by modified rice husk. **Helijon**, v. 8, n. 4, p. e09261, 2022.

HOMEM, Natália Cândido *et al.* Surface modification of a polyethersulfone microfiltration membrane with graphene oxide for reactive dyes removal. **Applied Surface Science**, v. 486, p. 499-507, 2019.

HO, Yuhshan S.; MCKAY, Gordon. A comparison of chemisorption kinetic models applied to pollutant removal on various sorbents. **Process safety and environmental protection**, v. 76, n. 4, p. 332-340, 1998.

HUNGER, Klaus. (Ed.). **Industrial dyes: chemistry, properties, applications**. John Wiley & Sons, 2007.

JANUÁRIO, Eduarda Freitas Diogo *et al.* Advanced graphene oxide-based membranes as a potential alternative for dyes removal: A review. **Science of The Total Environment**, v. 789, p. 147957, 2021.

JAVAID, Rahat; QAZI, Umair Yaqub. Catalytic oxidation process for the degradation of synthetic dyes: an overview. **International journal of environmental research and public health**, v. 16, n. 11, p. 2066, 2019.

JAWAD, Ali H. *et al.* Zwitterion composite chitosan-epichlorohydrin/zeolite for adsorption of methylene blue and reactive red 120 dyes. **International Journal of Biological Macromolecules**, v. 163, p. 756-765, 2020.

JIANG, Wenyan *et al.* Adsorption of cationic dye from water using an iron oxide/activated carbon magnetic composites prepared from sugarcane bagasse by microwave method. **Environmental technology**, v. 42, n. 3, p. 337-350, 2021.

JIMENEZ, Ricardo Sarti; DAL BOSCO, Sandra Maria; CARVALHO, Wagner Alves. Remoção de metais pesados de efluentes aquosos pela zeólita natural escolecita-influência da temperatura e do pH na adsorção em sistemas monoelementares. **Química nova**, v. 27, p. 734-738, 2004.

JUN, Byung-Moon *et al.* Adsorption of selected dyes on Ti₃C₂Tx MXene and Al-based metal-organic framework. **Ceramics International**, v. 46, n. 3, p. 2960-2968, 2020.

KADIRVELU, Kavipriya *et al.* Utilization of various agricultural wastes for activated carbon preparation and application for the removal of dyes and metal ions from aqueous solutions. **Bioresource technology**, v. 87, n. 1, p. 129-132, 2003.

KANNAN, Nagarethinam; SUNDARAM, Mariappan Meenakshi. Kinetics and mechanism of removal of methylene blue by adsorption on various carbons—a comparative study. **Dyes and pigments**, v. 51, n. 1, p. 25-40, 2001.

KANT, Rita. Textile dyeing industry an environmental hazard. 2011.

KANT, Rita. Adsorption of dye eosin from an aqueous solution on two different samples of activated carbon by static batch method. **Journal of Water Resource and Protection**, 2012.

KATHERESAN, Vanitha; KANSEDO, Jibrail; LAU, Sie Yon. Efficiency of various recent wastewater dye removal methods: A review. **Journal of environmental chemical engineering**, v. 6, n. 4, p. 4676-4697, 2018.

KAVEESHWAR, Aditya Rajeev *et al.* Pecan shell based activated carbon for removal of iron (II) from fracking wastewater: adsorption kinetics, isotherm and thermodynamic studies. **Process Safety and Environmental Protection**, v. 114, p. 107-122, 2018.

KÉMEUZÉ, V.A. Entandrophragma cylindricum (Sprague) Sprague. In: Louppe, D., Oteng-Amoako, A.A. & Brink, M. (Editors). **PROTA (Plant Resources of Tropical Africa / Ressources végétales de l'Afrique tropicale)**, 2008.

KHAKI, Mohammad Reza Delsouz *et al.* Evaluating the efficiency of nano-sized Cu doped TiO₂/ZnO photocatalyst under visible light irradiation. **Journal of Molecular Liquids**, v. 258, p. 354-365, 2018.

KHASRI, Azduwin *et al.* Adsorption of Remazol Brilliant Violet 5R dye from aqueous solution onto melunak and rubberwood sawdust based activated carbon: interaction mechanism, isotherm, kinetic and thermodynamic properties. **DWT**, v. 216, p. 401-411, 2021.

KHODABAKHSHI, Abbas; AMIN, Mohammad Mehdi. Determination of malachite green in trout tissue and effluent water from fish farms. **International Journal of Environmental Health Engineering**, v. 1, n. 1, 2012.

LANGMUIR, Irving. The adsorption of gases on plane surface of glass, mica and platinum. **Journal of American Chemical Society**, v. 40, p. 1361-1403, 1918

LAGERGREN, Stan. Zur theorie der sogenannten adsorption geloster stoffe. *Kungliga Svenska Vetenskapsakademiens Handlingar*, [s. l.], v. 24, n. 4, p. 1–39, 1898.

LEE, Jae-Wook *et al.* Evaluation of the performance of adsorption and coagulation processes for the maximum removal of reactive dyes. **Dyes and pigments**, v. 69, n. 3, p. 196-203, 2006.

LIMA, Eder C. *et al.* A critical review of the estimation of the thermodynamic parameters on adsorption equilibria. Wrong use of equilibrium constant in the Van't Hoof equation for calculation of thermodynamic parameters of adsorption. **Journal of molecular liquids**, v. 273, p. 425-434, 2019.

LIVANI, Milad Jamal; GHORBANI, Mohsen; MEHDIPOUR, Hassan. Preparation of an activated carbon from hazelnut shells and its hybrids with magnetic NiFe₂O₄ nanoparticles. **New Carbon Materials**, v. 33, n. 6, p. 578-586, 2018.

LIU, Tonghao *et al.* Adsorption of methylene blue from aqueous solution by graphene. **Colloids and Surfaces B: Biointerfaces**, v. 90, p. 197-203, 2012.

MAIAN – Disponível em: <https://maian.com.br/services/corante-azul-brilhante/> Acesso: 13 de Novembro de 2022.

MEEZ, Elie; RAHDAR, Abbas; KYZAS, George Z. Sawdust for the removal of heavy metals from water: a review. **Molecules**, v. 26, n. 14, p. 4318, 2021.

MISHRA, G.; TRIPATHY, M. A critical review of the treatments for decolourization of textile effluent. **Colourage**, v. 40, p. 35-35, 1993.

MOHAN, Dinesh *et al.* Cadmium and lead remediation using magnetic oak wood and oak bark fast pyrolysis bio-chars. **Chemical Engineering Journal**, v. 236, p. 513-528, 2014.

MOOSAVI, Seyedehmaryam *et al.* Application of efficient magnetic particles and activated carbon for dye removal from wastewater. **ACS omega**, v. 5, n. 33, p. 20684-20697, 2020.

NADA, Amr A. *et al.* Elaboration of nano titania-magnetic reduced graphene oxide for degradation of tartrazine dye in aqueous solution. **Solid State Sciences**, v. 78, p. 116-125, 2018.

NANDI, B. K.; GOSWAMI, A.; PURKAIT, M. K. Removal of cationic dyes from aqueous solutions by kaolin: kinetic and equilibrium studies. **Applied Clay Science**, v. 42, n. 3-4, p. 583-590, 2009.

NASCIMENTO, Ronaldo Ferreira do *et al.* Adsorção: aspectos teóricos e aplicações ambientais. 2020.

NAVIA-MENDOZA, Jennifer María *et al.* Advances in the application of nanocatalysts in photocatalytic processes for the treatment of food dyes: A review. **Sustainability**, v. 13, n. 21, p. 11676, 2021.

OFOMAJA, Augustine E. Sorptive removal of Methylene blue from aqueous solution using palm kernel fibre: Effect of fibre dose. **Biochemical Engineering Journal**, v. 40, n. 1, p. 8-18, 2008.

OMER, Omer Sakin *et al.* Adsorption thermodynamics of cationic dyes (methylene blue and crystal violet) to a natural clay mineral from aqueous solution between 293.15 and 323.15 K. **Arabian Journal of Chemistry**, v. 11, n. 5, p. 615-623, 2018.

ORTIZ-MARTÍNEZ, A. K. *et al.* Preparation of modified carbon paste electrodes from orange peel and used coffee ground. New materials for the treatment of dye-contaminated solutions using electro-Fenton processes. **Electrochimica Acta**, v. 390, p. 138861, 2021.

PAIXÃO, Rebecca Manesco *et al.* Deposition of graphene nanoparticles associated with tannic acid in microfiltration membrane for removal of food colouring. **Environmental Technology**, v. 42, n. 3, p. 351-357, 2021.

PAREDES-LAVERDE, Marcela *et al.* Understanding the removal of an anionic dye in textile wastewaters by adsorption on ZnCl₂ activated carbons from rice and coffee husk wastes: A combined experimental and theoretical study. **Journal of Environmental Chemical Engineering**, v. 9, n. 4, p. 105685, 2021.

PATRA, Biswa R. *et al.* Biochar production, activation and adsorptive applications: a review. **Environmental Chemistry Letters**, v. 19, n. 3, p. 2237-2259, 2021a.

PATRA, Biswa R. *et al.* Taguchi-based process optimization for activation of agro-food waste biochar and performance test for dye adsorption. **Chemosphere**, v. 285, p. 131531, 2021b.

PEREIRA, Antonio GB. *et al.* Recent advances on composite hydrogels designed for the remediation of dye-contaminated water and wastewater: A review. **Journal of Cleaner Production**, v. 284, p. 124703, 2020.

PERIYASAMY, Aravin Prince; MILITKY, Jiri. Sustainability in textile dyeing: recent developments. **Sustainability in the Textile and Apparel Industries**, p. 37-79, 2020.

PICCIN, Jeferson Steffanello *et al.* Adsorption isotherms in liquid phase: experimental, modeling, and interpretations. In: **Adsorption processes for water treatment and purification**. Springer, Cham, 2017. p. 19-51.

POTERA, Carol. Diet and nutrition: the artificial food dye blues. **Environmental Health Perspectives**, v. 118, n. 10, 2010.

PURKAIT, M. K.; DASGUPTA, S.; DE, S. Adsorption of eosin dye on activated carbon and its surfactant based desorption. **Journal of environmental management**, v. 76, n. 2, p. 135-142, 2005.

QUESADA, Heloise Beatriz *et al.* Surface water pollution by pharmaceuticals and an alternative of removal by low-cost adsorbents: A review. **Chemosphere**, v. 222, p. 766-780, 2019.

RÁPÓ, Eszter; TONK, Szende. Factors affecting synthetic dye adsorption; desorption studies: A review of results from the last five years (2017–2021). **Molecules**, v. 26, n. 17, p. 5419, 2021.

RAZI, Mohd Adib Mohammad; HISHAMMUDIN, Mimi Nur Attahirah Mohd; HAMDAN, Rafidah. Factor affecting textile dye removal using adsorbent from activated carbon: A review. In: **MATEC Web of Conferences**. EDP Sciences, 2017. p. 06015.

REHMAN, Muhammad Saif Ur; KIM, Ilgook; HAN, Jong-In. Adsorption of methylene blue dye from aqueous solution by sugar extracted spent rice biomass. **Carbohydrate polymers**, v. 90, n. 3, p. 1314-1322, 2012.

ROCHA, Luciana S. *et al.* Recent advances on the development and application of magnetic activated carbon and char for the removal of pharmaceutical compounds from waters: A review. **Science of the Total Environment**, 718, 137272.

ROGERS, Peter P.; LLAMAS, M. Ramón.; CORTINA, Luis Martinez (Ed.). **Water crisis: myth or reality?**. CRC Press, 2005.

ROY, Mouni; SAHA, Rajnarayan. Dyes and their removal technologies from wastewater: A critical review. **Intelligent Environmental Data Monitoring for Pollution Management**, p. 127-160, 2021.

RSR (Rapport Stratégique Regional). Vision stratégique et industrialization de la filière bois dans les 6 pays du bassin du Congo Horizon 2030. **FRM Ingénierie**, p. 33-232, 2018.

RUTHVEN, Douglas M. **Principles of Adsorption and Adsorption Processes**. John Wiley & Sons. New York, 1984

SALLEH, Mohamad Amran Mohd *et al.* Cationic and anionic dye adsorption by agricultural solid wastes: a comprehensive review. **Desalination**, v. 280, n. 1-3, p. 1-13, 2011.

SAMIYAMMAL, P. *et al.* Adsorption of brilliant green dye onto activated carbon prepared from cashew nut shell by KOH activation: studies on equilibrium isotherm. **Environmental Research**, v. 212, p. 113497, 2022.

SCHIO, Rejiane Da Rosa. Síntese de uma espuma composta de poliuretano/quitosana para adsorção do corante vermelho nº 40 em batelada e leito fixo. Dissertação (Mestrado em Engenharia Química) - Universidade Federal de Santa Maria, Santa Maria, 2019.

ŠĆIBAN, Marina *et al.* Adsorption of heavy metals from electroplating wastewater by wood sawdust. **Bioresource technology**, v. 98, n. 2, p. 402-409, 2007

SEKAR, M.; SAKTHI, V.; RENGARAJ, S. Kinetics and equilibrium adsorption study of lead (II) onto activated carbon prepared from coconut shell. **Journal of colloid and interface science**, v. 279, n. 2, p. 307-313, 2004.

ŞENTÜRK, İlknur; ALZEIN, Mazen. Adsorption of acid violet 17 onto acid-activated pistachio shell: isotherm, kinetic and thermodynamic studies. **Acta Chimica Slovenica**, v. 67, n. 1, p. 55-69, 2020.

SHABBIR, Sadaf *et al.* Evaluating role of immobilized periphyton in bioremediation of azo dye amaranth. **Bioresource Technology**, v. 225, p. 395-401, 2017.

SHEN, Dazhong *et al.* Adsorption kinetics and isotherm of anionic dyes onto organo-bentonite from single and multisolute systems. **Journal of hazardous materials**, v. 172, n. 1, p. 99-107, 2009.

SILVA, Alfredo José Ferreira da. **Adsorção dos íons de cobre usando pó da palha da carnaúba e bentonita: estudo cinético, termodinâmico e de equilíbrio**. 2019. Tese

(Doutorado em Engenharia Química) - Universidade Federal do Rio grande do Norte, Natal, RN, 2019.

SILVA, A. T. Da. **Influência da temperatura na adsorção do corante azul de metileno utilizando serragem de Pinus elliottii como um adsorvente alternativo: um modelo para o tratamento de efluentes têxteis.** Trabalho de conclusão de curso (Graduação em Química) – Universidade Federal de Santa Catarina, Florianópolis, SC, 2005.

SINGH, N. B. *et al.* Water purification by using Adsorbents: A Review. *Environmental Technology & Innovation*, v. 11, p. 187–240, 2018.

SIVASUBRAMANIAM, D.; FRANKS, A. E. Bioengineering microbial communities: their potential to help, hinder and disgust. **Bioengineered**, v. 7, n. 3, p. 137-144, 2016

SKODRAS. G. *et al.* Kinetic studies of elemental mercury adsorption in activated carbon fixed bed reactor. *Journal Hazardous Materials*, v. 158, p. 1-13, 2008.

SULTANA, Marzia. *et al.* A review on experimental chemically modified activated carbon to enhance dye and heavy metals adsorption. **Cleaner Engineering and Technology**, v. 6, p. 100382, 2022.

TAHIR, M. Asif; BHATTI, Haq Nawaz; IQBAL, Munawar. Solar Red and Brittle Blue direct dyes adsorption onto Eucalyptus angophoroides bark: Equilibrium, kinetics and thermodynamic studies. **Journal of Environmental Chemical Engineering**, v. 4, n. 2, p. 2431-2439, 2016.

THANG, Nguyen Hoc *et al.* Methylene blue adsorption mechanism of activated carbon synthesised from cashew nut shells. **RSC advances**, v. 11, n. 43, p. 26563-26570, 2021.

THUE, Pascal S. *et al.* Single-step pyrolysis for producing magnetic activated carbon from tucumã (*Astrocaryum aculeatum*) seed and nickel (II) chloride and zinc (II) chloride. Application for removal of nicotinamide and propanolol. **Journal of Hazardous Materials**, v. 398, p. 122903, 2020.

TRAN, Hai Nguyen *et al.* Thermodynamic parameters of liquid-phase adsorption process calculated from different equilibrium constants related to adsorption isotherms: A comparison study. **Journal of Environmental Chemical Engineering**, v. 9, n. 6, p. 106674, 2021.

THOMMES, Matthias *et al.* Physisorption of gases, with special reference to the evaluation of surface area and pore size distribution (IUPAC Technical Report). **Pure and applied chemistry**, v. 87, n. 9-10, p. 1051-1069, 2015.

VIDOVIX, Taynara Basso *et al.* Bisfenol A adsorption using a low-cost adsorbent prepared from residues of babassu coconut peels. **Environmental Technology**, v. 42, n. 15, p. 2372-2384, 2021.

VIEIRA, Laís Helena Sousa et al. Strategic design of magnetic carbonaceous nanocomposites and its application as multifunctional adsorbent. **Carbon**, v. 161, p. 758-771, 2020.

WANG, Panfeng et al. Adsorptive performance for methylene blue of magnetic Ni@activated carbon nanocomposites. **Functional Materials Letters**, v. 8, n. 02, p. 1550024, 2015.

WANG, Yan et al. Enhanced brilliant blue FCF adsorption using microwave-hydrothermal synthesized hydroxyapatite nanoparticles. **Journal of Dispersion Science and Technology**, v. 41, n. 9, p. 1346-1355, 2020.

WEKOYE, Joan N. *et al.* Kinetic and equilibrium studies of Congo red dye adsorption on cabbage waste powder. **Environmental Chemistry and Ecotoxicology**, v. 2, p. 24-31, 2020.

WORCH, Eckhard. Adsorption technology in water treatment: Fundamentals, processes, and modeling. Berlin/Boston: Walter de Gruyter GmbH & Co, 2012.

YAGUB, Mustafa T. et al. Dye and its removal from aqueous solution by adsorption: A review. **Advances in Colloid and Interface Science**, v. 209, p. 172– 184, 2014.

ZANONI Maria V. Boldrin; YAMANAKA, Hideko. Corantes: Caracterização química, toxicológica, métodos de detecção e tratamento. **Editora Cultura Acadêmica**, 1. ed. São Paulo, 2016.

YANG, Yongli; CANNON, Fred S. Biomass activated carbon derived from pine sawdust with steam bursting pretreatment; perfluorooctanoic acid and methylene blue adsorption. **Bioresource technology**, v. 344, p. 126161, 2022.

YEOW, Peck Kah; WONG, Sie Wei; HADIBARATA, Tony. Removal of azo and anthraquinone dye by plant biomass as adsorbent—a review. **Biointerface Research in Applied Chemistry**, v. 11, p. 8218-8232, 2021.

YOU, Xun *et al.* Adsorption of dyes methyl violet and malachite green from aqueous solution on multi-step modified rice husk powder in single and binary systems: Characterization, adsorption behavior and physical interpretations. **Journal of Hazardous Materials**, v. 430, p. 128445, 2022.

YU, Ang *et al.* Rapid synthesis of colloidal silver triangular nanoprisms and their promotion of TiO₂ photocatalysis on methylene blue under visible light. **Catalysis Communications**, v. 90, p. 75-78, 2017.

ZAZYCKI, Maria Amélia. **Preparação de biochar a partir de matérias-primas alternativas e sua aplicação na adsorção de corantes**. 2019. Tese (Doutorado em Engenharia Química) - Universidade Federal de Santa Maria, Santa Maria, RS, 2019.

ZHANG, Zhen *et al.* Adsorption of Pb (II) and Cd (II) by magnetic activated carbon and its mechanism. **Science of the Total Environment**, v. 757, p. 143910, 2021.

ZHOU, Yanbo *et al.* Recent advances for dyes removal using novel adsorbents: a review. **Environmental pollution**, v. 252, p. 352-365, 2019.

ZOLLINGER, Heinrich. Color chemistry: syntheses, properties, and applications of organic dyes and pigments. **John Wiley & Sons**, 2003.